In presenting the dissertation as a partial fulfillment of the requirements for an advanced degree from the Georgia Institute of Technology, I agree that the Library of the Institution shall make it available for inspection and circulation in accordance with its regulations governing materials of this type. I agree that permission to copy from, or to publish from, this dissertation may be granted by the professor under whose direction it was written, or, in his absence, by the Dean of the Graduate Division when such copying or publication is solely for scholarly purposes and does not involve potential financial gain. It is understood that any copying from, or publication of, this dissertation which involves potential financial gain will not be allowed without written permission.

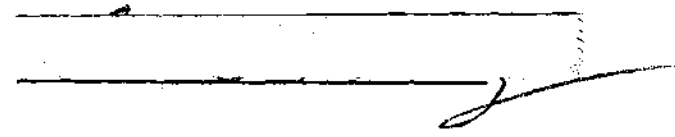

DEVELOPMENT OF AN EXPERIMENTAL METHOD FOR THE DETERMINATION OF LOCAL HEAT FLUX IN SMALL DIAMETER, COOLED NOZZLES

A THESIS

Presented to

The Faculty of the Graduate Division

by

Eric Gibson Kunz

In Partial Fulfillment

of the Requirements for the Degree

Master of Science in Mechanical Engineering

Georgia Institute of Technology

December, 1964

DEVELOPMENT OF AN EXPERIMENTAL METHOD FOR THE DETERMINATION OF LOCAL HEAT FLUX IN SMALL DIAMETER, COOLED NOZZLES

Approved:

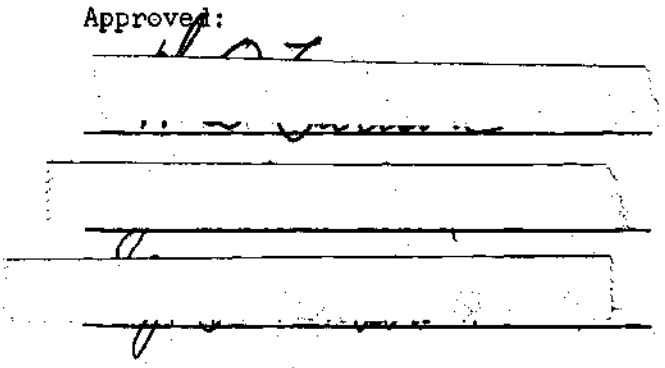

Date approved by Chairman:

18 May 1964

ACKNOWLEDGMENTS

The author is indebted to the many individuals who have contributed to the success of this work. In particular, he would like to express his sincere appreciation to his Thesis Advisor, Dr. Walter O. Carlson, for suggesting the problem and for his continued encouragement and advice. He would also like to express his gratitude to Dr. J. Edward Sunderland for his helpful suggestions throughout the progress of this work and for serving as a member of the thesis committee. The author would also like to express his sincere appreciation to Professor James E. Hubbartt for serving as a member of the thesis committee.

An extreme debt of gratitude is owed to his mother and his wife's parents for their aid and continuous encouragement throughout the progress of his graduate education. His deepest appreciation goes to his wife and daughter for their continuous patience and their unending source of strength.

Finally the author would like to dedicate this work to his father, Dr. Harold George Kunz, who would have been a better engineer than the author will ever be.

TABLE OF CONTENTS

APPENDIX (Continued) Page

LIST OF TABLES

LIST OF ILLUSTRATIONS

SUMMARY

A new experimental method is developed for the determination of the axial distribution of local heat flux on the inner surface of axially symmetric supersonic nozzles. The type of supersonic nozzle considered is thick-walled, of small diameter, and externally cooled. The gas, either argon or nitrogen, is considered to be at sufficiently high temperatures to be at least partially dissociated and possibly partially ionized. Under these conditions the method is based on two-dimensional steady state conduction in the nozzle wall with convection heat transfer on all four surfaces.

In the first step of the developed method, the steady state, two-dimensional heat conduction equation is solved for the temperature distribution within the nozzle wall. The finite difference technique for solving differential equations with complex boundary conditions is used to obtain the wall temperature distribution. The finite difference technique is used since an exact analytical solution is not available and since the accuracy of the results is a primary concern.

The next step in the developed method is to obtain sufficient experimental data to determine as accurately as possible: (1) the nozzle wall outer surface temperature distribution, (2) the two nozzle wall end surface temperature distributions, (3) the temperature distribution within the nozzle wall near the inner surface, (4) the total amount of heat removed from the nozzle by the coolant, and (5) the free stream stagnation temperature of the gas flowing through the nozzle. An initial one-

dimensional estimate is then made for the nozzle wall temperature distribution and inner surface combined convection and radiation heat transfer coefficient distribution.

In the final step the two-dimensional temperature distribution within the nozzle wall is calculated on a high speed digital computer using the finite difference two-dimensional temperature distribution equations, the measured surface temperature distributions, the one-dimensional estimate of the wall temperature distribution and the estimated heat transfer coefficient distribution. The calculated and measured values for the temperatures near the inner surface are compared and the estimate of the inner surface heat transfer coefficient is adjusted accordingly if the two temperature distributions do not match. The process of calculating, comparing and adjusting is continued until the calculated and measured temperatures match. The wall temperature distribution and the inner surface heat transfer coefficient distribution obtained when the calculated and measured temperatures match are the actual values for those parameters. The actual axial distribution of the local heat flux on the inner surface of the nozzle is then calculated as the final result. The computer programs necessary for the calculations are included for the Burroughs 220 Data-Processing System.

The design of the apparatus necessary to utilize this new experimental technique is presented for a specific size and shape nozzle having a particular range of operating conditions. The specific axially symmetric nozzle shape and size are: (1) three inch entrance inner diameter, (2) one half inch throat inner diameter, (3) two inch exit inner diameter, (4) 30 degree convergence half angle, (5) 15 degree divergence

half angle, and (6) a constant one inch wall thickness. The range of operating conditions considered are: (1) one half to one atmosphere gas pressure at the nozzle entrance, (2) gas temperatures up to approximately 10,000°K, (3) gas mass flow rates greater than 0.01 lbm/sec and (4) exit Mach numbers up to five. The nozzle wall material is pure copper and water is used as the coolant. The coolant passages, surface and internal thermocouple materials and methods of construction are presented in detail. Also, methods for construction, calibration, installation and operation of the nozzle are presented. The nozzle was not constructed, however, and experimental data were not obtained.

The accuracy of the overall method is estimated based on the operating conditions for the presented nozzle design. The estimated error in the axial distribution of the local heat flux for those conditions is plus or minus 7 per cent. The estimated cost for the experimental nozzle including the thermocouples but not including the measurement instruments is five hundred dollars. Further, it is concluded from the development of the method and the design of a specific experimental nozzle that the method is readily adaptable to nozzles having shapes, sizes and operating conditions different from those of the designed nozzle.

NOMENCLATURE

Symbol			Units
a	=	Thermal conductivity equation constant	Btu/hr-ft^2-°F
A_{c1}	=	Convection surface area--Equation 49	ft^2
A_{c2}	=	Convection surface area--Equation 70	ft^2
A_{c3}	=	Convection surface area--Equation 81	ft^2
A_{x1}	=	Gas flow cross sectional area--Figure 12	ft^2
b	=	Thermal conductivity equation constant	Btu/hr-ft-(°F)^2
C_1	=	Function defined by Equation 6	ft
C_2	=	Function defined by Equation 7	ft
C_3	=	Function defined by Equation 8	ft
C_4	=	Function defined by Equation 9	ft
C_5	=	Function defined by Equation 12	ft^2
C_6	=	Function defined by Equation 13	ft
C_7	=	Function defined by Equation 14	ft
C_8	=	Function defined by Equation 31	ft
C_9	=	Function defined by Equation 32	ft
C_{10}	=	Function defined by Equation 25	ft^2
C_{11}	=	Function defined by Equation 26	ft
C_{12}	=	Function defined by Equation 19	ft
C_{13}	=	Function defined by Equation 20	ft
C_{14}	=	Function defined by Equation 21	ft
C_{15}	=	Function defined by Equation 22	ft

Symbol			Units
E_{in}	=	Electrical energy rate to torch heating unit	$\frac{Btu}{hr}$
g_o	=	Dimensional conversion factor	32.2 ft-lbm/lb_f-sec^2
h_m	=	Local combined convection and radiation heat transfer coefficient--inner surface	Btu/hr-ft^2-°F
h_m^a	=	Approximate local combined heat transfer coefficient	Btu/hr-ft^2-°F
H_1	=	Gas static enthalpy--Figure 12	Btu/lbm
Ho_2	=	Gas stagnation enthalpy--Figure 12	Btu/lbm
J	=	Mechanical equivalent of heat unit conversion factor	778 ft-lbf/Btu
ko	=	Nozzle wall thermal conductivity evaluated at t_o	Btu/hr-ft-°F
k(t)	=	Temperature dependent thermal conductivity--Equation 36	Btu/hr-ft-°F
k*	=	Thermal conductivity evaluated at nozzle wall outer surface temperature	Btu/hr-ft-°F
$\bar{k}_1$	=	Integrated average thermal conductivity--Equation 43	Btu/hr-ft-°F
$\bar{k}_2$	=	Integrated average thermal conductivity--Equation 44	Btu/hr-ft-°F
$\bar{k}_3$	=	Integrated average thermal conductivity--Equation 45	Btu/hr-ft-°F
$\bar{k}_4$	=	Integrated average thermal conductivity--Equation 46	Btu/hr-ft-°F
$\bar{k}_5$	=	Integrated average thermal conductivity--Equation 59	Btu/hr-ft-°F
$\bar{k}_6$	=	Integrated average thermal conductivity--Equation 78	Btu/hr-ft-°F
L_1	=	Grid system dimension constant--Figure 6 or 7	ft

Symbol			Units
L_2	=	Grid system dimension constant--Figure 6 or 7	ft
ln	=	Logarithm to the base e	
$\dot{m}$	=	Gas mass flow rate	lbm/hr
P_1	=	Gas static wall pressure--Figure 12	p.s.i.a.
P_2	=	Gas static wall pressure--Figure 12	p.s.i.a.
$q\Big\vert_{m,n+1}^{m,n}$	=	Heat conducted from grid point m,n+1 to grid point m,n	Btu/hr
$\bar{q}_o''$	=	Average outer surface heat flux	Btu/hr-ft^2
$q_{m,i}''$	=	Local inner surface grid point heat flux	Btu/hr-ft^2
$q_{m,i}$	=	Local inner surface grid point total heat transfer	Btu/hr
q_{conv}	=	Local inner surface grid point combined convection and radiation heat transfer	Btu/hr
Q_a	=	Heat removed from torch region by coolant	Btu/hr
Q_b	=	Heat removed from plenum chamber by coolant	Btu/hr
r_i	=	Local inner surface radius	ft
r_o	=	Local outer surface radius	ft
$r_{m,n}$	=	Radius from nozzle axis to grid point m,n	ft
t_o	=	Local outer surface temperature--measured	°F
t_i^a	=	Approximate local inner surface temperature	°F
$t_{m,n}$	=	Temperature of grid point m,n	°F
$t_{m,n}^a$	=	Approximate temperature of grid point m,n	°F
$t_{m,1}$	=	Outer surface grid point temperature from measured distribution	°F
T_{og}	=	Gas free stream stagnation temperature	°F

Symbol			Units
$V\Big\|_{m+1,n-1}^{m,n}$	=	Ratio of partial element volume to complete volume for conduction region between grid points m+1,n-1 and m,n	
z_m	=	Axial coordinate distance from the nozzle entrance end surface to the m^{th} radial grid line	ft
ρ	=	Gas mass density	lbm/ft^3
Δr	=	Constant-radial distance between axial grid lines	ft
T_{og}	=	Gas free stream stagnation temperature	°F

CHAPTER I

INTRODUCTION

Statement of Problem

The work reported herein is concerned with the development of an experimental technique to determine the axial distribution of local heat flux on the inner surface of axially symmetric nozzles. The specific type of nozzle and its operating conditions define the particular type of system for which an experimental technique is to be developed. This thesis does not include the construction of the nozzle or the collection and correlation of experimental data.

The nozzle is a thick-walled, small-diameter throat, supersonic, axially symmetric nozzle. The throat and exit diameters are to be of the order of magnitude of one half of an inch and two inches, respectively. The gas is to be accelerated within the nozzle to a Mach number of three or higher and is to be considered at a sufficiently high temperature to be at least partially dissociated and possibly at high enough temperatures to be partially ionized. Finally, the nozzle is to be adequately cooled so that long duration operation is possible.

These operating conditions and nozzle characteristics not only define the special case for which an experimental method for determining the axial distribution of local heat flux is to be developed, but also require the technique to take into consideration two-dimensional conduction of heat through the nozzle wall.

Survey of Related Literature

The amount of research on the topic of heat transfer in rocket nozzles, which has been conducted in the past few years, and the publications which have resulted from this research, permit only a brief listing of some of the typical methods developed by the work done in each area of this field of research. The order of presentation of the experimental techniques for determining the axial distribution of local heat flux in nozzles is by grouping the various techniques into two cases determined by the operating conditions for which the techniques were developed. The first case is defined by operating conditions such that steady state conduction of the heat through the nozzle wall occurs and the second case is defined by operating conditions such that transient conduction of the heat through the nozzle wall occurs.

Steady State Conduction

For the case of steady state conduction in the nozzle wall there have been only two significantly different methods developed. The first of these methods is generally called the calorimetric method.[1-11*] With this method, steady state conditions are achieved by cooling the nozzle with water forced through small, rectangular, circumferential passageways within the nozzle wall. These passages are located very close to the inner surface of the nozzle wall so that the actual wall thickness between the hot gas stream and the coolant water is very thin. The passages are usually very narrow and are placed side by side for the entire extent of the nozzle. The effects achieved by this construction are

---

* Superscript numbers refer to references in Bibliography.

two-fold. First, since the wall thickness through which the heat is conducted is very thin, conduction is entirely in the radial direction. The second effect is that semi-local values of the heat flux are easily calculated from measurements of the temperature rise and flow rate of the water for each passageway combined with knowledge of the amount of nozzle wall inner surface area cooled by each passageway. Also, semi-local values of the inner surface combined radiation and convection heat transfer coefficient can be determined if values for the free stream gas temperature and the inner surface wall temperatures are known. Although this is one of the better methods, the results obtained from tests using this method have not been found to correlate very well with the results of tests on thick-walled nozzles employing other methods.[8,9,10,11]

In the second method developed for the case of steady state conduction, a nozzle with a thicker wall in the radial direction than in the first method is used and the entire nozzle outer surface is cooled with a single water passage.[6,12] At several locations along the axis of the nozzle the radial temperature distributions are measured. The method of measuring these distributions involves driving of plugs into holes drilled radially into the nozzle wall at the locations where the local heat fluxes are desired. Each plug has two or more thermocouples embedded along the plug axis such that when the plug is in place the radial temperature distribution is measured at that location. The method of heat flux calculation for this technique requires the assumption of only radial conduction.

However, since the nozzle wall is not thin, heat conduction is generally in both the radial and axial directions and thus the resulting

heat fluxes so calculated are not entirely correct. Plots of the temperature distribution within the nozzle wall in fact do clearly indicate the two dimensional pattern of heat conduction.[12]

Transient Conduction

In the case of transient conduction conditions in the nozzle wall there are several similar methods generally employed. All of the transient methods have three common features. First, the nozzle wall is not cooled except for the heat which radiates away to the surroundings due only to the temperature level of the nozzle wall outer surface. Second, the nozzle walls are much thicker than those of the steady state conduction calorimetric method. Third, all of the techniques basically assume that the heat conduction is entirely radial. Two-dimensional conduction is not considered.

The first general method in the transient conduction case employs the same type of radial thermocouple plugs as are used in the second method for the steady state heat conduction case.[5,6,8,10,13,14,15,16]

In this case, the radial temperature distributions are obtained at all locations at uniform intervals of time after the gas starts flowing. Thus, time histories of the temperature distributions at each of the desired locations are obtained before the gas flow must be stopped to avoid charring or melting the nozzle wall inner surface.

The evaluation of heat fluxes from the data obtained can be accomplished by several different techniques and thus several different sub-cases are presented. First, the most common method of analysis is that of fitting a curve to each of the temperature distributions obtained and then obtaining a fifth or higher order polynomial equation to fit the

curves. Using these equations for the temperature distributions, the distribution of heat flux at the nozzle inner surface is determined by finite difference techniques applied to the transient, one-dimensional heat conduction equation aided by the use of high speed digital computers.[5,6,10,11,14,16]

The rest of the various methods for evaluating the heat fluxes from the plug time histories of the temperature distributions are various techniques for obtaining approximate analytical solutions to the transient, one dimensional heat conduction equation. These various techniques are: the integration method, the Cresci-Libby method and the semi-log extrapolation method.[15]

The second general method in the transient conduction case does not use time histories of the radial temperature distributions but uses time histories of the inner surface wall temperatures.[17,18] The temperature-time histories are obtained by direct measurement with special thermocouples designed for this purpose. The heat flux and total transfer to the nozzle wall for any given length of time are obtained by still another approximate integral solution to the transient, one-dimensional heat conduction equation.[17]

The third general method in the transient conduction case is usually called the Greenfield Method.[15,19] This method employs a nozzle with a very thick wall. Circumferential slots are cut into the nozzle wall almost all the way through to the inner surface of the nozzle wall. These slots essentially divide the nozzle into many separate axial segments. Each segment is assumed to approximate a short hollow cylinder thermally insulated from the next segment by the air gaps and thus each

is considered to be an independent thermal capacitor. A single thermocouple is embedded within each axial segment at the location of the segment average temperature as calculated from Schmidt plots of the nozzle wall. The average temperature gradient in time for each of the segments is then obtained by graphical integration. The average heat flux for each setment is assumed to be equal to the product of the segment weight, the specific heat of the segment and the integrated average temperature gradient in time divided by the segment's inner surface area.

In all of the transient cases the one common condition that is apparent is that one-dimensional heat transfer is assumed to occur. However, in all of the transient cases the nozzle wall is thick in the radial direction. The heat conduction is, therefore, generally in both the radial and axial directions rather than just the radial direction as assumed, with the exception of the Greenfield Method, and thus the resulting heat fluxes so calculated are not entirely correct.

Purpose of Research

The purpose of this research is to extend and improve the field of experimental determination of local heat flux in rocket nozzles. In order to extend the field, a new experimental method for determining the axial distribution of the local heat flux will be developed such that the case of steady state operating conditions is extended from considering only one dimensional heat conduction to considering two-dimensional heat conduction within the nozzle wall.

The experimental method will be developed so that it will yield results which have greater accuracy than the results obtained with the

previous methods. This increase in accuracy will be obtained by considering two-dimensional heat conduction within the nozzle wall and thereby avoiding the inherent inaccuracy in considering only one-dimensional conduction. At the same time the new method will incorporate experimental measurement techniques at least as accurate as those used by previous methods, thus permitting a greater overall accuracy to be obtained.

CHAPTER II

ANALYTICAL DEVELOPMENT OF DATA REDUCTION TECHNIQUE

General Method

The proposed method of experimentally determining the axial distribution of local heat flux on the inner surface of an axially symmetric, thick-walled, cooled nozzle basically consists of a four-step procedure. In the first step the steady state, two-dimensional heat conduction equation is solved for the temperature distribution within a nozzle wall having convection heat transfer boundary conditions on all four surfaces. The finite difference technique for solving differential equations with complex boundary conditions is used to obtain the solution.

The next step is to obtain sufficient experimental data so that the following are known as accurately as possible: (1) the nozzle wall outer surface temperature distribution, (2) the two nozzle wall end surface temperature distributions, (3) the temperature distribution within the nozzle wall near the inner surface, (4) the total amount of heat removed from the nozzle by the coolant and (5) the free stream stagnation temperature of the gas flowing through the nozzle. An average value of the heat flux at the outer nozzle surface is then calculated by dividing the total heat removed from the nozzle by the outer nozzle wall surface area.

The third step is to make an estimate of the nozzle wall inner surface combined convection and radiation heat transfer coefficient. To

make this estimate, an approximation is first made for the nozzle wall inner surface temperature distribution by solving the steady state, one dimensional equation for heat conduction through the wall of a hollow tube in the radial direction at each axial location for which a value of the outer surface temperature is known. The approximation for the inner surface temperature distribution is then:

$$t_i^a = \frac{(\bar{q}_o'')(r_o)\ln(r_o/r_i)}{k_o} + t_o \qquad (1)$$

where: $\bar{q}_o''$ = average outer surface heat flux

k_o = nozzle wall thermal conductivity evaluated at t_o

t_o = local outer surface temperature--measured

r_o = local outer surface radius

r_i = local inner surface radius

t_i^a = approximate local inner surface temperature

The estimate of the axial distribution of the wall inner surface heat transfer coefficient can then be obtained from:

$$h_m^a = \frac{(\bar{q}_o'')(r_o/r_i)}{(T_{og} - t_i^a)} \qquad (2)$$

where: $\bar{q}_o''$ = average outer surface heat flux

r_o = local outer surface radius

r_i = local inner surface radius

t_i^a = approximate local inner surface temperature

T_{og} = free stream stagnation temperature of the gas

h_m^a = approximate local combined heat transfer coefficient

In the final step the axial distribution of the local heat flux is determined. Using the experimentally measured values of the temperature distributions along the wall outer surface and both of the wall end surfaces, the free stream stagnation gas temperature and the estimate of the wall inner surface combined heat transfer coefficient, the entire temperature distribution within the nozzle wall is calculated from the finite difference solution to the steady state, two-dimensional heat conduction equation. A high speed digital computer is used to perform these calculations. Next, the measured values of the temperatures of the nozzle wall near the inner surface are compared to the corresponding values in the calculated temperature distribution. If the temperatures at each point where measured values were obtained do not match those temperatures at the corresponding points in the calculated distribution, the estimate of the axial distribution of the combined heat transfer coefficient is adjusted accordingly and the entire nozzle wall temperature distribution is recalculated.

The calculating, comparing and altering process is repeated until the measured temperatures and the calculated temperatures match. Then, provided both the measured temperatures and the calculated temperatures are sufficiently sensitive to slight changes in the axial distribution of the inner surface combined heat transfer coefficient, the value of the heat transfer coefficient distribution that was used in the final temperature calculations is the actual axial distribution of the combined heat transfer coefficient on the inner surface of the nozzle wall. Also, the final calculated value of the entire nozzle wall temperature distribu-

tion yields the actual nozzle wall inner surface temperature distribution since it is calculated as part of the entire nozzle wall temperature distribution. Both the combined heat transfer coefficient distribution and the nozzle wall inner surface temperature distribution are the actual values to within the accuracy limits of the method and the experimental data.

The axial distribution of the inner surface heat flux is calculated directly from Equation 3 using the combined heat transfer coefficient distribution and wall inner surface temperature distribution just obtained.

$$q''_{m,i} = h_m(T_{og} - t_{m,i}) \tag{3}$$

where: $q''_{m,i}$ = local inner surface heat flux

$t_{m,i}$ = local inner surface temperature

T_{og} = gas free stream stagnation temperature

h_m = local inner surface combined heat transfer coefficient

Derivation of Equations

In order to consider steady state, two-dimensional heat conduction within the nozzle walls it is necessary to obtain a solution to the two-dimensional conduction equation subject to the convection boundary conditions of a nozzle. Many analytical solutions to this equation in cylindrical coordinates have been obtained, each one for a different set of boundary conditions.[21,22,23] A solution has not yet been found, however, for the particular case of convection boundary conditions on a

body having the shape of an axially-symmetric, convergent-divergent nozzle. The interdependence of the two cylindrical coordinates at both the inner and outer wall surfaces is probably the major reason why such an analytical solution has not been obtained.

The alternative to an exact analytical solution of the conduction equation considered is to use one of the many approximate solution techniques. Since the accuracy of results is a primary concern, the method of the finite differences is used to obtain a set of equations for the temperature distribution within the nozzle wall which can then be solved on a high speed digital computer. The presentation of the finite difference technique herein is limited to how it is used to solve the steady state, two-dimensional conduction equation subject to the nozzle convection boundary conditions. For the brief review of the finite difference technique as it is used in solving general heat transfer problems, the heat transfer texts by Gebhart[24] or Schneider[25] are recommended. A reasonably complete development of the finite difference technique for heat transfer calculations with many illustrative examples can be found in Dusinberre's text[26] on the subject.

Grid System

The first step in obtaining a finite difference solution is to divide the nozzle wall axial cross sectional area into small elemental areas with a grid system. The nozzle wall axial cross sectional area is chosen because the temperature distribution within it completely represents the temperature distribution within the nozzle wall for the two-dimensional conduction case considered. The two general features which define the grid system used are the type of grid system and the

size of the grid system.

The choice of the type of grid system is limited by two characteristics which it must have so that the set of equations for the temperature distribution within the nozzle wall, which comprise the finite difference solution to the conduction equation, will be relatively simple. Further, rough approximations for surface boundary conditions are thereby avoided. The first grid system characteristic is that the lines forming the grid system should coincide with the cylindrical coordinate axes. Second, all grid lines should terminate on the boundary surfaces only at grid line intersection points. The grid system which has these important characteristics is shown in Figure 1.

The details of this type of grid system become apparent when this system is constructed as follows. First, the axial grid lines are drawn so that the nozzle wall is divided into equal radial increments. The number of these increments is determined by the size of the grid system chosen. The radial grid lines are then drawn so that each terminates at an intersection point of the nozzle wall inner surface and an axial grid line. The end surfaces of the nozzle wall are determined from the position of the radial grid line nearest the desired nozzle inner surface diameter for each end. The inner surface contour of the nozzle is continued to the desired diameter on each end of the nozzle by shaping the gas side surface of the nozzle end coolant passages accordingly. Since the radial grid line nearest the desired nozzle inner surface diameter is used, the continuation of the nozzle inner surface contour by the gas side surface of the end coolant passages will be less than the distance between two radial grid lines at that point. For a grid system

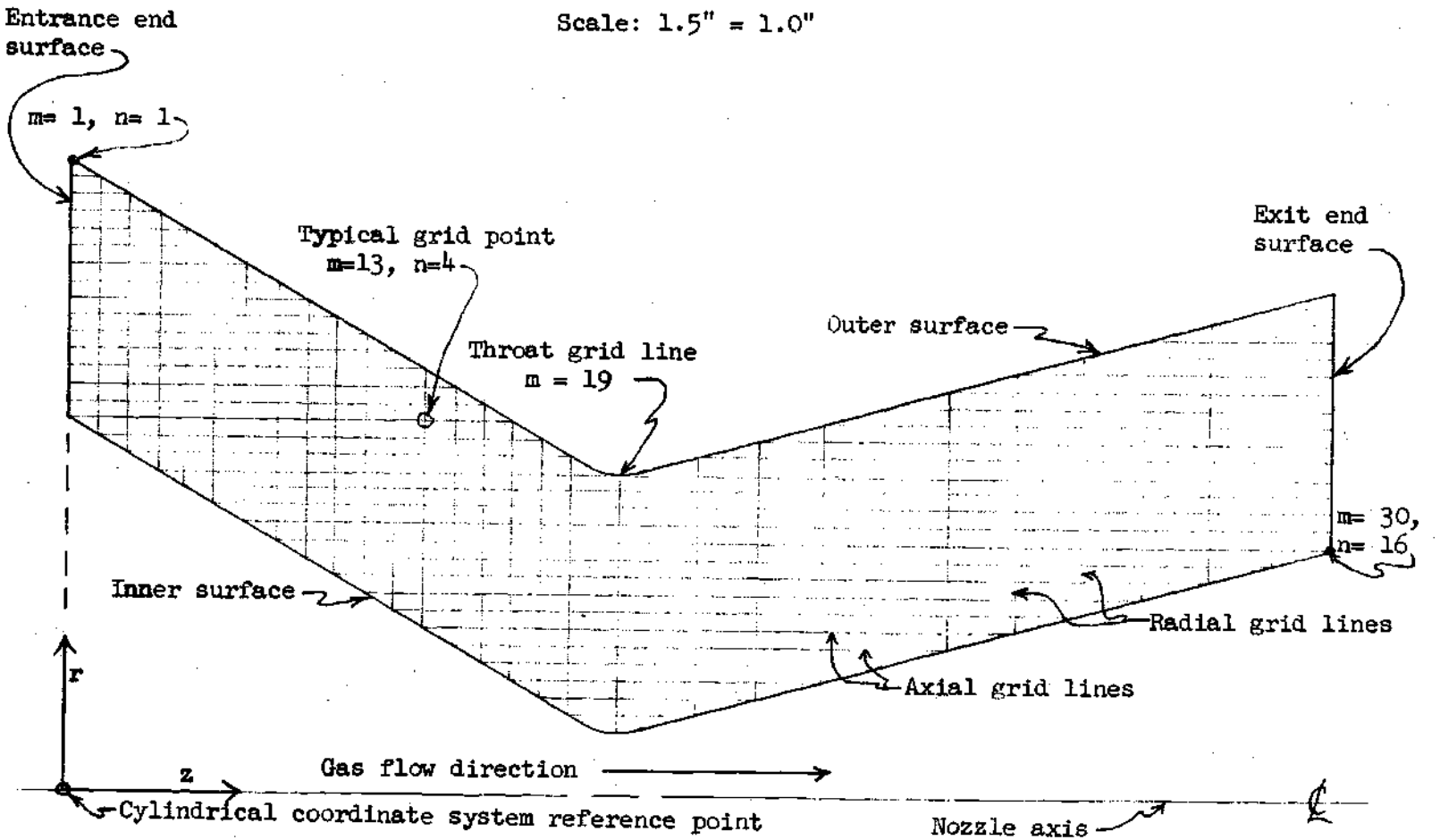

Figure 1. Grid System for Convergent-Divergent Nozzle Wall Axial Cross Sectional Area

fine enough for accurate results, this distance will be much less than the width of the coolant passage necessary for sufficient cooling. The details of this design are shown in Figure 2 for one end of the nozzle. The other nozzle end surface is treated in the same manner. The result of designing the nozzle wall end surfaces in this way is to obtain a grid system which has both of the important grid system characteristics so that rough approximations for the boundary conditions can be avoided and the set of temperature distribution equations are reasonably simple.

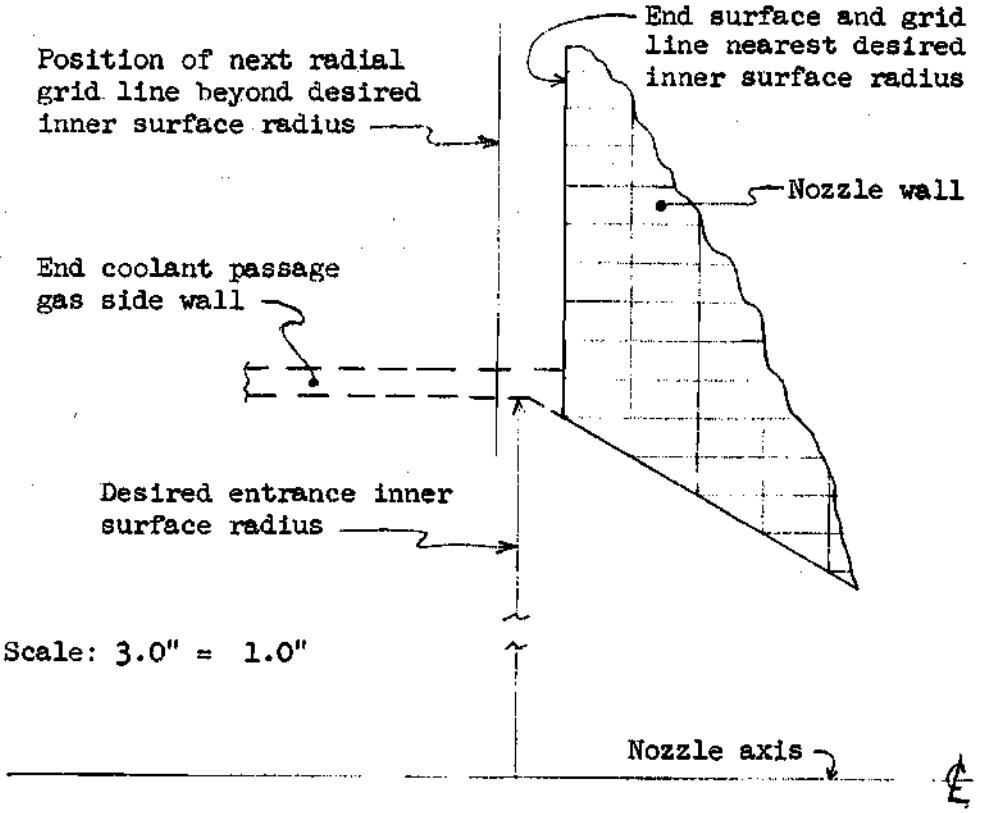

Figure 2. Nozzle End Surface Design Detail

The second general feature of the grid system is its size. The size of the grid system means the size of the elemental areas into which

it divides the axial cross sectional area of the nozzle wall. Therefore, as the size of the grid system decreases, the size of each elemental area decreases, the number of elemental areas and grid lines increases, the accuracy of the finite difference approximation increases and the overall accuracy of the results increases. Because of this effect on the accuracy of the results, the grid system size must be small enough so that if a smaller grid size is used neither the magnitude nor the shape of the resulting axial distribution of local heat flux is altered significantly. The size of the grid system which meets these requirements for the range of nozzle operating conditions for which the method is developed is shown in Figure 1.

Energy Balances and Resulting Temperature Distribution Equations

Once the type and size of grid system have been established the next step in solving the conduction equation for the temperature distribution within the nozzle wall is to write an energy balance for each of the grid line intersection points. In the derivation of these energy balances, the significant approximations made in the finite difference technique become apparent. These approximations are as follows: (1) The heat is conducted between grid points only along the grid line segments connecting the grid points. (2) The conduction along each grid line is one-dimensional conduction in the direction of the grid line. (3) The volume element for the one-dimensional conduction along each line segment is the area surrounding the line segment, for the segment length and extending half way to the next grid line on each side, times the circumference of the nozzle at that location. (4) The temperature gradient causing the conduction along a grid line between two grid points

is taken as the difference in temperatures of the two grid points divided by the length of the grid line segment between those points. (5) The thermal conductivity for the element of material considered by each grid line segment is the integrated average conductivity. This average is obtained by integrating the conductivity versus temperature equation using the temperatures of the two grid points as limits and then dividing the result by the difference of those two temperatures. For the case of a linear variation of thermal conductivity with temperature, the integrated average becomes the arithmetic average of the conductivity evaluated at each of the two grid point temperatures.

The number of actual energy balances derived can be reduced by writing an energy balance for each typical type of grid point using two subscripts to designate the grid point position. Each grid point, then, is distinguished by two integer subscripts. The numbering of the grid points is performed as follows: (1) The radial grid lines are numbered consecutively from the entrance end to the exit end with the entrance end surface as the first and the exit end surface as the last radial grid line. Thus, the radial grid line, on which the grid point falls, is the first subscript value. (2) The second subscript value designates how many axial grid lines into the nozzle wall along a radial grid line a particular grid point is from the outer surface at that radial grid line. Thus, grid point m,n is on the m^{th} radial grid line counting from the entrance end of the nozzle and is n axial grid lines in from the nozzle outer surface. As a further example, referring to the grid system in Figure 1, the grid point at the throat of the nozzle on the nozzle wall inner surface would be grid point number 19,16. This numbering system

reduces the number of energy balances necessary for the grid system in Figure 1 from 420 to only 7.

The seven necessary energy balances are for the following grid points: (1) a typical interior grid point for the converging section, (2) a typical inner surface grid point for the converging section, (3) a typical interior grid point for the radial grid line at the nozzle throat, (4) the first grid point inside the inner surface on the nozzle throat radial grid line, (5) the inner surface grid point on the nozzle throat radial grid line, (6) a typical interior grid point for the diverging section and (7) a typical inner surface grid point for the diverging section. Energy balances for the grid points on the entrance end surface, on the exit end surface and on the outer surface are not necessary since the temperature distributions along those surfaces are obtained as data and, therefore, the temperatures at the grid points on those surfaces are not calculated. Further, since those surface grid point temperatures are known, no other boundary condition information is necessary for those surfaces in the finite difference solution for the nozzle wall temperature distribution.

The finite difference technique for obtaining the temperature distribution equations from the set of energy balance equations is called the relaxation method. This method alters the energy balances by setting each one equal to a variable called a residual instead of equating them to zero as a steady state energy balance should be. The method is then to assume a temperature for every grid point for which the energy balances apply. These values of the grid point temperatures are used in their appropriate energy balance and the values of the residuals are cal-

culated for each grid point. If all of the residuals are zero then the temperature distribution used to calculate those residuals is the actual temperature distribution for the boundary conditions used in the calculations. If one or more of the residuals is not equal to zero then at least one of the temperatures in the assumed distribution is wrong. When this occurs, the temperature distribution must be altered so as to reduce all of the residuals to as close to zero as possible.

Any reasonably systematic process for reducing those residuals by altering the temperature distribution becomes very complex and lengthy for the grid system used for a nozzle wall. However, if the energy balances are left equal to zero and solved for the temperature of the grid point for which they are derived, a simple straightforward temperature calculation procedure results. Therefore, the energy balances are solved for the temperature of the grid point for which each energy balance is derived. The method of calculating the actual nozzle wall temperature distribution using these equations is presented in the following section in detail.

A typical grid point diagram, the energy balance and the resulting temperature equation for each of the seven general grid points follow. All of the finite difference approximations are used in their derivations. The complete derivations of these equations are presented in Appendix A. In the derivations the thermal conductivity of the nozzle wall is assumed to be a linear function of temperature. The grid system size used to determine the range of grid points for which each equation is valid is the grid system shown in Figure 1.

Not to Scale

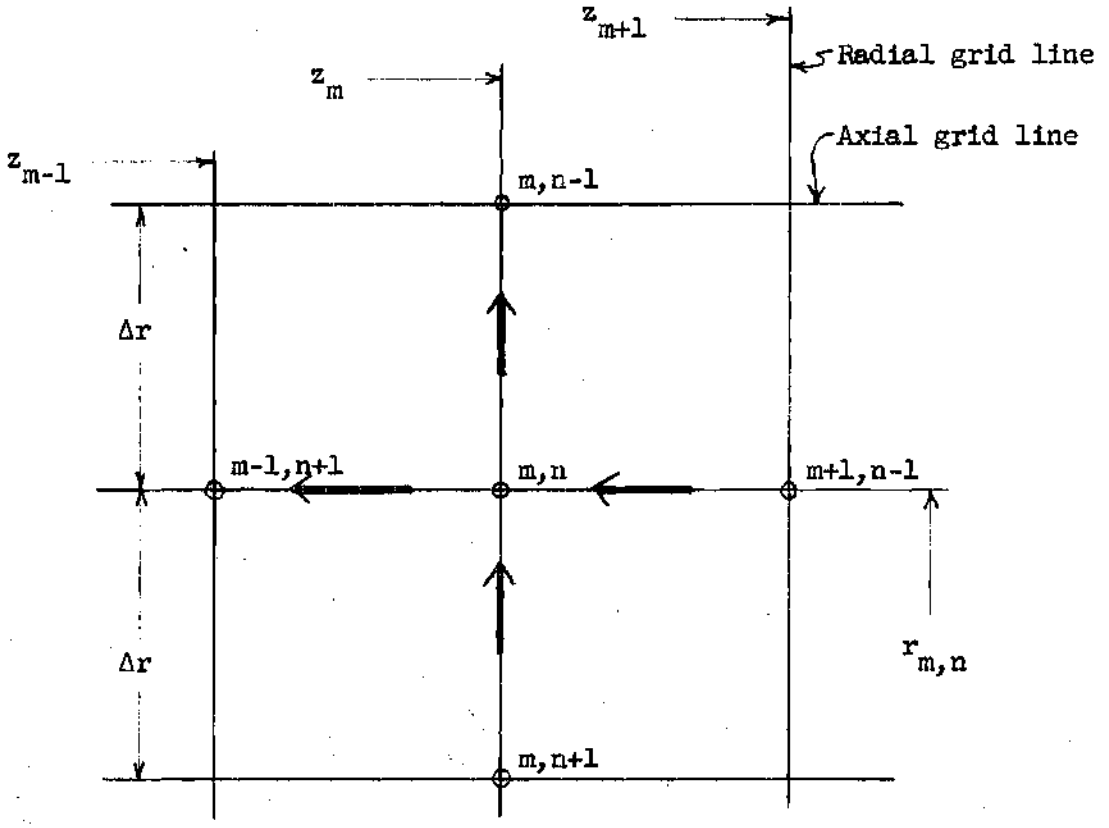

Note: (1) Arrows on grid lines indicate assumed direction of heat flow.
(2) r - coordinate dimensions referenced to nozzle centerline.
(3) z - coordinate dimensions referenced to nozzle entrance end surface.

Figure 3. A Typical Interior Grid Point for the Converging Section

A typical interior grid point for the converging section of the nozzle is shown in Figure 3.

The steady state energy balance for this grid point m,n is:*

$$\bar{k}_1 \left(\frac{2r_{m,n}\Delta r}{z_{m+1} - z_m}\right)\left(t_{m+1,n-1} - t_{m,n}\right) - \bar{k}_2 \left(\frac{2r_{m,n}\Delta r}{z_m - z_{m-1}}\right)\left(t_{m,n} - t_{m-1,n+1}\right) \quad (4)$$

$$+ \bar{k}_3 \left(\frac{z_{m+1} - z_{m-1}}{\ln(r_{m,n}) - \ln(r_{m,n} - \Delta r)}\right)\left(t_{m,n} - t_{m,n-1}\right)$$

$$- \bar{k}_4 \left(\frac{z_{m+1} - z_{m-1}}{\ln(r_{m,n} + \Delta r) - \ln(r_{m,n})}\right)\left(t_{m,n} - t_{m,n-1}\right) = 0$$

Solving this energy balance for the temperature of the grid point, number m,n, yields:

$$t_{m,n} = \frac{\bar{k}_1 C_1 t_{m+1,n-1} + \bar{k}_2 C_2 t_{m-1,n+1} + \bar{k}_3 C_3 t_{m,n+1} + \bar{k}_4 C_4 t_{m,n-1}}{\bar{k}_1 C_1 + \bar{k}_2 C_2 + \bar{k}_3 C_3 + \bar{k}_4 C_4} \quad (5)$$

where:

$$C_1 = \left(\frac{2r_{m,n}\Delta r}{z_{m+1} - z_m}\right) \quad (6)$$

$$C_2 = \left(\frac{2r_{m,n}\Delta r}{z_m - z_{m-1}}\right) \quad (7)$$

$$C_3 = \left(\frac{z_{m+1} - z_{m-1}}{\ln(r_{m,n}) - \ln(r_{m,n} - \Delta r)}\right) \quad (8)$$

---

* Refer to Nomenclature for a complete listing of symbol definitions.

Not to Scale

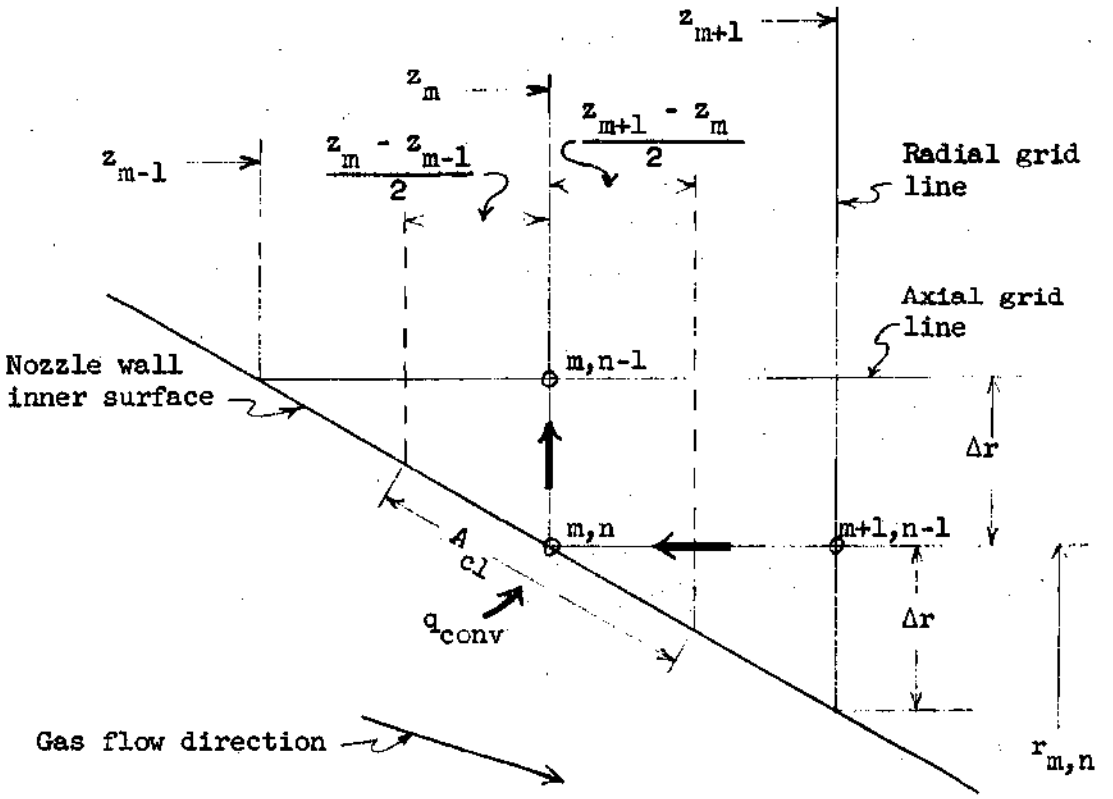

Note: (1) Arrows on grid lines indicate assumed direction of heat flow.
(2) r - coordinate dimensions referenced to nozzle centerline.
(3) z - coordinate dimensions referenced to nozzle entrance end surface.

Figure 4. A Typical Inner Surface Grid Point for the Converging Section

$$C_4 = \left(\frac{z_{m+1} - z_{m-1}}{\ln(r_{m,n} + \Delta r) - \ln(r_{m,n})}\right) \tag{9}$$

for: $2 \leq m \leq 18$ and $2 \leq n \leq 15$.

A typical inner surface grid point for the converging section of the nozzle is shown in Figure 4. The steady state energy balance for this grid point m,n is then:

$$0 = h_m(2r_{m,n})\sqrt{(\Delta r)^2 + \left(\frac{z_{m+1} - z_{m-1}}{2}\right)^2}\left(T_{og} - t_{m,n}\right) \tag{10}$$

$$+ \bar{k}_1\left(\frac{\frac{3}{2} r_{m,n}\Delta r + \frac{1}{8}(\Delta r)^2}{z_{m+1} - z_m}\right)\left(t_{m+1,n-1} - t_{m,n}\right)$$

$$+ \bar{k}_4\left[\frac{(z_{m+1} - z_m)(2r_{m,n} + \Delta r) + (z_m - z_{m-1})(r_{m,n} + \frac{3}{4}\Delta r)}{(2r_{m,n} + \Delta r)\left[\ln(r_{m,n} + \Delta r) - \ln(r_{m,n})\right]}\right]\left(t_{m,n-1} - t_{m,n}\right)$$

Solving this energy balance for the temperature of the grid point, number m,n, yields:

$$t_{m,n} = \frac{h_m C_5 T_{og} + \bar{k}_1 C_6 T_{m+1,n-1} + \bar{k}_4 C_7 t_{m,n-1}}{h_m C_5 + \bar{k}_1 C_6 + \bar{k}_4 C_7} \tag{11}$$

where:
$$C_5 = (2r_{m,n})\left[(\Delta r)^2 + \left(\frac{z_{m+1} - z_{m-1}}{2}\right)^2\right]^{\frac{1}{2}} \tag{12}$$

$$C_6 = \left(\frac{\frac{3}{2} r_{m,n}\Delta r + \frac{1}{8}(\Delta r)^2}{z_{m+1} - z_m}\right) \tag{13}$$

$$C_7 = \left[\frac{(z_{m+1} - z_m)(2r_{m,n} + \Delta r) + (z_m - z_{m-1})(r_{m,n} + \frac{3}{4}\Delta r)}{(2r_{m,n} + \Delta r)\{\ln(r_{m,n} + \Delta r) - \ln(r_{m,n})\}}\right] \quad (14)$$

for: $2 \leq m \leq 18$ and $n = 16$.

A typical interior grid point for the radial grid line at the nozzle throat is shown in Figure 5. The steady state energy balance for this grid point m,n is then:

$$\bar{k}_5 \left(\frac{2r_{m,n}\Delta r}{z_{m+1} - z_m}\right)(t_{m+1,n+1} - t_{m,n}) + \bar{k}_2 \left(\frac{2r_{m,n}\Delta r}{z_m - z_{m-1}}\right)(t_{m-1,n+1} - t_{m,n}) \quad (15)$$

$$+ \bar{k}_3 \left(\frac{z_{m+1} - z_{m-1}}{\ln(r_{m,n}) - \ln(r_{m,n} - \Delta r}\right)(t_{m,n+1} - t_{m,n})$$

$$+ \bar{k}_4 \left(\frac{z_{m+1} - z_{m-1}}{\ln(r_{m,n} + \Delta r) - \ln(r_{m,n})}\right)(t_{m,n-1} - t_{m,n}) = 0$$

Solving this energy balance for the temperature of the grid point, number m,n, yields:

$$t_{m,n} = \frac{\bar{k}_5 C_1 t_{m+1,n+1} + \bar{k}_2 C_2 t_{m-1,n+1} + \bar{k}_3 C_3 t_{m,n+1} + \bar{k}_4 C_4 t_{m,n-1}}{\bar{k}_5 C_1 + \bar{k}_2 C_2 + \bar{k}_3 C_3 + \bar{k}_4 C_4} \quad (16)$$

for: $m = 19$ and $2 \leq n \leq 14$.

Not to Scale

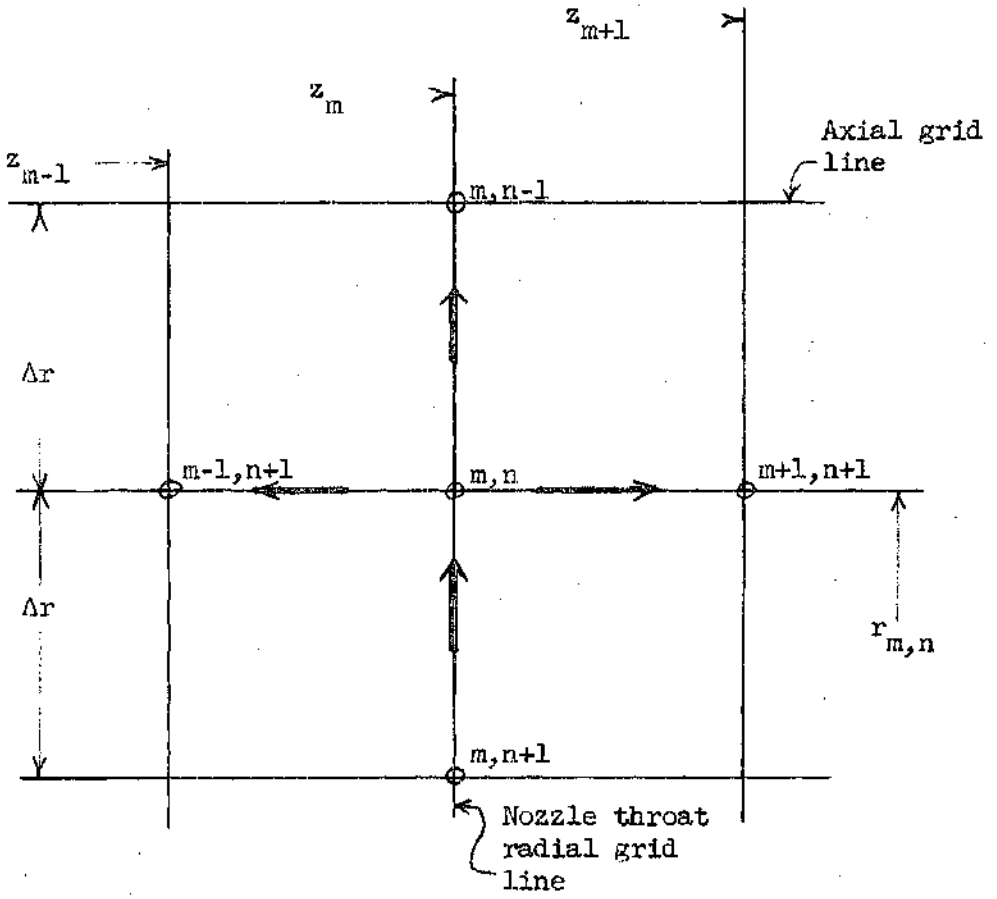

Note: (1) Arrows on grid lines indicate assumed direction of heat flow.
(2) r - coordinate dimensions referenced to nozzle centerline.
(3) z - coordinate dimensions referenced to nozzle entrance end surface.

Figure 5. A Typical Interior Grid Point for the Nozzle Throat Radial Grid Line

Not to Scale

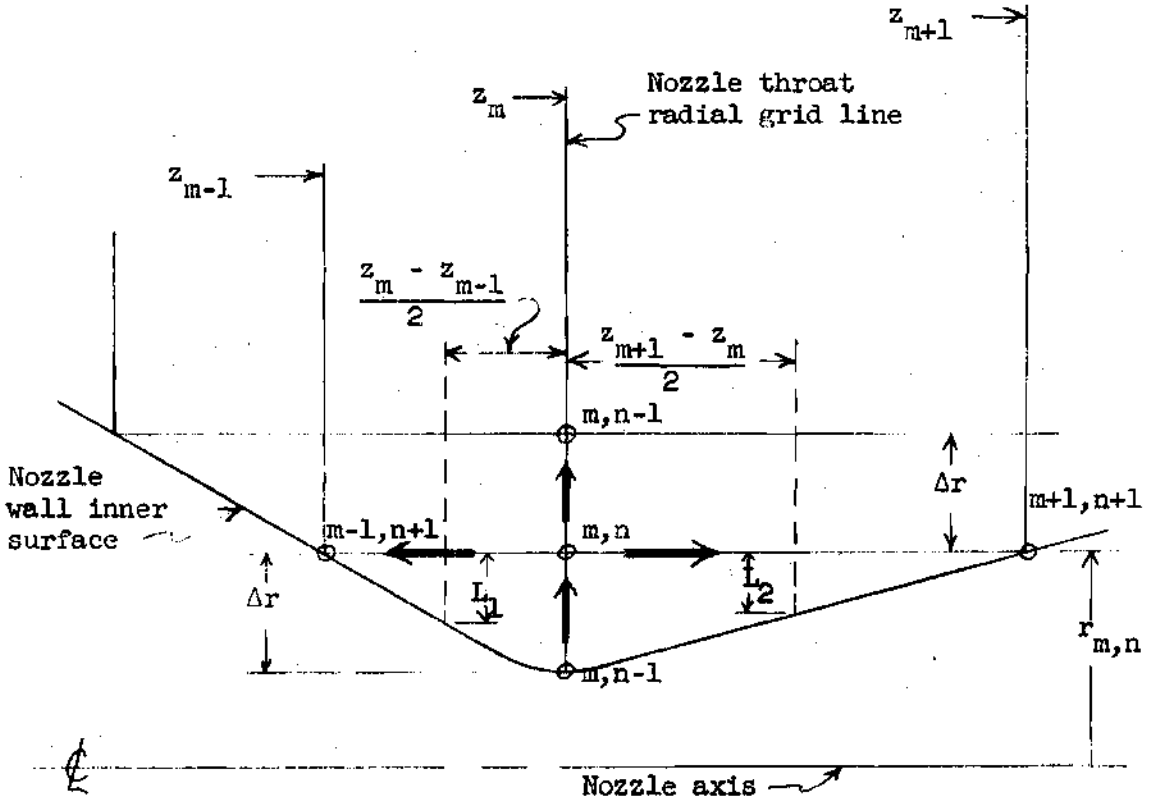

Note: (1) Arrows on grid lines indicate assumed direction of heat flow.
(2) r - coordinate dimensions referenced to nozzle centerline.
(3) z - coordinate dimensions referenced to nozzle entrance end surface.

Figure 6. The First Grid Point Inside the Inner Surface on the Nozzle Throat Radial Grid Line

The first grid point inside the inner surface on the nozzle throat radial grid line is shown in Figure 6. The steady state energy balance for this grid point m,n is then:

$$\bar{k}_3\left[\frac{(z_m - z_{m-1})\left[(\Delta r + L_1)\left(r_{m,n} - \frac{\Delta r}{4} - \frac{L_1}{4}\right) - \frac{1}{12}(\Delta r - L_1)^2\right]}{\left[\ln(r_{m,n}) - \ln(r_{m,n} - \Delta r)\right]\left[2r_{m,n}\Delta r - (\Delta r)^2\right]}\right](t_{m,n+1} - t_{m,n}) \tag{17}$$

$$+ \bar{k}_3\left[\frac{(z_{m+1} - z_m)\left[(\Delta r + L_2)\left(r_{m,n} - \frac{\Delta r}{4} - \frac{L_2}{4}\right) - \frac{1}{12}(\Delta r - L_2)^2\right]}{\left[\ln(r_{m,n}) - \ln(r_{m,n} - \Delta r)\right]\left[2r_{m,n}\Delta r - (\Delta r)^2\right]}\right](t_{m,n+1} - t_{m,n})$$

$$+ \bar{k}_4\left[\frac{(z_{m+1} - z_{m-1})}{\ln(r_{m,n} + \Delta r) - \ln(r_{m,n})}\right](t_{m,n-1} - t_{m,n})$$

$$+ \bar{k}_5\left[\frac{\left[r_{m,n}\Delta r + \frac{1}{4}(\Delta r)^2 + \frac{3}{2}r_{m,n}L_2 - \frac{2}{3}(L_2)^2\right]}{(z_{m+1} - z_{m-1})}\right](t_{m+1,n+1} - t_{m,n})$$

$$+ \bar{k}_2\left[\frac{\left[r_{m,n}\Delta r + \frac{1}{4}(\Delta r)^2 + \frac{3}{2}r_{m,n}L_2 - \frac{2}{3}(L_2)^2\right]}{(z_m - z_{m-1})}\right](t_{m-1,n+1} - t_{m,n}) = 0$$

Solving this energy balance for the temperature of the grid point number m,n yields:

$$t_{m,n} = \frac{\bar{k}_3 C_{12} t_{m,n+1} + \bar{k}_4 C_{13} t_{m,n-1} + \bar{k}_5 C_{14} t_{m+1,n+1} + \bar{k}_2 C_{15} t_{m-1,n+1}}{\bar{k}_3 C_{12} + \bar{k}_4 C_{13} + \bar{k}_5 C_{14} + \bar{k}_2 C_{15}} \tag{18}$$

where: $$C_{12} = \frac{(z_m - z_{m-1})\left[(\Delta r + L_1)(r_{m,n} - \frac{1}{4}\Delta r - \frac{1}{4}L_1) - \frac{1}{12}(\Delta r - L_1)^2\right]}{\left[2r_{m,n}\Delta r - (\Delta r)^2\right]\left[\ln(r_{m,n}) - \ln(r_{m,n} - \Delta r)\right]}$$

(19)

$$+ \frac{(z_{m+1} - z_m)\left[(\Delta r + L_2)(r_{m,n} - \frac{1}{4}\Delta r - \frac{1}{4}L_2) - \frac{1}{12}(\Delta r - L_2)^2\right]}{\left[2r_{m,n}\Delta r - (\Delta r)^2\right]\left[\ln(r_{m,n}) - \ln(r_{m,n} - \Delta r)\right]}$$

$$C_{13} = \frac{(z_{m+1} - z_{m-1})}{\left[\ln(r_{m,n} + \Delta r) - \ln(r_{m,n})\right]} \tag{20}$$

$$C_{14} = \frac{\left[r_{m,n}\Delta r + \frac{1}{4}(\Delta r)^2 + \frac{3}{2}(r_{m,n}L_2) - \frac{2}{3}(L_2)^2\right]}{(z_{m+1} - z_m)} \tag{21}$$

$$C_{15} = \frac{\left[r_{m,n}\Delta r + \frac{1}{4}(\Delta r)^2 + \frac{3}{2}(r_{m,n}L_2) - \frac{2}{3}(L_2)^2\right]}{(z_m - z_{m-1})} \tag{22}$$

for: m = 19 and n = 15.

The inner surface grid point on the nozzle throat radial grid line is shown in Figure 7. The steady state energy balance for this grid point m,n is then:

$$h_m(2r_{m,n} + \Delta r - L_1)\left[(\Delta r - L_1)^2 + (\frac{z_m - z_{m-1}}{2})^2\right]^{\frac{1}{2}}(T_{og} - t_{m,n}) \tag{23}$$

$$+ h_m(2r_{m,n} + \Delta r - L_2)\left[(\Delta r - L_2)^2 + (\frac{z_{m+1} - z_m}{2})^2\right]^{\frac{1}{2}}(T_{og} - t_{m,n})$$

$$- \bar{k}_4\left[\frac{(z_m - z_{m-1})\left[r_{m,n}(\Delta r - L_1) + (\Delta r)^2 - \frac{1}{3}(\Delta r - L_1)^2\right]}{\left[2r_{m,n}\Delta r + (\Delta r)^2\right]\left[\ln(r_{m,n} + \Delta r) - \ln(r_{m,n})\right]}\right](t_{m,n} - t_{m,n-1})$$

Not to Scale

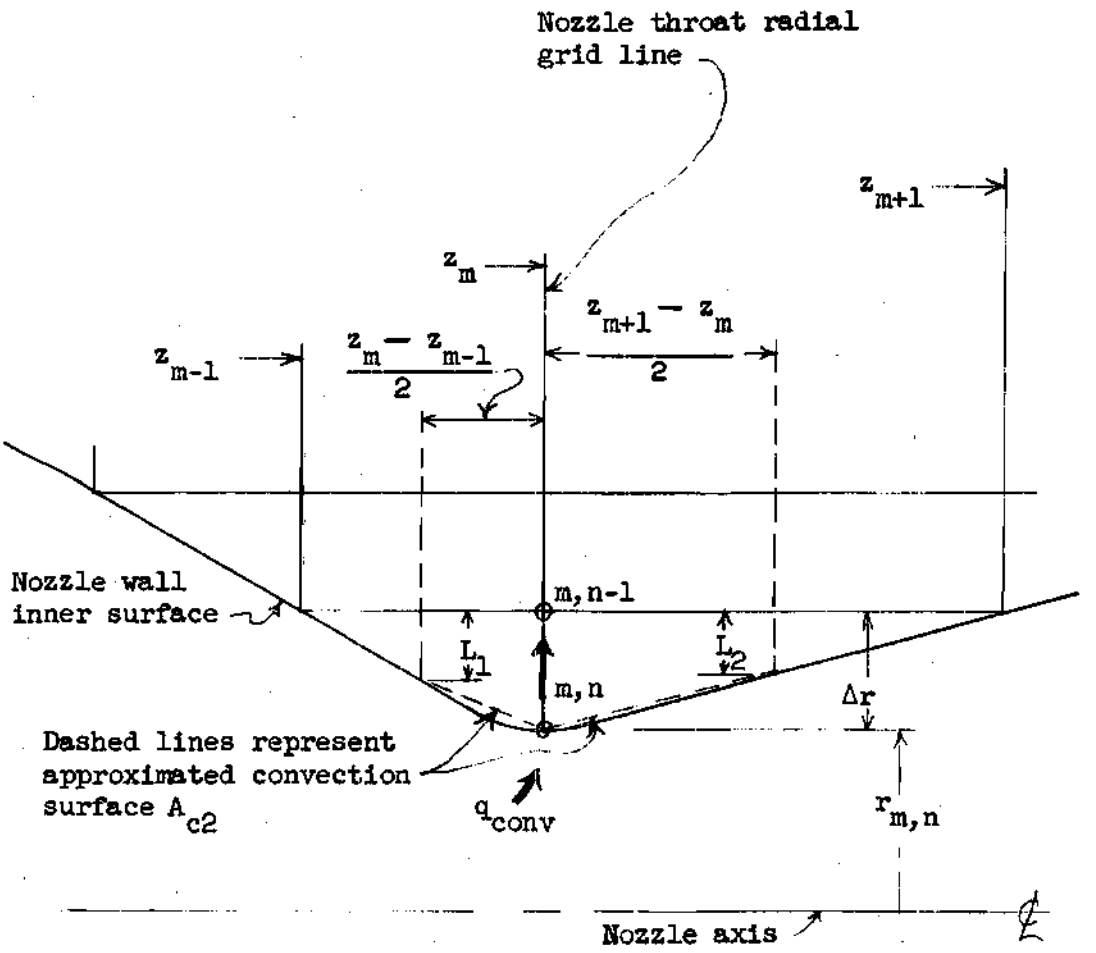

Note: (1) Arrow on grid line indicates assumed direction of heat flow.
(2) r - coordinate dimensions referenced to nozzle centerline.
(3) z - coordinate dimensions referenced to nozzle entrance end surface.

Figure 7. The Inner Surface Grid Point on the Nozzle Throat Radial Grid Line

$$- \bar{k}_4 \left[\frac{(z_{m+1} - z_m)\left[r_{m,n}(\Delta r + L_2) + (\Delta r)^2 - \frac{1}{3}(\Delta r - L_2)^2\right]}{\left[2r_{m,n}\Delta r + (\Delta r)^2\right]\left[\ln(r_{m,n} + \Delta r) - \ln(r_{m,n})\right]} \right] (t_{m,n} - t_{m,n-1}) = 0$$

Solving this energy balance for the temperature of the grid point, number m,n yields:

$$t_{m,n} = \frac{h_m C_{10} T_{og} + \bar{k}_4 C_{11} t_{m,n-1}}{h_m C_{10} + \bar{k}_4 C_{11}} \tag{24}$$

where:
$$C_{10} = (2r_{m,n} + \Delta r - L_1)\left[(\Delta r - L_1)^2 + \frac{1}{4}(z_m - z_{m-1})^2\right]^{\frac{1}{2}} + (2r_{m,n} + \Delta r - L_2)\left[(\Delta r - L_2)^2 + \frac{1}{4}(z_{m+1} - z_m)^2\right]^{\frac{1}{2}} \tag{25}$$

$$C_{11} = \frac{(z_m - z_{m-1})\left[r_{m,n}(\Delta r + L_1) + (\Delta r)^2 - \frac{1}{3}(\Delta r - L_1)^2\right]}{\left[2r_{m,n}\Delta r + (\Delta r)^2\right]\left[\ln(r_{m,n} + \Delta r) - \ln(r_{m,n})\right]} + \frac{(z_{m+1} - z_m)\left[r_{m,n}(\Delta r + L_2) + (\Delta r)^2 - \frac{1}{3}(\Delta r - L_2)^2\right]}{\left[2r_{m,n}\Delta r + (\Delta r)^2\right]\left[\ln(r_{m,n} + \Delta r) - \ln(r_{m,n})\right]} \tag{26}$$

for: m = 19 and n = 16.

A typical interior grid point for the diverging section of the nozzle is shown in Figure 8. The steady state energy balance for this grid point m,n is then:

$$\bar{k}_5 \left(\frac{2r_{m,n}\Delta r}{z_{m+1} - z_m}\right)(t_{m+1,n+1} - t_{m,n}) + \bar{k}_6 \left(\frac{2r_{m,n}\Delta r}{z_m - z_{m-1}}\right)(t_{m-1,n-1} - t_{m,n}) + \bar{k}_3 \left(\frac{z_{m+1} - z_{m-1}}{\ln(r_{m,n}) - \ln(r_{m,n} - \Delta r)}\right)(t_{m,n+1} - t_{m,n}) \tag{27}$$

Not to Scale

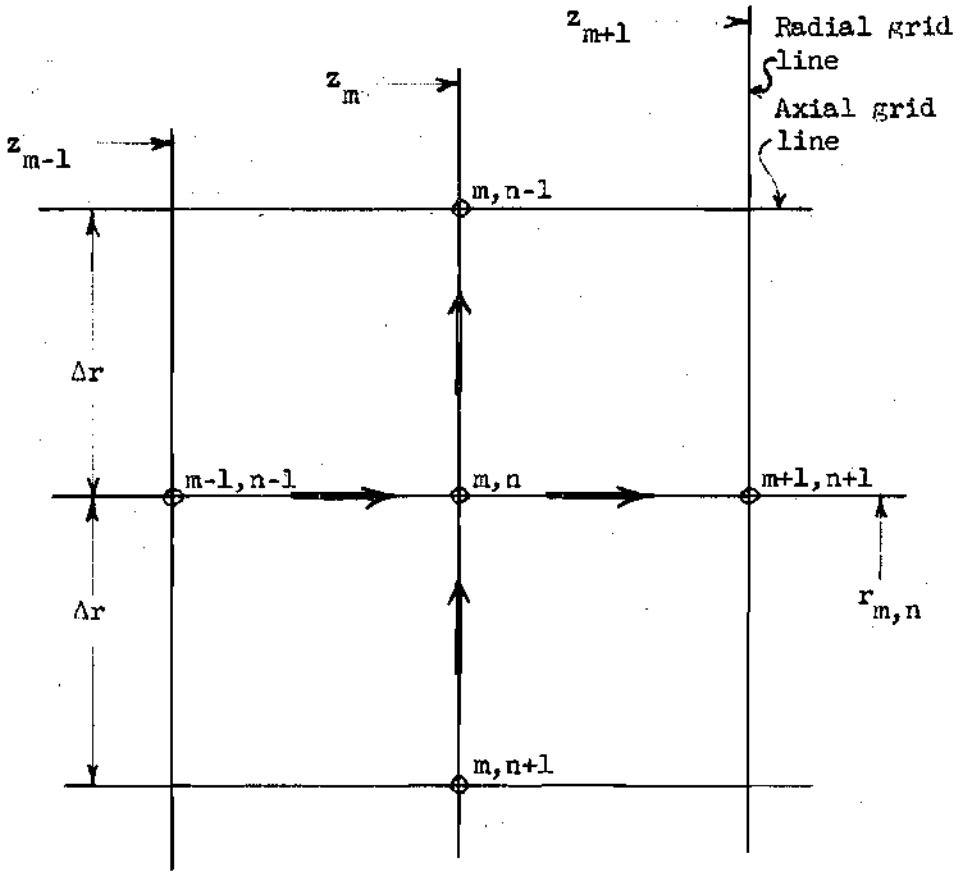

Note: (1) Arrows on grid lines indicate assumed direction of heat flow.
(2) r - coordinate dimensions referenced to nozzle centerline.
(3) z - coordinate dimensions referenced to nozzle entrance end surface.

Figure 8. A Typical Interior Grid Point for the Diverging Section

$$+ \bar{k}_4 \left(\frac{z_{m+1} - z_{m-1}}{\ln(r_{m,n} + \Delta r) - \ln(r_{m,n})}\right)(t_{m,n-1} - t_{m,n}) = 0 \qquad (27)$$

Solving this energy balance for the temperature of the grid point, number m,n yields:

$$t_{m,n} = \frac{\bar{k}_5 C_1 t_{m+1,n+1} + \bar{k}_6 C_2 t_{m-1,n-1} + \bar{k}_3 C_3 t_{m,n+1} + \bar{k}_4 C_4 t_{m,n-1}}{\bar{k}_5 C_1 + \bar{k}_6 C_2 + \bar{k}_3 C_3 + \bar{k}_4 C_4} \qquad (28)$$

where C_1, C_2, C_3, and C_4 are as before, for: $20 \leq m \leq 29$ and $2 \leq n \leq 15$.

A typical inner surface grid point for the diverging section of the nozzle is shown in Figure 9. The steady state energy balance for this grid point m,n is then:

$$h_m (2r_{m,n})\left[(\Delta r)^2 + \left(\frac{z_{m+1} - z_{m-1}}{2}\right)^2\right]^{\frac{1}{2}} (T_{og} - t_{m,n}) \qquad (29)$$

$$+ \bar{k}_6 \left[\frac{\frac{3}{2}(r_{m,n}\Delta r) + \frac{1}{8}(\Delta r)^2}{(z_m - z_{m-1})}\right](t_{m-1,n-1} - t_{m,n})$$

$$+ \bar{k}_4 \left[\frac{(z_m - z_{m-1})(2r_{m,n} + \Delta r) + (z_{m+1} - z_m)(r_{m,n} + \frac{3}{4}\Delta r)}{(2r_{m,n} + \Delta r)\left[\ln(r_{m,n} + \Delta r) - \ln(r_{m,n})\right]}\right](t_{m,n-1} - t_{m,n}) = 0$$

Solving this energy balance for the temperature of the grid point, number m,n yields:

$$t_{m,n} = \frac{h_m C_5 T_{og} + \bar{k}_6 C_8 t_{m-1,n-1} + \bar{k}_4 C_9 t_{m,n-1}}{h_m C_5 + \bar{k}_6 C_8 + \bar{k}_4 C_9} \qquad (30)$$

Not to Scale

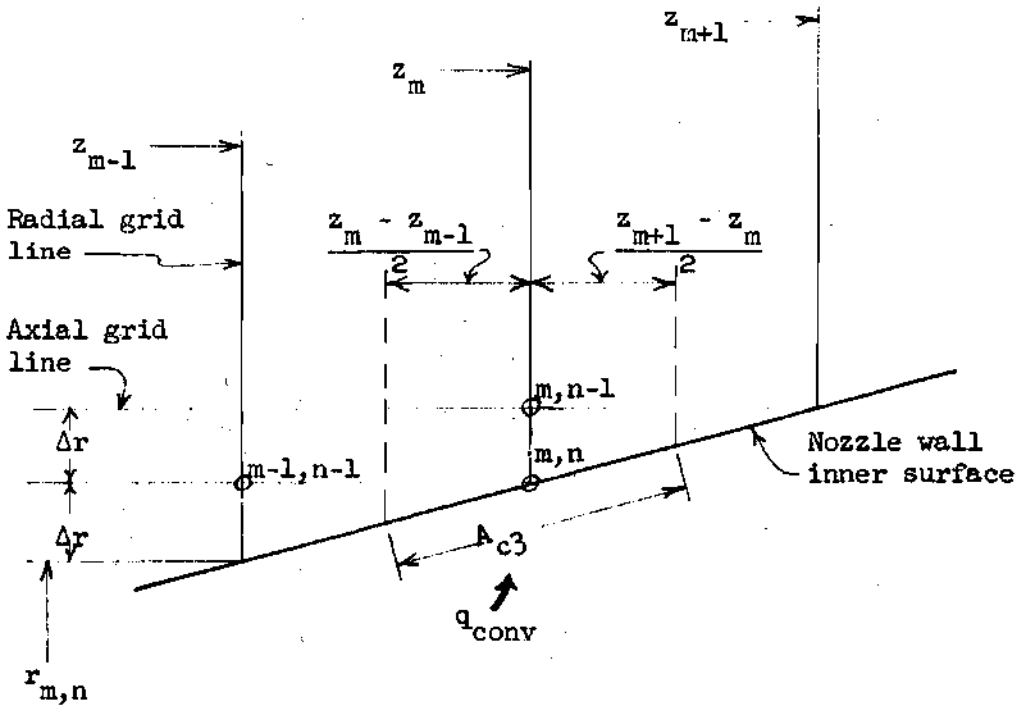

Note: (1) Arrows on grid lines indicate assumed direction of heat flow.
(2) r - coordinate dimensions referenced to nozzle centerline.
(3) z - coordinate dimensions referenced to nozzle entrance end surface.

Figure 9. A Typical Inner Surface Grid Point for the Diverging Section

where C_5 is as before and:

$$C_8 = \frac{[\frac{3}{2}(r_{m,n}\Delta r) + \frac{1}{8}(\Delta r)^2]}{[z_m - z_{m-1}]} \tag{31}$$

$$C_9 = \frac{(z_m - z_{m-1})(2r_{m,n}+\Delta r) + (z_{m+1} - z_m)(r_{m,n}+\frac{3}{4}\Delta r)}{(2r_{m,n}+\Delta r)[\ln(r_{m,n}+\Delta r) - \ln(r_{m,n})]} \tag{32}$$

for: $20 \leq m \leq 29$ and $n = 16$.

Solution of Equations and Data Reduction

Before the set of seven general grid point temperature equations can be solved, two types of data are necessary. The first type of data is that which is determined by the nozzle size and shape, by the size of the grid system chosen and by the equation for the nozzle wall thermal conductivity. The second type of data is that which is experimentally measured.

The data determined by the shape and size of the nozzle are: (1) the distance from the entrance end surface of each radial grid line, (2) the nozzle wall outer surface radius at the entrance end surface (grid point 1,1), and (3) the dimensions L_1 and L_2. The values for these quantities are directly obtained from the equations for the grid lines and for the lines representing the nozzle wall surfaces in terms of the r and z coordinates. The only values which must be specified to write the equations are those of the nozzle shape and size and the distance between axial grid lines. However, since these quantities are specified as exact values, the data obtained from the resulting equations are exact

and therefore no error is introduced with these data.

Next, the coefficients of the equation for the nozzle wall thermal conductivity as a linear function of temperature are determined from the best available conductivity data for the nozzle wall material chosen. If accurate conductivity data are not available for the nozzle wall material over the estimated range of nozzle wall operating temperatures, a sample of the nozzle wall material should be used to accurately determine such conductivity data.

The data obtained by experimental measurement during nozzle tests are: (1) the nozzle wall outer surface temperature distribution, (2) the entrance and exit end surface temperature distributions, (3) the temperature distribution within the nozzle wall near the inner surface, and (4) the temperature rise and flow rate of the coolant water. The temperature distributions on the nozzle wall outer and end surfaces are determined by placing a sufficient number of thermocouples along those surfaces so that their temperature distributions can be accurately plotted. Once having accurate plots of the surface temperature distributions, the temperatures of the grid points on those surfaces are obtained directly from the plots.

The temperatures near the inner surface are also measured by thermocouples. These thermocouples should be imbedded in the nozzle wall at actual grid point locations since they are to be compared with calculated grid point temperatures. If they are not imbedded at grid point locations, a complex interpolation is required to obtain values from the calculated distribution to compare with the measured values. For the imbedded thermocouples to be placed as close to the inner surface as

possible, they are imbedded at grid points which are only one axial grid line in from the inner surface. The grid points whose temperatures are so measured are shown in Figure 10. The two conditions used in choosing these grid points are: (1) a sufficient number of temperatures are measured so that slight changes in the axial distribution of the local heat transfer rates are observable as changes in some or all of these temperatures and (2) the number of thermocouples imbedded does not significantly alter the pattern of heat conduction within the nozzle wall.

The final data necessary are values for the free stream stagnation temperature of the gas flowing through the nozzle. The size of the nozzle and its operating conditions do not permit direct measurement of this temperature. It must be determined, therefore, by forming a thermodynamic energy balance for the entire system including the gas heating system and the ducts through which the gas passes before entering the nozzle itself. The technique used to determine this temperature is the same technique as is used in the calorimetric method of determining the axial distributions of local heat transfer rates for similar nozzle operating conditions.[1,2,3,4]

Since the design of all of the associated equipment, besides the nozzle itself, determines the specific details of this technique, only a general description of it is possible without specifying the design of the rest of the equipment preceding the nozzle. In general, then, the free stream stagnation temperature is determined from the measured static pressure at the exit end of the plenum chamber wall and the enthalpy of the gas at that location. The gas enthalpy is computed by subtracting all of the heat transferred to the coolant prior to the

Circled grid points show locations of nozzle wall internal temperature measurement points near inner surface

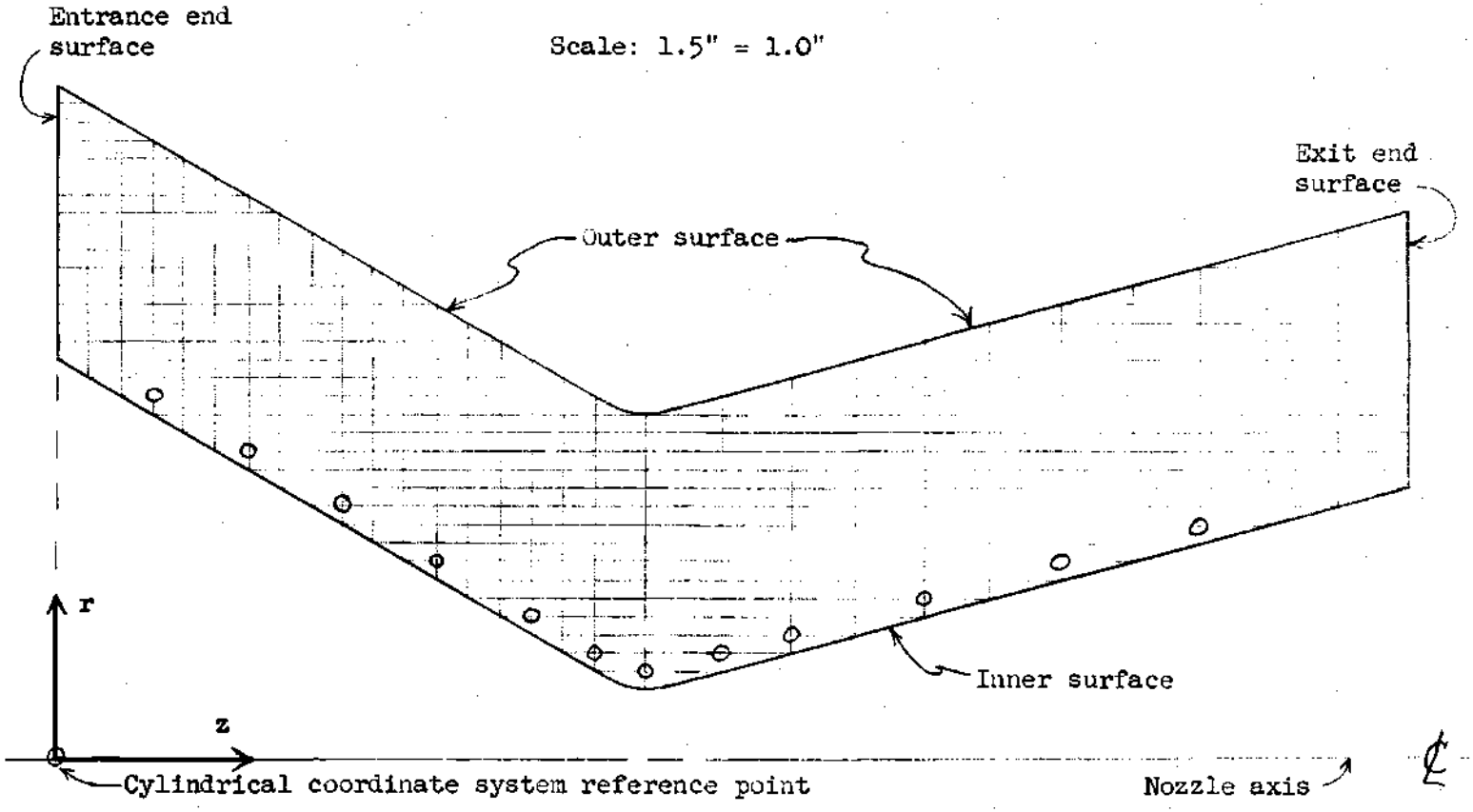

Figure 10. Internal Temperature Measurement Grid Point Locations

nozzle from the energy added to the gas during the heating of the gas and the enthalpy of the gas as it enters the system. If the gas is cooled to a comparatively low temperature before it leaves the system, the total heat added to the gas can be compared to the total heat removed by the coolant in all of the sections of the system to check on the accuracy of this method.[1,2,3,4] A sketch of a typical system with its energy balance is presented in Appendix B as an example of this method.

To reduce all of the data using the finite difference set of grid point temperature equations an initial estimate of both the distribution of the heat transfer coefficient on the inner surface and the temperature distribution within the wall are necessary. The method of making an initial estimate of the heat transfer coefficient on the nozzle wall inner surface is as presented in the General Method section of this chapter. The initial estimate of the nozzle wall temperature distribution is obtained in a similar manner.

By rewriting the steady state, radial heat conduction equation for a hollow tube, equation (1), using the grid system two-subscript notation, a one-dimensional initial estimate is obtained for the entire nozzle wall temperature distribution. That is:

$$t^{a}_{m,n} = \frac{(\bar{q}''_{\odot})(r_{m,1})\ln\left(\frac{r_{m,1}}{r_{m,n}}\right)}{k_{\odot}} + t_{m,1} \qquad (33)$$

where: $t^{a}_{m,n}$ = estimate of nozzle wall grid point temperature distribution

$t_{m,1}$ = outer surface grid point temperatures from measured

distribution

$\bar{q}''_o$ = average nozzle wall outer surface heat flux

$r_{m,1}$ = radius of nozzle wall outer surface grid points

$r_{m,n}$ = radius of nozzle wall grid points

k_o = nozzle wall thermal conductivity evaluated at $t_{m,1}$

for: $2 \leq m \leq 29$ and $2 \leq n \leq 16$ for the grid system shown in Figure 1.

This one-dimensional estimate of the nozzle wall temperature distribution and the initial estimate of the distribution of the inner surface heat transfer coefficient along with the measured temperature distributions on the outer surface and the two end surfaces are used for the initial calculation of the two-dimensional conduction grid point temperature distribution within the nozzle wall. The seven grid point equations are used to calculate this temperature distribution on a high speed digital computer. The computer program for these calculations is in Appendix E in the standard Algol language for the Burroughs 220 Data-Processing System.

The computer program uses the seven grid point temperature equations to calculate the two-dimensional conduction grid point temperature distribution in the nozzle wall for any given axial distribution of the inner surface heat transfer coefficient. Since the seven grid point temperature equations evaluate each grid point temperature by averaging the temperatures of the surrounding grid points, the computer program uses one temperature distribution for the entire nozzle wall to calculate a new temperature distribution. Each grid point temperature in the new distribution then, is an average of the temperatures of the surrounding grid points using the old distribution temperatures for those surrounding

grid point temperature values. The old temperature distribution is then replaced by this new temperature distribution and from it the grid point equations are used to calculate still another temperature distribution. Because the equations are for the steady state conditions, this process of calculating a new temperature distribution from the previous temperature distribution will eventually yield a temperature distribution after which each subsequent temperature distribution is identical. Thus, a plot of the calculated temperature of any grid point would follow one of the two patterns shown in Figure 11 depending on whether its initial estimated value was too high or too low.

This iterative method of temperature distribution calculations is a form of the Jacobi method of simultaneous displacements. In order to insure that the temperatures converge to the final solution for each heat transfer coefficient distribution used, each of the coefficients in the temperature calculation equations must be positive and greater than zero. If this criterion is satisfied the temperature distribution calculated by the equations is a stable and unique solution and there is no possibility of divergence.[31] The criterion, therefore, specifies that the distance between axial grid lines must be less than the radius of the nozzle wall inner surface at the throat, which is the point of minimum radius. For the grid system shown in Figure 1, the inner surface throat radius is one-fourth of an inch and the distance between axial grid lines is one-fifteenth of an inch. Thus, the criterion is satisfied and convergence is insured.

The only exceptions to this pattern of changing temperatures are the temperatures of the outer surface and two end surface grid points.

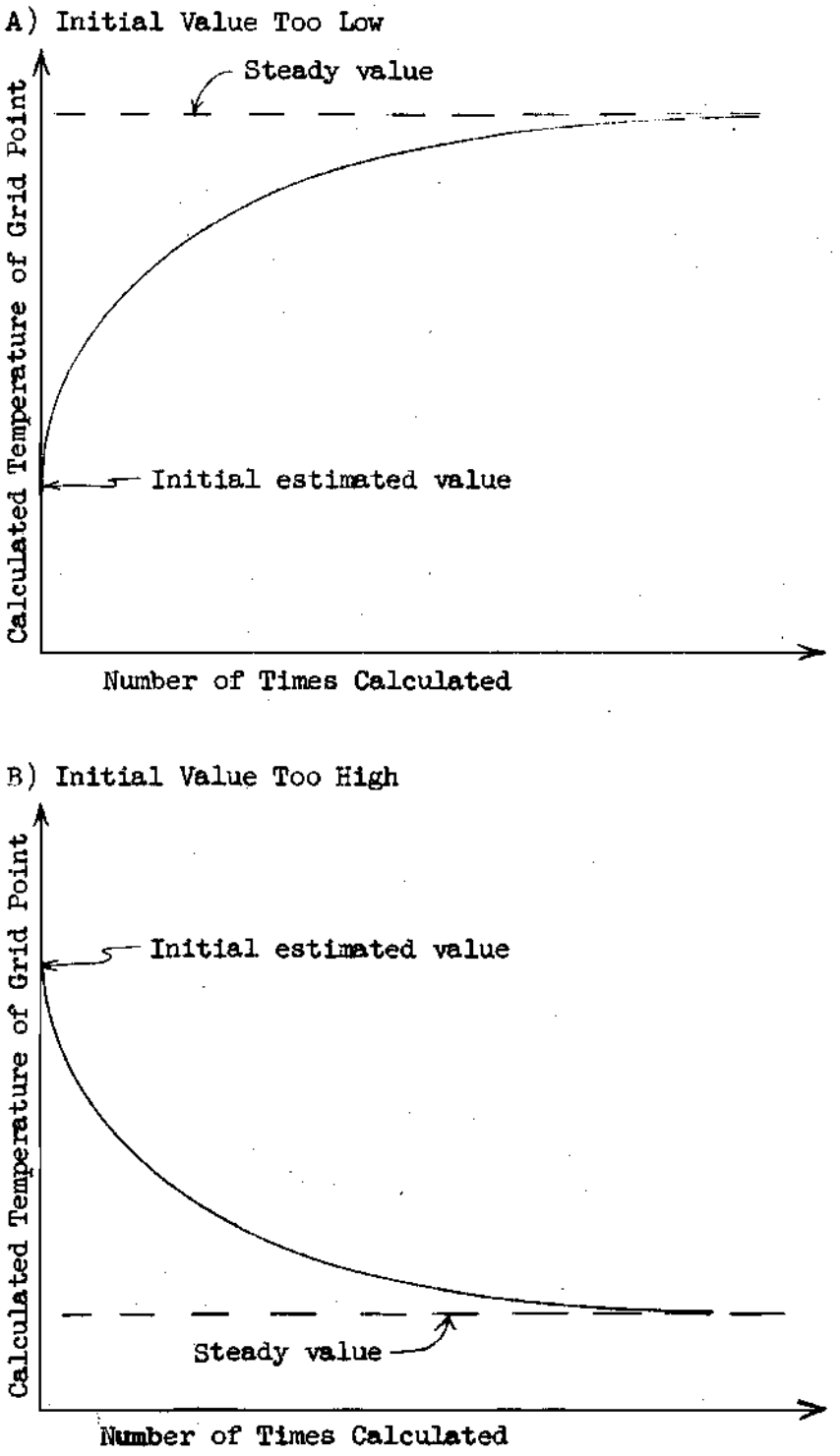

Figure 11. Typical Patterns of Grid Point Temperatures for Sequential Calculations

The values of the temperatures for these grid points are known since they are obtained as data. Therefore, the program does not calculate the temperature of those grid points but maintains them at their measured values in every temperature distribution. The boundary conditions on those three surfaces are thus defined by their temperature distributions alone.

The temperature distribution in which every grid point temperature has reached its steady value is, then, the two-dimensional conduction temperature distribution for the nozzle wall. This temperature distribution is not, however, the actual temperature distribution in the nozzle wall since only an estimate for the axial distribution of the inner surface heat transfer coefficient is used in its calculation. Therefore, the temperatures of the grid points near the inner surface which are obtained as data are compared with the calculated values for those grid points. For the regions where the measured values are higher than the calculated values the estimate of the heat transfer coefficient in that region is increased. It is decreased in the regions where the measured temperature values are lower than the calculated values of the grid point temperatures. The new estimate of the heat transfer coefficient distribution on the inner surface is then used in calculating a new two-dimensional conduction steady temperature distribution. The steady temperature distribution obtained with the previous estimate of the heat transfer coefficient distribution is used as the initial temperature distribution for this sequence of temperature distribution calculations.

The process of calculating a new two-dimensional conduction steady temperature distribution, comparing the calculated values of the grid point temperatures near the inner surface with the measured values for those grid points, altering the heat transfer coefficient distribution accordingly and recalculating the two-dimensional conduction steady temperature distribution is repeated until the calculated temperatures of the grid points near the inner surface match the measured values for those grid points. Once the measured and calculated temperatures of the grid points near the inner surface match, the two-dimensional conduction steady temperature distribution and the heat transfer coefficient distribution used to calculate it are the actual values provided both the measured temperatures and the calculated temperatures which were matched are sufficiently sensitive to slight changes in the heat transfer coefficient distribution.

The final step in reducing the data is to calculate the inner surface axial distribution of the heat flux, the axial distribution of the inner surface heat transfer and the total heat transferred to the nozzle wall. All of these values are directly calculated using a second computer program, which is also presented in Appendix E in the standard Algol language for the Burroughs 220 Data-Processing System. This program computes the axial distribution of the inner surface heat flux from the inner surface grid point temperature distribution, which is part of the final two-dimensional steady temperature distribution, using Equation 3 where the subscript i represents the value of n on the inner surface.

The program also calculates the inner surface convection area for

each grid point. Using these area values, it then calculates the axial distribution of the local heat transfer on the inner surface using:

$$q_{m,i} = q''_{m,i}(A_c) \tag{34}$$

where: $q_{m,i}$ = local inner surface grid point total heat transfer

$q''_{m,i}$ = local inner surface grid point heat flux

A_c = local inner surface grid point convection area

With the calculation of the axial distribution of the local heat flux on the nozzle wall inner surface, the desired results are obtained. The procedure for calculating these results for subsequent sets of data in a series of tests on the same nozzle is slightly different and shorter. First, a one dimensional estimate for the heat transfer coefficient distribution is not necessary. For the same nozzle with only a moderate difference in operating conditions, the heat transfer coefficient distribution calculated for the first set of data in the test series is a better estimate for the initial heat transfer coefficient distribution for the next set of data for that nozzle than a one-dimensional estimate. Second, the one-dimensional estimate for an initial nozzle wall grid point temperature distribution is not necessary. The final nozzle wall temperature distribution for the first set of data is a better estimate for the initial temperature distribution for the next set of data for the same nozzle than a one-dimensional estimate. The only change in that distribution necessary is that the outer surface and two end surface grid point temperatures are changed to the values for the new data

set to be analyzed. Other than these changes, the calculation procedure remains the same for each subsequent set of data in a series of tests on the same nozzle.

Accuracy of Data Reduction Technique

The accuracy of the data reduction technique primarily depends on the sensitivity of the grid point temperatures near the inner surface to variations in the heat transfer coefficient distribution and the size of the grid system chosen. The sensitivity of the temperatures of the grid points near the inner surface shown in Figure 10 is sufficient for less than a 2 per cent variation in the heat transfer coefficient distribution to cause a measurable change in those grid point temperatures for a copper nozzle with assumed operating conditions similar to those of the small diameter nozzle calorimetric method tests performed by the California Institute of Technology.[1,2,3,4]

The grid size effect on the accuracy of the data reduction technique is essentially eliminated if the grid size is chosen correctly. When the chosen grid size is small enough so that if a smaller grid size is used, the resulting heat transfer coefficient distribution is not altered more than one half of 1 per cent, the effect on the accuracy of the data reduction technique due to grid size choice is negligible in comparison with the error in the results due to the other factor. The accuracy of the data reduction technique itself is, therefore, within plus or minus 2 per cent. This does not include any error introduced by experimental measurement accuracy. The error due to the experimental measurement techniques is discussed in the next chapter with the presen-

tation of a typical nozzle and its associated equipment.

CHAPTER III

DEVELOPMENT OF EXPERIMENTAL APPARATUS AND MEASUREMENT TECHNIQUES

Apparatus

The design of the apparatus presented herein is for a specific nozzle having a particular range of operating conditions. The general features of the design are not, however, necessarily restricted to these conditions and can be used to design a similar apparatus for almost any size and shape nozzle with different ranges of operating conditions.

Nozzle

The specific axially symmetric nozzle shape and size are: (1) entrance diameter of three inches, (2) a throat diameter of one half inch, (3) an exit diameter of two inches, (4) an entrance convergence half angle of 30 degrees, (5) an exit divergence half angle of 15 degrees, (6) a constant wall thickness of one inch and (7) a wall throat region curvature of one fourth of an inch in radius. This nozzle shape, however, is altered to match the chosen grid system at the entrance end and exit end surfaces by the method described in Chapter II. The resulting nozzle shape is shown in Figure 1 and Figure 13.*

The range of nozzle operating conditions are: (1) one half to one atmosphere gas pressure at the nozzle entrance, (2) either argon or

---

* Figures 13 through 31 are in the Appendix.

nitrogen as the gas heated by a plasma arc, (3) gas temperatures up to approximately 10,000°K, (4) mass flow rates greater than 0.01 lbm/sec and (5) exit Mach numbers up to five. From the California Institute of Technology's tests on nozzles having similar operating conditions using the calorimetric method,[1,2,3,4] the total heat transferred to the nozzle wall is of the order of magnitude of 25,000 Btu/hr.

The nozzle material is pure copper. There are several reasons for this choice. First, accurate conductivity data is readily available for pure copper. Second, the maximum temperature levels reached in the nozzle wall are kept to approximately 250°F or less and therefore the thermocouple design problems are minimized. Third, the use of single wire thermocouples for surface temperatures is possible using constantan as one leg and the nozzle wall itself as the second leg. Also, construction is easier since silver soldering is possible where other materials such as steel would require welding.

The nozzle is to be operated for long durations so that it must be cooled on the outer and end surfaces. The coolant channels for the end surfaces are formed by two end caps. The entrance end cap, consisting of the two end plates shown in Figure 14, 15, 16, and 17, forms the coolant passage for the entrance end surface in which the coolant flows circumferentially around the nozzle end surface. The coolant enters the channel through a pipe and leaves through a second pipe located right next to the inlet pipe. A thin wall between the two pipes separates the inlet and outlet pipe openings in the channel and forces the flow into a circumferential pattern as shown in Figure 23. The nozzle entrance end surface forms the complete passage when the first end plate and nozzle

body are silver soldered together as shown in Figure 24. There is also a second coolant passage in the entrance end cap that is formed when the two plates of the end cap are assembled. This coolant passage is necessary since the entrance end cap forms part of the end of a plenum chamber preceding the nozzle section. The heat transferred to the end plate from the plenum chamber must be kept separate from the nozzle wall end surface coolant in order to maintain each section of the entire system a separate unit for energy balance purposes.

The exit end surface is cooled in the same manner as the entrance end surface. The exit end cap forming the exit end coolant passage is shown in Figures 18 and 19. The material for this end cap, as for the two components of the entrance end cap, is brass. The use of brass for these components adds strength to the entire unit and permits stronger connections for the fittings threaded into the caps. The exit end cap has a channel in it for sealant material to form a sealing ring when it is joined to the following constant diameter duct section. The lip in the entrance end cap fits into a similar sealant channel in the wall of the plentum chamber. Both of these sealant channels are shown in Figure 24.

The coolant channel along the outer surface is formed by a brass cover shown in Figure 20. This axial cover is formed by silver soldering the two sections of the cover together. When the cover is silver soldered in place, the height of the channel in the radial direction is only one tenth of an inch. This channel height is determined from the necessity of high Reynolds numbers for sufficient cooling. The inlet and outlet from this axial passage are through circumferential slots at

each end. The slots lead into collector rings as shown in Figures 21 and 24. These collector rings are used to prevent direct local impingement of coolant on the nozzle wall outer surface at the coolant pipe connections since the coolant pipes are connected on the sides of these collector rings. The inlet and outlet pipes connect to the collector rings at the points where the cover slots are blocked which further prevents direct local impingement as shown in Figure 27.

Thermocouples

There are two types of thermocouples used to measure the desired temperatures. First, the internal wall temperatures near the inner surface are measured with copper sheathed thermocouple elements such as shown in Figure 22. These elements are imbedded in holes in the wall, sealed and locked in place as shown in Figures 25 and 26. The location of these internal thermocouples are as shown in Figure 25 and Table 4 in Appendix C. The spacing of these thermocouples circumferentially about the nozzle axis provides that each thermocouple does not lie in the same axial plane with any other internal thermocouple. This feature, combined with the very small diameter of the thermocouple elements, minimizes the chance of one thermocouple affecting the reading of another because of heat pattern alteration due to the presence of the thermocouples in the wall.

The second type of thermocouple is that used to measure the entrance end surface, the exit end surface and the outer surface wall temperatures. As was previously mentioned, since the nozzle wall material is pure copper, the nozzle wall itself can be used as one leg of the surface thermocouples. The formation of these surface thermo-

couples, then, is by peening constantan wires to the surfaces at the desired locations for these thermocouples. Several copper lead wires are similarly attached to provide electrical connections of the second leg. The junctions are formed at the desired locations by accurately scribing circumferential lines on the surfaces at the desired locations and peening the wires on those lines. The positions of the scribed locating lines are shown in Figures 28, 29, 30 and 31 and Tables 2 and 3 in Appendix C.

The thermocouple wires, both the copper and constantan, are lacquered B and S gauge 33 single-strand thermocouple wires. They are led away from the junction points flush to the wall surface. The surface directly under the wires is coated first, then the wires are held to the surface by another coat of sealant. The wires go along the surface to the nearest thermocouple tube and pass out of the nozzle in the tube as shown in Figures 26 and 27. The advantage of this construction is the minimization of thermocouple junction area and coolant flow disturbance near the thermocouple junctions.

Both the internal and surface temperatures should be measured with a laboratory standard millivolt potentiometer such as a Leeds and Northrup (Cat. No. 8686). This type of accurate potentiometer is necessary since the accuracy of the temperatures is of primary importance. Only one such potentiometer is needed since the cooled nozzle operates under steady state conduction conditions and thus the temperatures do not have to be measured at the same time. Also, the cold or reference junction should be an ice bath sufficiently large to insure a constant temperature for the entire duration of each test run.

Coolant Facilities

The nozzle coolant passages are designed to provide sufficient cooling for long duration runs. The size of the passages were determined by considering water as the coolant and at least 25,000 Btu/hr would have to be removed by the water without local boiling within the passages. This value of heat removal was based on values from the California Institute of Technology calorimetric studies.[1,2,3,4] The convection heat transfer correlation equation for non-boiling turbulent flow through annuli by W. H. McAdams, et al[25] was used for the axial coolant passage calculations. The modified Sieder and Tate formula given by M. Jakob[26] for rectangular, curved passages was used for the end surface passage calculations. The results of these calculations indicated a water flow rate of about 50 gallons per minute in the axial passage and approximately four gallons per minute in each end passage are necessary for the range of nozzle operating conditions considered.

In Chapter II it was indicated that measurement of the coolant flow rates and temperature rises for each section of the entire system are necessary for determination of the free stream stagnation gas temperature. Coolant flow rates can be measured by any of the more accurate flow measurement devices available such as a calibrated flow nozzle. A particular type of system is not specified since the coolant flow rates of all the sections in the entire system will have to be measured and the overall flow measurement requirements might alter a decision based on the nozzle section alone. Also, the overall cost of the necessary devices has to be balanced with the accuracy obtained. An accuracy to within 1 per cent or less is necessary for a sufficiently accurate free stream

stagnation gas temperature determination.

The temperature rise of the coolant for each channel is determined by inserting a shielded thermocouple through the wall of each of the inlet and outlet pipes of the coolant passages as close to the connections between the pipes and the passages as possible. These thermocouples should be the same type as used for the internal temperature measurement in the nozzle wall. A typical installation is shown in Figure 27.

Construction Sequence

The sequence of construction of the nozzle section is determined by the design of its component parts. Because of the complexity of the design there is only one construction sequence possible. Only the general pattern of this sequence is presented in this section. The complete detailed sequence is presented in Appendix D. Before construction can be started the following are necessary: (1) all parts of the nozzle section are made to the specifications on the detailed drawings in Appendix C, (2) the thermocouple location lines have been scribed on the surfaces as specified in Appendix C, (3) all of the specified sealants, fittings and thermocouple wires have been obtained and (4) the thermocouple wires have been threaded into the appropriate tubes and checked for electrical short circuits.

The first step, once the above have been completed, is to assemble the exit end cap portion of the nozzle section. To assemble this portion the thermocouple tube for the exit end surface is screwed into the nozzle wall and tightened. The thermocouple wires are then bent along the wall end surface to form the pattern shown in Figure 29 and the wires are peened and sealed. The exit end cap divider grooves are lined with

sealant, the divider is put in place and the cap is silver soldered to the nozzle wall. The coolant passage pipe fittings are added and the thermocouple tube locking unit is put in place and locked.

The second step is to assemble the entrance and cap portion of the nozzle section. The thermocouple tube is again inserted first and the thermocouple wires are peened and sealed in the pattern shown in Figure 28. The first entrance end plate with its divider plate and sealant in place, is then soldered in place. The thermocouple tube is next sealed with the sealer disk and an O-ring. The thermocouple tube is then bent and the second entrance end plate with its divider plate and sealant is soldered in place. To complete the entrance end cap the coolant passage pipe fittings are added and the thermocouple tube locking unit is locked in place.

The third step is to assemble the axial coolant passage portion of the nozzle section. First the two thermocouple tubes are inserted and the surface thermocouples are peened in place. They are then sealed in the pattern shown in Figures 30 and 31. The two parts of the cover plate are then located and soldered together in place. Next, the collector rings are located and soldered together in place at each end of the axial cover. The internal thermocouples are then inserted into their holes and the tops of the holes are sealed at the nozzle wall surface. Next the coolant connectors are soldered to the collector rings. Once the internal thermocouple sealant has dried, the thermocouple locking units are added and tightened to complete the axial coolant passage portion of the nozzle section.

The final step in the construction of the nozzle section is to

insert all of the coolant water thermocouples into the coolant pipes and lock them in place. Once these thermocouples are in place, the nozzle section is complete. Only the calibration of the thermocouples is necessary before the nozzle section can be connected to the system in which it is to be used.

Calibration

Before the constructed nozzle is installed, the thermocouples are calibrated. The method of calibration is to submerge the entire nozzle section in a tank of water. The coolant passages are left open so that they are filled with water. The thermocouples are connected to terminals leading through the tank wall. A laboratory standard thermocouple is also inserted into the water and connected to wall terminals. The tank is then closed, sealed and pressurized to 80 p.s.i.a. The tank is then heated while the water is stirred to insure an isothermal condition. The temperatures are measured with the laboratory standard millivolt potentiometer. All the thermocouples are monitored in sequence until all of them reach a steady value. At that time all of the thermocouples are read and the values recorded along with the value from the standard thermocouple.

This process is repeated until at least 25 calibration points are obtained for the range of temperatures between 50°F and 300°F. Before the nozzle is removed from the tank, however, the calibration data are plotted for each of the thermocouples to insure that a sufficient number of points were obtained to permit smooth calibration curves to be drawn. If more calibration points are necessary, the extra data are obtained

in the same way as before and the nozzle is removed from the tank. Once the calibration curves are completed the nozzle is ready to be installed.

Installation

The installation of the nozzle into the system is relatively simple. The same type of sealant used on the divider plates is put into the sealant ring slot in the end of the plenum chamber wall. The nozzle section is then placed into position and bolted to the plenum chamber end. The sealant is also placed into the sealant slot in the exit end cap and the constant diameter duct following the nozzle section is bolted into place. Both of these connections are shown in Figure 24.

Before the coolant passage pipes are connected with the coolant pump system the passages are checked for leaks. The outlets of the coolant passages are closed with pipe plugs screwed into the outlet pipe connectors on the nozzle section. A tank of freon 12 is attached to one of the coolant passage inlets and the passage is pressurized. The entire nozzle section is then surveyed for leaks using an electronic halogen leak detector such as a General Electric Type H-7. If a leak is detected, the spot is marked and soldered or sealed, as the case may be, at the end of the leak testing procedure.

The pressurizing and checking is done to each of the coolant passages separately and then any leaks found are corrected. The outlet plugs are removed and the coolant inlet and outlet pipes are connected to the coolant supply and return system. Next, the thermocouples are connected to a switch which is directly connected to the millivolt potentiometer so that easy switching of the various thermocouple leads to

the potentiometer is possible. The last step in the installation procedure is to completely cover the nozzle section with a very thick layer of fiberglass insulation to insure against heat losses to the surroundings.

Operation

The operating procedure can only be specified generally since it is dependent on all of the equipment in the entire system besides that for the nozzle section. The first general step then is to start all of the coolant flows in the nozzle section and the other sections. The coolant should be started slowly at first to prevent the formation of air pockets in the coolant lines and passages. The coolant should be run until the temperature of the coolant as measured by the inlet and outlet thermocouples becomes steady before the gas flow is started. During this period any electronic measurement equipment that might be associated with other sections of the system should be turned on and allowed to warm up.

Since the nozzle inlet pressures will be between one half and one atmosphere, a vacuum system at the discharge end of the entire system will be necessary to achieve the desired pressure drops across the nozzle. Thus, the next step is to lower the pressure in the gas flow channel of the system, including the nozzle, to the necessary discharge pressure before the gas flow is started to insure shockless flow. Once the necessary vacuum is obtained and the gas is turned on producing shockless flow, the plasma torch for heating the gas is started.

When the torch is started, the internal thermocouples and the

coolant thermocouples are continuously checked to insure against overheating. If the temperature rise in the coolant flows begins to exceed about three degrees Fahrenheit, the coolant flows should be increased. They should also be increased if the internal thermocouples begin to exceed about 275°F. When all of the thermocouples indicate the temperatures have stabilized and thus steady state conduction conditions exist, the temperatures are recorded along with the flow rate measurement data. Data to be recorded at sections other than the nozzle should also be recorded at this time.

With all of the necessary data recorded the gas flow rate, torch or other operating conditions are altered for the next test run. The temperatures are again monitored until they are steady and the data are recorded. This is repeated for each set of desired conditions. When all of the various runs have been completed the torch is shut off first and then the gas flow. The coolant is left on until the nozzle internal temperatures return to the coolant temperature and then it is also shut off along with the recording equipment.

Accuracy and Cost

The effect on the accuracy of the results due to experimental error is dependent on several factors. First, the tolerances maintained during construction of the nozzle wall body, the scribing of the surface thermocouple location lines, the drilling of the internal thermocouple holes and the peening of the surface thermocouples to the outer surface on the location lines directly affect the accuracy of the results obtained. In order to obtain an estimate for the order of magnitude of

their effect, each of the variables were altered and their effect on the calculated internal temperatures for a test case based on data taken from the California Institute of Technology's calorimetric tests[1,2,3,4] was determined. From the effect on the calculated internal temperatures, the effect on the axial distribution of local heat flux was determined. For tolerances of plus or minus one thousandth of an inch for each of the variables, a possible cumulative error in the heat flux was plus or minus 1 per cent.

The second factor affecting the accuracy of the results is the accuracy of the thermal conductivity data for the nozzle wall material. For pure copper, in the range of temperatures of 50°F to 300°F, the linear approximation to the thermal conductivity versus temperature caused a far greater error than the error in the conductivity data itself. The two most widely different straight lines possible which represented the conductivity data were drawn and the equation for each one was determined. Using these two equations independently for the same test set of data as before, the maximum effect on the axial distribution of local heat flux was determined as plus or minus one half of 1 per cent.

The third factor affecting the results is the error in the measured temperatures. This error is the cumulative effect of the following: (1) the effect of a temperature gradient existing along the thermocouple wires, (2) surface thermocouple junctions not being exactly point contacts, (3) the internal thermocouples being only pressure contacted to the nozzle wall at the bottom of their holes and (4) the altering of the temperature pattern in the nozzle due to the presence of the thermocouples. The effect of a temperature gradient existing along

the thermocouples can be corrected by the methods presented by M. Jakob[29]. The net effect of the other influences, determined in the same manner as the previous factors, was determined to be approximately plus or minus 1 and 1/2 per cent on the axial distribution of local heat flux.

The final factor affecting the accuracy of the results is the error in determining the free stream stagnation gas temperature. The estimated error in the method of determining the free stream stagnation gas temperature using the energy balance technique presented in Chapter II is dependent on the accuracy of the coolant flow rate and temperature rise measurements and the assumptions of the technique. The California Institute of Technology's test indicates the error involved is approximately plus or minus 4 per cent for similar nozzle operating conditions.[1] By varying the free stream stagnation gas temperature by several values in the test data case, the effect of a plus or minus 4 per cent error in the free stream stagnation gas temperature was determined to be a plus or minus 4 per cent error in the distribution of the local heat flux. Combining this error cumulatively with all of the other experimental error yields a total approximate experimental error of plus or minus 7 per cent. However, if the coolant flow rates and coolant temperature rise measurements are made as accurately as possible, the error in the free stream stagnation gas temperature calculations should be approximately plus or minus 2 per cent or less. This improvement over the indicated error of the California Institute of Technology's tests is more than likely possible since fewer coolant channels are involved and thus fewer sources of error. The cumulative experimental error then is estimated as plus or minus 5 per cent.

The cost of the material, machining and construction of the nozzle section including the thermocouples is estimated at under five hundred dollars. This estimate does not include any of the measurement instruments since their cost depends on the make and model obtained and are common enough to be considered already on hand in a laboratory conducting tests of this nature.

CHAPTER IV

EFFECTS OF VARIATIONS OF ANALYTICAL AND EXPERIMENTAL PARAMETERS

Analytical Parameters

The analytical parameters considered are those parameters which are part of the data reduction technique itself rather than the experimental equipment. The two analytical parameters considered are the grid system and the form of the equation expressing the nozzle wall thermal conductivity as a function of temperature. If these parameters are altered from the size and forms presented in the previous chapters, changes in the equipment and computer programs are necessary.

Grid System

If the type and/or size of the grid system are changed from the type and size grid system presented in Figure 1, both the nozzle design and the computer program must be altered. Changing the type of grid system to a type other than that presented in Chapter II would require: (1) a completely new set of energy balances and temperature distribution equations, (2) entirely new computer programs for the new equations and (3) a new method of matching the nozzle design to the new grid system. In other words, the entire method would have to be altered.

Altering the size of the grid system from that shown in Figure 1 would require only a few minor changes. The first important effect is that the dimensions for the nozzle wall body length would have to be altered to have the end surfaces coincide with radial grid lines.

The procedure for this change was presented in Chapter II. Also, the amount of continuation of the nozzle wall inner surface contour on the end caps would have to be altered accordingly. At the same time the locations of the internal thermocouple holes and the axial cover holes would have to be changed to coincide with the altered positions of the internal grid points.

Changing the grid size also requires several changes in the computer programs. First, the values for the two grid point subscripts, m and n, must be revised to redefine the regions in which the temperature equations are valid. Second, the equations in the programs which are used to calculate the grid point radius matrix and the convection surface areas would have to be altered to correspond with the new grid size. Third, changing the grid size alters the number of data input and output values and thus the input and output program statements would have to be revised. Finally, changing the grid size affects both the accuracy of the results and the computer calculation run time. Increasing the grid size, a greater number of grid points, increases the computer run time and depending on the nozzle operating conditions might increase the accuracy of the results.

Conductivity Equations

As previously stated, the equation used to express the nozzle wall thermal conductivity as a function of temperature is a linear variation of conductivity with temperature. If the thermal conductivity variation is changed to be other than linear, then the conductivity equations in the computer program would have to be changed. All that is necessary to change those equations is the new conductivity versus temperature

equation must be integrated with respect to temperature with the temperatures of the two grid points as limits and the result divided by the difference of those two temperatures. This is the same procedure that was used for the linear conductivity variation as presented in Appendix A.

Experimental Parameters

The experimental parameters considered are those parameters which are altered if modifications are made to the experimental nozzle design presented in Chapter III. The two experimental parameters considered are the shape and material of the nozzle and the coolant system. If these parameters are altered from those used in the presented design then alterations are necessary in the equipment and the computer programs.

Nozzle Shape and Material

The two types of alterations to the nozzle shape which are considered are changing any or all of the nozzle dimensions and changing the nozzle from a constant wall thickness to one having a constant diameter outer surface. First, if any or all of the nozzle dimensions are changed, such as the convergence and divergence half angles or the entrance, throat or exit diameters or the wall thickness, the grid size would have to be altered. With a different grid size the programs would then also have to be altered as discussed under Analytical Parameters. Further, the internal thermocouple holes would have to be relocated and the design of the end caps and the axial cover altered. If the nozzle wall shape is changed to a constant diameter outer surface instead of a constant wall thickness while maintaining the same inner surface size and shape, the grid size does not have to be altered but the design of

the end caps and the axial cover do have to be changed. The second subscript, n, would then have to be referenced to the new outer surface shape which results in necessary changes in the programs. The radius matrix equations and the regions over which the temperature equations are valid would have to be altered.

Using a material other than pure copper for the nozzle wall body requires several design changes and the possibility of using other than a linear relationship for thermal conductivity as a function of temperature. If other than pure copper is used, the design of the surface thermocouples must be changed, since the nozzle wall itself could no longer be used as one leg of those thermocouples. Each surface thermocouple must be changed so that the junctions are formed from two thermocouple wires and that junction peened to the surface. Also, since a change in wall material would mean a lower thermal conductivity, the temperature levels in the wall would be higher and thus the type of thermocouple wires used would have to be changed to meet the higher temperature requirements. This would apply to both the internal and surface thermocouples.

Coolant System

The two parameters of the coolant system considered are the flow rate and the type of coolant used. Altering either would increase or decrease the heat transfer coefficient distribution on the outer surface. This, generally, only changes the level of all of the temperatures within the nozzle wall and therefore does not, to any great extent, alter the heat flux distribution on the inner surface.[30] Thus, changing either or both the flow rate or the type of coolant would only require possible alterations in the type of thermocouple material due to in-

creasing temperature levels. No other alterations would be required except, perhaps, to the coolant pumping system.

CHAPTER V

CONCLUSIONS AND RECOMMENDATIONS

A new experimental technique has been developed for the determination of the axial distribution of local heat flux on the inner surface of axially symmetric nozzles. In particular, the method developed considered steady state two-dimensional conduction in the nozzle wall. Further, an experimental nozzle has been designed to permit use of the method for a specific nozzle shape with a specified range of operating conditions. The conclusions regarding the method and the nozzle design are:

1. The field of experimental determination of local heat flux in rocket nozzles has been extended by the development of an experimental technique which provides a definite increase in the accuracy of the results by considering two-dimensional conduction conditions in the wall of the nozzle.

2. The estimated overall error in the axial distribution of the local heat flux for the experimental nozzle design as presented is plus or minus 7 per cent.

3. The estimated cost of the experimental nozzle design as presented is five hundred dollars, which is the same or less than the cost for similar nozzles used in previous techniques.

4. The amount of computer time necessary for each set of data is not prohibitive.

5. The method is adaptable to nozzles having shapes and sizes different from those of the experimental nozzle as presented since only minor changes in the computer programs are necessary.

The following items are recommended as a logical extension of the work which has been presented:

1. The two computer programs used in the calculations should be combined and prepared for use on a faster computer than the Burroughs 220 Data-Processing System. The Burroughs 5000 Data-Processing System or the I.B.M. 7090 System are suggested.

2. The computer program for the calculation of the nozzle wall two-dimensional temperature distribution should be altered so that the Gauss-Seidel method of successive displacements is used instead of the present Jacobi method of simultaneous displacements.[31] The changes necessary are minor and the net effect achieved is to reduce the computer calculation time by a factor of two.

3. An investigation should be made into the possibility of designing surface thermocouples in the range of 1/32 of an inch in diameter for measuring the nozzle wall inner surface temperature distribution. If measurement of the inner surface temperature distribution is possible, an increase in the sensitivity of the technique to the axial distribution of local heat fluxes would be obtained by using the inner surface temperatures as the comparison temperatures instead of the internal temperatures presently used.

4. An investigation should be made into the possibility of obtaining non-dimensionalized temperature profiles for general regions of the nozzle wall to aid in future predictions of nozzle wall two-

dimensional temperature distributions.

5. An investigation should be made to determine the possibility of using the finite difference technique for the case of transient two-dimensional conduction conditions in uncooled rocket nozzles.

A P P E N D I X

APPENDIX A

GRID POINT TEMPERATURE DISTRIBUTION EQUATION DERIVATIONS

In deriving each of the seven grid point temperature distribution equations, all of the significant approximations made in the finite difference technique are used. These approximations are as follows. (1) The heat is conducted between grid points only along the grid line segments connecting the grid points. (2) The conduction along each grid line is one-dimensional conduction in the direction of the grid line. (3) The volume element for the one-dimensional conduction along each grid line segment is the area surrounding the line segment length, extending half way to the next grid line on each side, times the circumference at that location. (4) The temperature gradient causing the conduction along a grid line between two grid points is taken as the difference in temperatures of the two grid points divided by the length of the grid line segment between those points. (5) The thermal conductivity for the element of material considered by each grid line segment is the integrated average conductivity.

For a linear relationship between the thermal conductivity and temperature, the integrated average becomes the arithmetic average. That is for:

$$k(t) = a + b \cdot t \tag{35}$$

and
$$\bar{k}_1 = \frac{\int_{t_{m,n}}^{t_{m+1,n-1}} k(t)dt}{(t_{m+1,n-1} - t_{m,n})} \tag{36}$$

then:
$$\bar{k}_1 = a + \frac{b}{2}(t_{m+1,n-1} - t_{m,n}) \tag{37}$$

where: $k(t)$ = linear relationship of thermal conductivity as a function of temperature

$\bar{k}_1$ = integrated average thermal conductivity for the conduction equation between two grid points, m,n and m+1, n-1

This average thermal conductivity is used for each conduction equation in the grid point temperature distribution equation derivations with the appropriate grid point temperatures.

A Typical Interior Grid Point for the Converging Section

The diagram for a typical interior grid point for the converging section is shown in Figure 3. The general steady state energy balance for this grid point is:

$$q\Big|_{m+1,n-1}^{m,n} + q\Big|_{m,n+1}^{m,n} - q\Big|_{m,n}^{m-1,n+1} - q\Big|_{m,n}^{m,n-1} = 0 \tag{38}$$

The one-dimensional conduction equations for each of these terms, therefore, are:

$$q\Big|_{m+1,n-1}^{m,n} = \frac{\bar{k}_1\pi\left[\left(r_{m,n} + \frac{\Delta r}{2}\right)^2 - \left(r_{m,n} - \frac{\Delta r}{2}\right)^2\right]}{(z_{m+1} - z_m)}(t_{m+1,n-1} - t_{m,n}) \tag{39}$$

$$q\Big|_{m,n}^{m-1,n+1} = \frac{\bar{k}_2\pi\left[\left(r_{m,n} + \frac{\Delta r}{2}\right)^2 - \left(r_{m,n} - \frac{\Delta r}{2}\right)^2\right]}{z_m - z_{m-1}}\left(t_{m,n} - t_{m-1,n+1}\right) \quad (40)$$

$$q\Big|_{m,n+1}^{m,n} = \frac{2\pi\bar{k}_3\left(\frac{z_{m+1} - z_m}{2} + \frac{z_m - z_{m-1}}{2}\right)\left(t_{m,n+1} - t_{m,n}\right)}{\ln(r_{m,n}) - \ln(r_{m,n} - \Delta r)} \quad (41)$$

$$q\Big|_{m,n}^{m,n-1} = \frac{2\pi\bar{k}_4\left(\frac{z_{m+1} - z_{m-1}}{2}\right)\left(t_{m,n} - t_{m,n-1}\right)}{\ln(r_{m,n} + \Delta r) - \ln(r_{m,n})} \quad (42)$$

Substituting these equations into the heat balance and simplifying yields:

$$\bar{k}_1\left(\frac{2r_{m,n}\Delta r}{z_{m+1} - z_m}\right)\left(t_{m+1,n-1} - t_{m,n}\right) - \bar{k}_2\left(\frac{2r_{m,n}\Delta r}{z_m - z_{m-1}}\right)\left(t_{m,n} - t_{m-1,n+1}\right)$$

$$+ \bar{k}_3\left(\frac{z_{m+1} - z_{m-1}}{\ln(r_{m,n}) - \ln(r_{m,n} - \Delta r)}\right)\left(t_{m,n+1} - t_{m,n}\right) \quad (4)$$

$$- \bar{k}_4\left(\frac{z_{m+1} - z_{m-1}}{\ln(r_{m,n} + \Delta r) - \ln(r_{m,n})}\right)\left(t_{m,n} - t_{m,n-1}\right) = 0$$

Solving this equation for the temperature of grid point m,n yields:

$$t_{m,n} = \frac{\bar{k}_1C_1t_{m+1,n-1} + \bar{k}_2C_2t_{m-1,n+1} + \bar{k}_3C_3t_{m,n+1} + \bar{k}_4C_4t_{m,n-1}}{\bar{k}_1C_1 + \bar{k}_2C_2 + \bar{k}_3C_3 + \bar{k}_4C_4} \quad (5)$$

where:

$$C_1 = \frac{2r_{m,n}\Delta r}{z_{m+1} - z_m} \tag{6}$$

$$C_2 = \frac{2r_{m,n}\Delta r}{z_m - z_{m-1}} \tag{7}$$

$$C_3 = \frac{z_{m+1} - z_{m-1}}{\ln(r_{m,n}) - \ln(r_{m,n} - \Delta r)} \tag{8}$$

$$C_4 = \frac{z_{m+1} - z_{m-1}}{\ln(r_{m,n} + \Delta r) - \ln(r_{m,n})} \tag{9}$$

$$\bar{k}_1 = a + \frac{b}{2}(t_{m+1,n-1} + t_{m,n}) \tag{43}$$

$$\bar{k}_2 = a + \frac{b}{2}(t_{m-1,n+1} + t_{m,n}) \tag{44}$$

$$\bar{k}_3 = a + \frac{b}{2}(t_{m,n+1} + t_{m,n}) \tag{45}$$

$$\bar{k}_4 = a + \frac{b}{2}(t_{m,n-1} + t_{m,n}) \tag{46}$$

A Typical Inner Surface Grid Point for the Convergent Section

The diagram for a typical inner surface grid point for the converging section is shown in Figure 4. The general steady state energy balance for this grid point is:

$$q_{conv.} + q\Big|_{m+1,n-1}^{m,n} - q\Big|_{m,n}^{m,n-1} = 0 \tag{47}$$

where:
$$q_{conv.} = h_m A_{cl}(T_{og} - t_{m,n}) \tag{48}$$

and A_{cl} is the convection area for this grid point, the lateral surface area of a right circular truncated cone:

$$A_{Cl} = \pi(2r_{m,n})\left[(\Delta r)^2 + \left(\frac{z_{m+1} - z_{m-1}}{2}\right)^2\right]^{\frac{1}{2}} \tag{49}$$

Each of the conduction terms must be modified since the element for each is only a partial element. The technique used to modify these conduction terms is to write the conduction equations assuming they are for complete elements and then multiply each term by the ratio of the partial element volume to the complete element volume. The complete element conduction terms are:

$$q\Big|_{m+1,n-1}^{m,n} = \frac{\pi\bar{k}_1\left[\left(r_{m,n} + \frac{\Delta r}{2}\right)^2 - \left(r_{mn} - \frac{\Delta r}{2}\right)^2\right]\left(t_{m+1,n-1} - t_{m,n}\right)}{(z_{m+1} - z_m)} \tag{50}$$

and

$$q\Big|_{m,n}^{m,n-1} = \frac{2\pi\bar{k}_4\left(\frac{z_{m+1} - z_{m-1}}{2}\right)\left(t_{m,n} - t_{m,n-1}\right)}{\ln(r_{m,n} + \Delta r) - \ln(r_{m,n})} \tag{51}$$

The modifying volume ratios for these terms are:

$$V\Big|_{m+1,n-1}^{m,n} = \frac{\pi\left[\left(r_{m,n} + \frac{\Delta r}{2}\right)^2 - \left(r_{m,n} - \frac{\Delta r}{2}\right)^2\right]\left(\frac{z_{m+1} - z_m}{2}\right)}{\pi\left[\left(r_{m,n} + \frac{\Delta r}{2}\right)^2 - \left(r_{m,n} - \frac{\Delta r}{2}\right)^2\right](z_{m+1} - z_m)}$$

$$+ \frac{\pi\left[\left(r_{m,n} + \frac{\Delta r}{2}\right)^2 - \left(r_{m,n}\right)^2\right]\left(\frac{z_{m+1} - z_m}{2}\right)}{\pi\left[\left(r_{m,n} + \frac{\Delta r}{2}\right)^2 - \left(r_{m,n} - \frac{\Delta r}{2}\right)^2\right](z_{m+1} - z_m)} \tag{52}$$

and

$$V\Big|_{m,n}^{m,n-1} = \frac{\pi\left[\left(r_{m,n} + \Delta r\right)^2 - \left(r_{m,n}\right)^2\right]\left(\frac{z_{m+1} - z_m}{2}\right)}{\pi\left[\left(r_{m,n} + \Delta r\right)^2 - \left(r_{m,n}\right)^2\right]\left(\frac{z_{m+1} - z_{m-1}}{2}\right)}$$

$$+ \frac{\pi\left[\left(r_{m,n} + \Delta r\right)^2 - \left(r_{m,n} + \frac{\Delta r}{2}\right)^2\right]\left(\frac{z_m - z_{m-1}}{2}\right)}{\pi\left[\left(r_{m,n} + \Delta r\right)^2 - \left(r_{m,n}\right)^2\right]\left(\frac{z_{m+1} - z_{m-1}}{2}\right)} \tag{53}$$

Combining these terms, simplifying and substituting into the energy balance yields:

$$0. = h_m(2r_{m,n})\sqrt{(\Delta r)^2 + \left(\frac{z_{m+1} - z_{m-1}}{2}\right)^2}\left(T_{og} - t_{m,n}\right)$$

$$+ \bar{k}_1 \frac{\frac{3}{2} r_{m,n}\Delta r + \frac{1}{8}(\Delta r)^2}{z_{m+1} - z_m}\left(t_{m+1,n-1} - t_{m,n}\right) \tag{10}$$

$$+ \bar{k}_4 \left[\frac{(z_{m+1} - z_m)(2r_{m,n} + \Delta r) + (z_m - z_{m-1})(r_{m,n} + \frac{3}{4}\Delta r)}{(2r_{m,n} + \Delta r)\left|\ln(r_{m,n} + \Delta r) - \ln(r_{m,n})\right|}\right]\left(t_{m,n-1} - t_{m,n}\right)$$

Solving this equation for the temperature of grid point m,n

yields:

$$t_{m,n} = \frac{h_m C_5 T_{og} + \bar{k}_1 C_6 T_{m+1,n-1} + \bar{k}_4 C_7 t_{m,n-1}}{h_m C_5 + \bar{k}_1 C_6 + \bar{k}_4 C_7} \tag{11}$$

where:

$$C_5 = (2r_{m,n})\left[(\Delta r)^2 + \left(\frac{z_{m+1} - z_{m-1}}{2}\right)^2\right]^{\frac{1}{2}} \tag{12}$$

$$C_6 = \left[\frac{\frac{3}{2} r_{m,n}\Delta r + \frac{1}{8}(\Delta r)^2}{z_{m+1} - z_m}\right] \tag{13}$$

$$C_7 = \left[\frac{(z_{m+1} - z_m)(2r_{m,n} + \Delta r) + (z_m - z_{m-1})(r_{m,n} + \frac{3}{4}\Delta r)}{(2r_{m,n} + \Delta r)\{\ln(r_{m,n} + \Delta r) - \ln(r_{m,n})\}}\right] \tag{14}$$

$\bar{k}_1$ and $\bar{k}_4$ are the same as before.

A Typical Interior Grid Point for the Nozzle Throat Grid Line

The diagram for a typical interior grid point for the nozzle throat grid line is shown in Figure 5. The general steady state energy balance for this grid point is:

$$-q\Big|_{m,n}^{m+1,n+1} + q\Big|_{m,n+1}^{m,n} - q\Big|_{m,n}^{m-1,n+1} - q\Big|_{m,n}^{m,n-1} = 0 \tag{54}$$

The one-dimensional conduction equations for each of these terms, therefore, are:

$$q\Big|_{m,n}^{m+1,n+1} = \frac{\pi \bar{k}_5\left[\left(r_{m,n} + \frac{\Delta r}{2}\right)^2 - \left(r_{m,n} - \frac{\Delta r}{2}\right)^2\right]}{(z_{m+1} - z_m)}(t_{m,n} - t_{m+1,n+1}) \quad (55)$$

$$q\Big|_{m,n}^{m-1,n+1} = \frac{\pi \bar{k}_2\left[\left(r_{m,n} + \frac{\Delta r}{2}\right)^2 - \left(r_{m,n} - \frac{\Delta r}{2}\right)^2\right]}{(z_m - z_{m-1})}(t_{m,n} - t_{m-1,n+1}) \quad (56)$$

$$q\Big|_{m,n+1}^{m,n} = \frac{2\pi\bar{k}_3\left(\frac{z_{m+1} - z_{m-1}}{2}\right)(t_{m,n+1} - t_{m,n})}{\ln(r_{m,n}) - \ln(r_{m,n} - \Delta r)} \quad (57)$$

$$q\Big|_{m,n}^{m,n-1} = \frac{2\pi\bar{k}_4\left(\frac{z_{m+1} - z_{m-1}}{2}\right)(t_{m,n} - t_{m,n-1})}{\ln(r_{m,n} + \Delta r) - \ln(r_{m,n})} \quad (58)$$

Substituting these equations into the heat balance and simplifying yields:

$$\bar{k}_5\left(\frac{2r_{m,n}\Delta r}{z_{m+1} - z_m}\right)(t_{m+1,n+1} - t_{m,n}) + \bar{k}_2\left(\frac{2r_{m,n}\Delta r}{z_m - z_{m-1}}\right)(t_{m-1,n+1} - t_{m,n})$$

$$+ \bar{k}_3\left(\frac{z_{m+1} - z_{m-1}}{\ln(r_{m,n}) - \ln(r_{m,n} - \Delta r)}\right)(t_{m,n+1} - t_{m,n}) \quad (15)$$

$$+ \bar{k}_4\left(\frac{z_{m+1} - z_{m-1}}{\ln(r_{m,n} + \Delta r) - \ln(r_{m,n})}\right)(t_{m,n-1} - t_{m,n}) = 0$$

Solving this equation for the temperature of grid point m,n yields:

$$t_{m,n} = \frac{\bar{k}_5 C_1 t_{m+1,n+1} + \bar{k}_2 C_2 t_{m-1,n+1} + \bar{k}_3 C_3 t_{m,n+1} + \bar{k}_4 C_4 t_{m,n-1}}{\bar{k}_5 C_1 + \bar{k}_2 C_2 + \bar{k}_3 C_3 + \bar{k}_4 C_4} \quad (16)$$

where: C_1, C_2, C_3, C_4, $\bar{k}_2$, $\bar{k}_3$ and $\bar{k}_4$ are as before and:

$$\bar{k}_5 = a + \frac{b}{2}(t_{m+1,n+1} + t_{m,n}) \quad (59)$$

The First Grid Point Inside the Inner Surface on the Nozzle Throat Radial Grid Line

The diagram for the first grid point inside the inner surface on the nozzle throat radial grid line is shown in Figure 6. The general steady state energy equation for this grid point is:

$$q\Big|_{m,n+1}^{m,n} - q\Big|_{m,n}^{m-1,n+1} - q\Big|_{m,n}^{m+1,n+1} - q\Big|_{m,n}^{m,n-1} = 0 \quad (60)$$

The first three terms must be modified using the volume ratio technique, as used for surface elements, since they are for partial elements. The last conduction term does not have to be modified since it is for a complete element. The complete element conduction terms, then, are:

$$q\Big|_{m,n+1}^{m,n} = \frac{2\pi\bar{k}_3\left(\frac{z_{m+1} - z_{m-1}}{2}\right)(t_{m,n+1} - t_{m,n})}{\ln(r_{m,n}) - \ln(r_{m,n} - \Delta r)} \quad (61)$$

$$q\Big|_{m,n}^{m-1,n+1} = \frac{\pi\bar{k}_2\left[\left(r_{m,n}+\frac{\Delta r}{2}\right)^2 - \left(r_{m,n}-L_2\right)^2\right]}{(z_m - z_{m-1})}\left(t_{m,n} - t_{m-1,n+1}\right) \quad (62)$$

$$q\Big|_{m,n}^{m+1,n+1} = \frac{\pi\bar{k}_5\left[\left(r_{m,n}+\frac{\Delta r}{2}\right)^2 - \left(r_{m,n}-L_2\right)^2\right]}{(z_{m+1} - z_{m-1})}\left(t_{m,n} - t_{m+1,n+1}\right) \quad (63)$$

$$q\Big|_{m,n}^{m,n-1} = \frac{2\pi\bar{k}_4\left(\frac{z_{m+1} - z_{m-1}}{2}\right)\left(t_{m,n} - t_{m,n-1}\right)}{\ln(r_{m,n} + \Delta r) - \ln(r_{m,n})} \quad (64)$$

The modifying volume ratios for the first three terms are:

$$V\Big|_{m,n+1}^{m,n} = \frac{(z_m - z_{m-1})\left[(\Delta r + L_1)\left(r_{m,n} - \frac{\Delta r}{4} - \frac{L_1}{4}\right) - \frac{1}{12}(\Delta r - L_1)^2\right]}{(z_{m+1} - z_{m-1})(2r_{m,n}\Delta r - \Delta r^2)}$$

$$+ \frac{(z_{m+1} - z_m)\left[(\Delta r + L_2)\left(r_{m,n} - \frac{\Delta r}{4} - \frac{L_2}{4}\right) - \frac{1}{12}(\Delta r - L_2)^2\right]}{(z_{m+1} - z_{m-1})(2r_{m,n}\Delta r - \Delta r^2)} \quad (65)$$

$$V\Big|_{m,n}^{m+1,n+1} = \frac{\pi\left(\frac{z_{m+1} - z_m}{2}\right)\left[\left(r_{m,n} + \frac{\Delta r}{2}\right)^2 - \left(r_{m,n} - L_2\right)^2\right]}{\pi(z_{m+1} - z_m)\left[\left(r_{m,n} + \frac{\Delta r}{2}\right)^2 - \left(r_{m,n} - L_2\right)^2\right]}$$

$$+ \frac{\pi\left(\frac{z_{m+1} - z_m}{2}\right)\left[\left(r_{m,n} + \frac{\Delta r}{2}\right)^2 - \frac{1}{4}\left\{\left(2r_{m,n} - L_2\right)^2 + \frac{1}{3}(L_2)^2\right\}\right]}{\pi(z_{m+1} - z_m)\left[\left(r_{m,n} + \frac{\Delta r}{2}\right)^2 - \left(r_{m,n} - L_2\right)^2\right]} \quad (66)$$

$$V\Big|_{m,n}^{m-1,n+1} = \frac{\pi\left(\frac{z_m - z_{m-1}}{2}\right)\left[\left(r_{m,n} + \frac{\Delta r}{2}\right)^2 - \left(r_{m,n} - L_2\right)^2\right]}{\pi(z_m - z_{m-1})\left[\left(r_{m,n} + \frac{\Delta r}{2}\right)^2 - \left(r_{m,n} - L_2\right)^2\right]} \quad (67)$$

$$+\frac{\pi\left(\frac{z_m - z_{m-1}}{2}\right)\left[\left(r_{m,n} + \frac{\Delta r}{2}\right)^2 - \frac{1}{4}\left\{\left(2r_{m,n} - L_2\right)^2 + \frac{1}{3}\left(L_2\right)^2\right\}\right]}{\pi\left(z_m - z_{m-1}\right)\left[\left(r_{m,n} + \frac{\Delta r}{2}\right)^2 - \left(r_{m,n} - L_2\right)^2\right]} \quad (67)$$

Combining these terms, simplifying and substituting into the energy balance yields:

$$\left[\frac{\bar{k}_3\left(z_m - z_{m-1}\right)\left[\left(\Delta r + L_1\right)\left(r_{m,n} - \frac{\Delta r}{4} - \frac{L_1}{4}\right) - \frac{1}{12}\left(\Delta r - L_1\right)^2\right]}{\left\{\ln\left(r_{m,n}\right) - \ln\left(r_{m,n} - \Delta r\right)\right\}\left\{2r_{m,n}\Delta r - (\Delta r)^2\right\}}\right. \quad (17)$$

$$\left. + \frac{\bar{k}_3\left(z_{m+1} - z_m\right)\left[\left(\Delta r + L_1\right)\left(r_{m,n} - \frac{\Delta r}{4} - \frac{L_2}{4}\right) - \frac{1}{12}\left(\Delta r - L_2\right)^2\right]}{\left\{\ln\left(r_{m,n}\right) - \ln\left(r_{m,n} - \Delta r\right)\right\}\left\{2r_{m,n}\Delta r - (\Delta r)^2\right\}}\right]\left(t_{m,n+1} - t_{m,n}\right)$$

$$+ \frac{\bar{k}_4\left(z_{m+1} - z_{m-1}\right)}{\ln\left(r_{m,n} + \Delta r\right) - \ln\left(r_{m,n}\right)}\left(t_{m,n-1} - t_{m,n}\right)$$

$$+ \frac{\bar{k}_5\left(r_{m,n}\Delta r + \frac{(\Delta r)^2}{4} + \frac{3}{2}r_{m,n}L_2 - \frac{2}{3}\left(L_2\right)^2\right)}{\left(z_{m+1} - z_{m-1}\right)}\left(t_{m+1,n+1} - t_{m,n}\right)$$

$$+ \frac{\bar{k}_2\left(r_{m,n}\Delta r + \frac{(\Delta r)^2}{4} + \frac{3}{2}r_{m,n}L_2 - \frac{2}{3}\left(L_2\right)^2\right)}{\left(z_m - z_{m-1}\right)}\left(t_{m-1,n+1} - t_{m,n}\right) = 0$$

Solving this equation for the temperature of grid point m,n yields:

$$t_{m,n} = \frac{\bar{k}_3 C_{12} t_{m,n+1} + \bar{k}_4 C_{13} t_{m,n-1} + \bar{k}_5 C_{14} t_{m+1,n+1} + \bar{k}_2 C_{15} t_{m-1,n+1}}{\bar{k}_3 C_{12} + \bar{k}_4 C_{13} + \bar{k}_5 C_{14} + \bar{k}_2 C_{15}} \quad (18)$$

where $\bar{k}_2$, $\bar{k}_3$, $\bar{k}_4$ and $\bar{k}_5$ are as before, and

$$C_{12} = \frac{(z_m - z_{m-1})\left[(\Delta r + L_1)\left(r_{m,n} - \frac{\Delta r}{4} - \frac{L_1}{4}\right) - \frac{1}{12}(\Delta r - L_1)^2\right]}{(2r_{m,n}\Delta r - (\Delta r)^2)\left[\ln(r_{m,n}) - \ln(r_{m,n} - \Delta r)\right]} \tag{19}$$

$$+ \frac{(z_{m+1} - z_m)\left[(\Delta r + L_2)\left(r_{m,n} - \frac{\Delta r}{4} - \frac{L_2}{4}\right) - \frac{1}{12}(\Delta r - L_2)^2\right]}{(2r_{m,n}\Delta r - (\Delta r)^2)\left[\ln(r_{m,n}) - \ln(r_{m,n} - \Delta r)\right]}$$

$$C_{13} = \frac{(z_{m+1} - z_{m-1})}{\left[\ln(r_{m,n} + \Delta r) - \ln(r_{m,n})\right]} \tag{20}$$

$$C_{14} = \frac{\left(r_{m,n}\Delta r + \frac{(\Delta r)^2}{4} + \frac{3}{2} r\ L_2 - \frac{2}{3}(L_2)^2\right)}{(z_{m+1} - z_{m-1})} \tag{21}$$

$$C_{15} = \frac{\left(r_{m,n}\Delta r + \frac{(\Delta r)^2}{4} + \frac{3}{2} r_{m,n} L_2 - \frac{2}{3}(L_2)^2\right)}{(z_m - z_{m-1})} \tag{22}$$

The Inner Surface Grid Point on the Nozzle Throat Radial Grid Line

The diagram for the inner surface grid point on the nozzle throat radial grid line is shown in Figure 7. The general steady state energy balance for this grid point is:

$$q_{conv} - q\Big|_{m,n}^{m,n-1} = 0 \tag{68}$$

where $$q_{conv} = h_m A_{c2}(T_{og} - t_{m,n}) \tag{69}$$

and A_{c2} is the convection area for this grid point, the lateral surface area of two right circular truncated cones:

$$A_{c2} = \pi\left(2r_{m,n} + \Delta r - L_1\right)\left[(\Delta r - L_1)^2 + \left(\frac{z_m - z_{m-1}}{2}\right)^2\right]^{\frac{1}{2}} \tag{70}$$

$$+ \pi\left(2r_{m,n} + \Delta r - L_2\right)\left[(\Delta r - L_2)^2 + \left(\frac{z_{m+1} - z_m}{2}\right)^2\right]^{\frac{1}{2}}$$

Again, the volume ratio technique is used to modify the conduction term since the element considered is only a partial element. The complete element conduction term is:

$$q\Big|_{m,n}^{m,n-1} = \frac{2\pi\bar{k}_4\left(\frac{z_{m+1} - z_{m-1}}{2}\right)\left(t_{m,n} - t_{m,n-1}\right)}{\ln\left(r_{m,n} + \Delta r\right) - \ln\left(r_{m,n}\right)} \tag{71}$$

The modifying volume ratio is:

$$V\Big|_{m,n}^{m,n-1} = \frac{\pi\left(\frac{z_m - z_{m-1}}{2}\right)\left\{\left(r_{m,n}+\Delta r\right)^2 - \frac{1}{4}\left[\left(2r_{m,n}+\Delta r-L_1\right)^2 + \frac{1}{3}\left(\Delta r-L_1\right)^2\right]\right\}}{\pi\left(\frac{z_{m+1} - z_{m-1}}{2}\right)\left[\left(r_{m,n} + \Delta r\right)^2 - \left(r_{m,n}\right)^2\right]} \tag{72}$$

$$+ \frac{\pi\left(\frac{z_{m+1} - z_m}{2}\right)\left\{\left(r_{m,n}+\Delta r\right)^2 - \frac{1}{4}\left[\left(2r_{m,n}+\Delta r-L_2\right)^2 + \frac{1}{3}\left(\Delta r-L_2\right)^2\right]\right\}}{\pi\left(\frac{z_{m+1} - z_{m-1}}{2}\right)\left[\left(r_{m,n} + \Delta r\right)^2 - \left(r_{m,n}\right)^2\right]}$$

Combining these terms, simplifying and substituting into the energy

balance yields:

$$\left[h_m \{(2r_{m,n} + \Delta r - L_1)\left[(\Delta r - L_1)^2 + \left(\frac{z_m - z_{m-1}}{2}\right)^2\right]^{\frac{1}{2}}\right. \tag{23}$$

$$+ h_m\{(2r_{m,n} + \Delta r - L_2)\left[(\Delta r - L_2)^2 + \left(\frac{z_{m+1} - z_m}{2}\right)^2\right]^{\frac{1}{2}}\}\left](T_{og} - t_{m,n})\right.$$

$$\left[\bar{k}_4 \{ \frac{(z_m - z_{m-1})\left[r_{mn}(\Delta r + L_1) + (\Delta r)^2 - \frac{1}{3}(\Delta r - L_1)^2\right]}{(2r_{mn}\Delta r + \Delta r^2)\left[\ln(r_{mn} + \Delta r) - \ln(r_{mn})\right]}\right.$$

$$\left. + k_4\{\frac{(z_{m+1} - z_m)\left[r_{m,n}(\Delta r + L_2) + (\Delta r)^2 - \frac{1}{3}(\Delta r - L_2)^2\right]}{(2r_{m,n}\Delta r + (\Delta r)^2)\left[\ln(r_{m,n} + \Delta r) - \ln(r_{m,n})\right]}\}\right](t_{m,n} - t_{m,n-1}) = 0$$

Solving this equation for the temperature of the grid point m,n yields:

$$t_{m,n} = \frac{h_m C_{10} T_{og} + \bar{k}_4 C_{11} t_{m,n-1}}{h_m C_{10} + \bar{k}_4 C_{11}} \tag{24}$$

where $\bar{k}_4$ is the same as before and

$$C_{10} = (2r_{m,n} + \Delta r - L_1)\left[(\Delta r - L_1)^2 + \frac{1}{4}(z_m - z_{m-1})^2\right]^{\frac{1}{2}} \tag{25}$$

$$+ (2r_{m,n} + \Delta r - L_2)\left[(\Delta r - L_2)^2 + \frac{1}{4}(z_{m+1} - z_m)^2\right]^{\frac{1}{2}}$$

$$C_{11} = \frac{(z_m - z_{m-1})\left[r_{m,n}(\Delta r + L_1) + (\Delta r)^2 - \frac{1}{3}(\Delta r - L_1)^2\right]}{(2r_{m,n}\Delta r + (\Delta r)^2)\left[\ln(r_{m,n} + \Delta r) - \ln(r_{m,n})\right]} \tag{26}$$

$$+ \frac{(z_{m+1} - z_m)\left[r_{m,n}(\Delta r + L_2) + \Delta r^2 - \frac{1}{3}(\Delta r - L_2)^2\right]}{(2r_{m,n}\Delta r + (\Delta r)^2)\left[\ln(r_{m,n} + \Delta r) - \ln(r_{m,n})\right]}$$

A Typical Interior Grid Point for the Diverging Section

The diagram for a typical interior grid point for the diverging section is shown in Figure 8. The general steady state energy balance for this grid point is:

$$- q\Big|_{m,n}^{m+1,n+1} + q\Big|_{m,n+1}^{m,n} + q\Big|_{m-1,n-1}^{m,n} - q\Big|_{m,n}^{m,n-1} = 0 \tag{73}$$

The one-dimensional conduction equations for each of these terms, therefore, are:

$$q\Big|_{m,n}^{m+1,n+1} = \frac{\pi\bar{k}_5\left[(r_{m,n} + \frac{\Delta r}{2})^2 - (r_{m,n} - \frac{\Delta r}{2})^2\right]}{(z_{m+1} - z_m)}(t_{m,n} - t_{m+1,n+1}) \tag{74}$$

$$q\Big|_{m,n+1}^{m,n} = \frac{2\pi\bar{k}_3\left[\frac{z_{m+1} - z_{m-1}}{2}\right]}{\ln(r_{m,n}) - \ln(r_{m,n} - \Delta r)}(t_{m,n+1} - t_{m,n}) \tag{75}$$

$$q\Big|_{m-1,n-1}^{m,n} = \frac{\pi\bar{k}_6\left[(r_{m,n} + \frac{\Delta r}{2})^2 - (r_{m,n} - \frac{\Delta r}{2})^2\right]}{(z_m - z_{m-1})}(t_{m-1,n-1} - t_{m,n}) \tag{76}$$

$$q\Big|_{m,n}^{m,n-1} = \frac{2\pi k_4\left[\frac{z_{m+1} - z_{m-1}}{z}\right]}{\ln(r_{m,n} + \Delta r) - \ln(r_{m,n})} \quad (t_{m,n} - t_{m,n-1}) \qquad (77)$$

Substituting these equations into the heat balance and simplifying yields:

$$\bar{k}_5\left(\frac{2r_{m,n}\Delta r}{z_{m+1} - z_m}\right)(t_{m+1,n+1} - t_{m,n}) + \bar{k}_6\left(\frac{2r_{m,n}\Delta r}{z_m - z_{m-1}}\right)(t_{m-1,n-1} - t_{m,n})$$

$$+ \bar{k}_3\left(\frac{z_{m+1} - z_{m-1}}{\ln(r_{m,n}) - \ln(r_{m,n} - \Delta r)}\right)(t_{m,n+1} - t_{m,n}) \qquad (27)$$

$$+ \bar{k}_4\left(\frac{z_{m+1} - z_{m-1}}{\ln(r_{m,n} + \Delta r) - \ln(r_{m,n})}\right)(t_{m,n-1} - t_{m,n}) = 0$$

Solving this equation for the temperature of grid point m,n yields:

$$t_{m,n} = \frac{\bar{k}_5 C_1 t_{m+1,n+1} + \bar{k}_6 C_2 t_{m-1,n-1}}{\bar{k}_5 C_1 + \bar{k}_6 C_2 + \bar{k}_3 C_3 + \bar{k}_4 C_4}$$

$$+ \frac{\bar{k}_3 C_3 t_{m,n+1} + \bar{k}_4 C_4 t_{m,n-1}}{\bar{k}_5 C_1 + \bar{k}_6 C_2 + \bar{k}_3 C_3 + \bar{k}_4 C_4} \qquad (28)$$

where C_1, C_2, C_3, C_4, $\bar{k}_3$, $\bar{k}_4$ and $\bar{k}_5$ are the same as before and

$$\bar{k}_6 = a + \frac{b}{2}\left(t_{m-1,n-1} - t_{m,n}\right) \tag{78}$$

A Typical Inner Surface Grid Point for the Diverging Section

The diagram for a typical inner surface grid point for the diverging section is shown in Figure 9. The general steady state energy balance for this grid point is:

$$q_{conv} + q\Big|_{m-1,n-1}^{m,n} - q\Big|_{m,n}^{m,n-1} = 0 \tag{79}$$

where:

$$q_{conv} = h_m A_{c3}\left(T_{og} - t_{m,n}\right) \tag{80}$$

and A_{c3} is the convection area for this grid point, the lateral surface area of a right circular truncated cone:

$$A_{c3} = \pi\left(2r_{m,n}\right)\left[(\Delta r)^2 + \left(\frac{z_{m+1} - z_{m-1}}{2}\right)^2\right]^{\frac{1}{2}} \tag{81}$$

As for the previous surface grid point equations the partial element conduction terms are obtained by multiplying the complete element conduction terms by the ratio of the partial element volume to the complete element volume. The complete element conduction terms, then, are:

$$q\Big|_{m-1,n-1}^{m,n} = \frac{\pi\bar{k}_6\left[\left(r_{m,n} + \frac{\Delta r}{2}\right)^2 - \left(r_{m,n} - \frac{\Delta r}{2}\right)^2\right]}{\left(z_m - z_{m-1}\right)}\left(t_{m-1,n-1} - t_{m,n}\right) \tag{82}$$

$$q\Big|_{m,n}^{m,n-1} = \frac{2\pi\bar{k}_4\left(\frac{z_{m+1} - z_{m-1}}{2}\right)}{\ln(r_{m,n} + \Delta r) - \ln(r_{m,n})}\left(t_{m,n} - t_{m,n-1}\right) \qquad (83)$$

The volume ratios for these terms are:

$$V\Big|_{m-1,n-1}^{m,n} = \frac{\pi\left[\left(r_{m,n} + \frac{\Delta r}{2}\right)^2 - \left(r_{m,n} - \frac{\Delta r}{2}\right)^2\right]\left(\frac{z_m - z_{m-1}}{2}\right)}{\pi\left[\left(r_{m,n} + \frac{\Delta r}{2}\right)^2 - \left(r_{m,n} - \frac{\Delta r}{2}\right)^2\right]\left(z_m - z_{m-1}\right)} \qquad (84)$$

$$+ \frac{\pi\left[\left(r_{m,n} + \frac{\Delta r}{2}\right)^2 - \left(r_{m,n}\right)^2\right]\left(\frac{z_m - z_{m-1}}{2}\right)}{\pi\left[\left(r_{m,n} + \frac{\Delta r}{2}\right)^2 - \left(r_{m,n} - \frac{\Delta r}{2}\right)^2\right]\left(z_m - z_{m-1}\right)}$$

$$V\Big|_{m,n}^{m,n-1} = \frac{\pi\left[\left(r_{m,n} + \Delta r\right)^2 - \left(r_{m,n}\right)^2\right]\left(\frac{z_m - z_{m-1}}{2}\right)}{\pi\left[\left(r_{m,n} + \Delta r\right)^2 - \left(r_{m,n}\right)^2\right]\left(\frac{z_{m+1} - z_{m-1}}{2}\right)} \qquad (85)$$

$$+ \frac{\pi\left[\left(r_{m,n} + \Delta r\right)^2 - \left(r_{m,n} + \frac{\Delta r}{2}\right)^2\right]\left(\frac{z_{m+1} - z_m}{2}\right)}{\pi\left[\left(r_{m,n} + \Delta r\right) - \left(r_{m,n}\right)^2\right]\left(\frac{z_{m+1} - z_{m-1}}{2}\right)}$$

Combining these terms, simplifying and substituting into the energy balance yields:

$$0 = h_m\left(2r_{m,n}\right)\left[(\Delta r)^2 + \left(\frac{z_{m+1} - z_{m-1}}{2}\right)^2\right]^{\frac{1}{2}}\left(T_{og} - t_{m,n}\right) \qquad (29)$$

$$+ \bar{k}_6\left(\frac{\frac{3}{2}r_{m,n}\Delta r + \frac{1}{8}(\Delta r)^2}{z_m - z_{m-1}}\right)\left(t_{m-1,n-1} - t_{m,n}\right)$$

$$+ \bar{k}_4 \left| \frac{(z_m - z_{m-1})(2r_{m,n} + \Delta r) + (z_{m+1} - z_m)(r_{m,n} + \frac{3}{4}\Delta r)}{(2r_{m,n} + \Delta r)\{\ln(r_{m,n} + \Delta r) - \ln(r_{m,n})\}} \right| (t_{m,n-1} - t_{m,n})$$

Solving this energy equation for the temperature of grid point m,n yields:

$$t_{m,n} = \frac{h_m C_5 T_{og} + \bar{k}_6 C_8 t_{m-1,n-1} + \bar{k}_4 C_9 t_{m,n-1}}{h_m C_5 + \bar{k}_6 C_8 + \bar{k}_4 C_9} \tag{30}$$

where C_5, $\bar{k}_4$ and $\bar{k}_6$ are as before and:

$$C_8 = \left(\frac{\frac{3}{2} r_{m,n} \Delta r + \frac{1}{8}(\Delta r)^2}{z_m - z_{m-1}} \right) \tag{31}$$

$$C_9 = \left| \frac{(z_m - z_{m-1})(2r_{m,n} + \Delta r) + (z_{m+1} - z_m)(r_{m,n} + \frac{3}{4}\Delta r)}{(2r_{m,n} + \Delta r)\{\ln(r_{m,n} + \Delta r) - \ln(r_{m,n})\}} \right| \tag{32}$$

APPENDIX B

GAS TEMPERATURE DETERMINATION TECHNIQUE

A general steady state energy balance for the system shown in Figure 12 between section 1 and section 2 is:

$$\dot{m}\left(H_1 + \frac{(V_1)^2}{g_o J}\right) + E_{in} - Q_a - Q_b = \dot{m}\left(H_{o2}\right) \tag{86}$$

where $\dot{m}$, E_{in}, Q_a and Q_b are measured. H_1 is determined from T_1 and P_1 measurements and enthalpy tables for the particular gas chosen. V_1 is determined from:

$$\dot{m} = \rho_1 A_{x1} V_1 \tag{87}$$

where ρ_1 is also obtained from property tables for the gas and T_1 and P_1. H_{o2} is directly calculated from Equation 86 once V_1 is obtained. T_{og}, the free stream stagnation gas temperature is then obtained from the enthalpy tables using P_2 and H_{o2}.

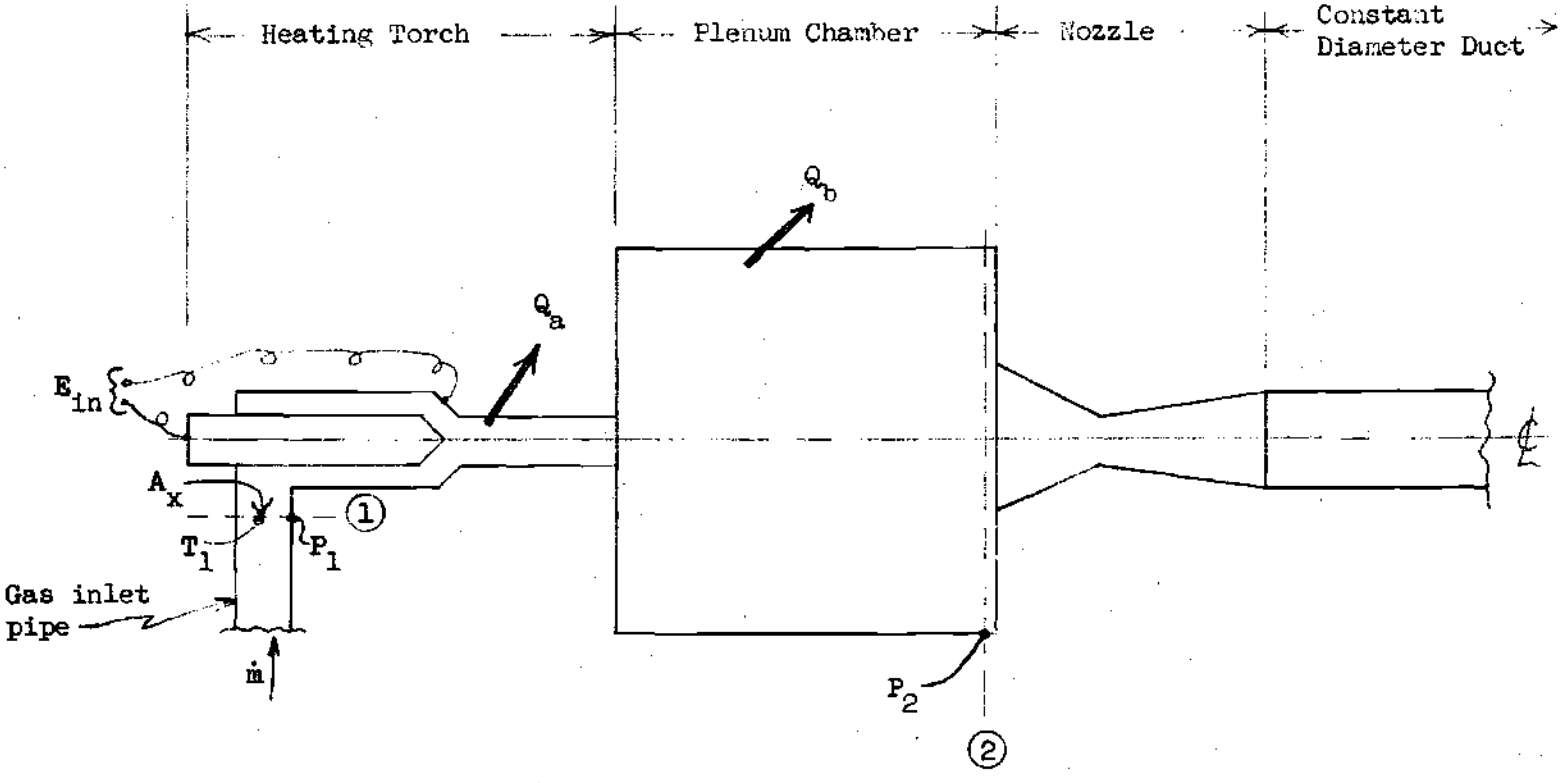

Figure 12. Diagram of Typical Plasma Gas Flow Study System

APPENDIX C

NOZZLE DESIGN

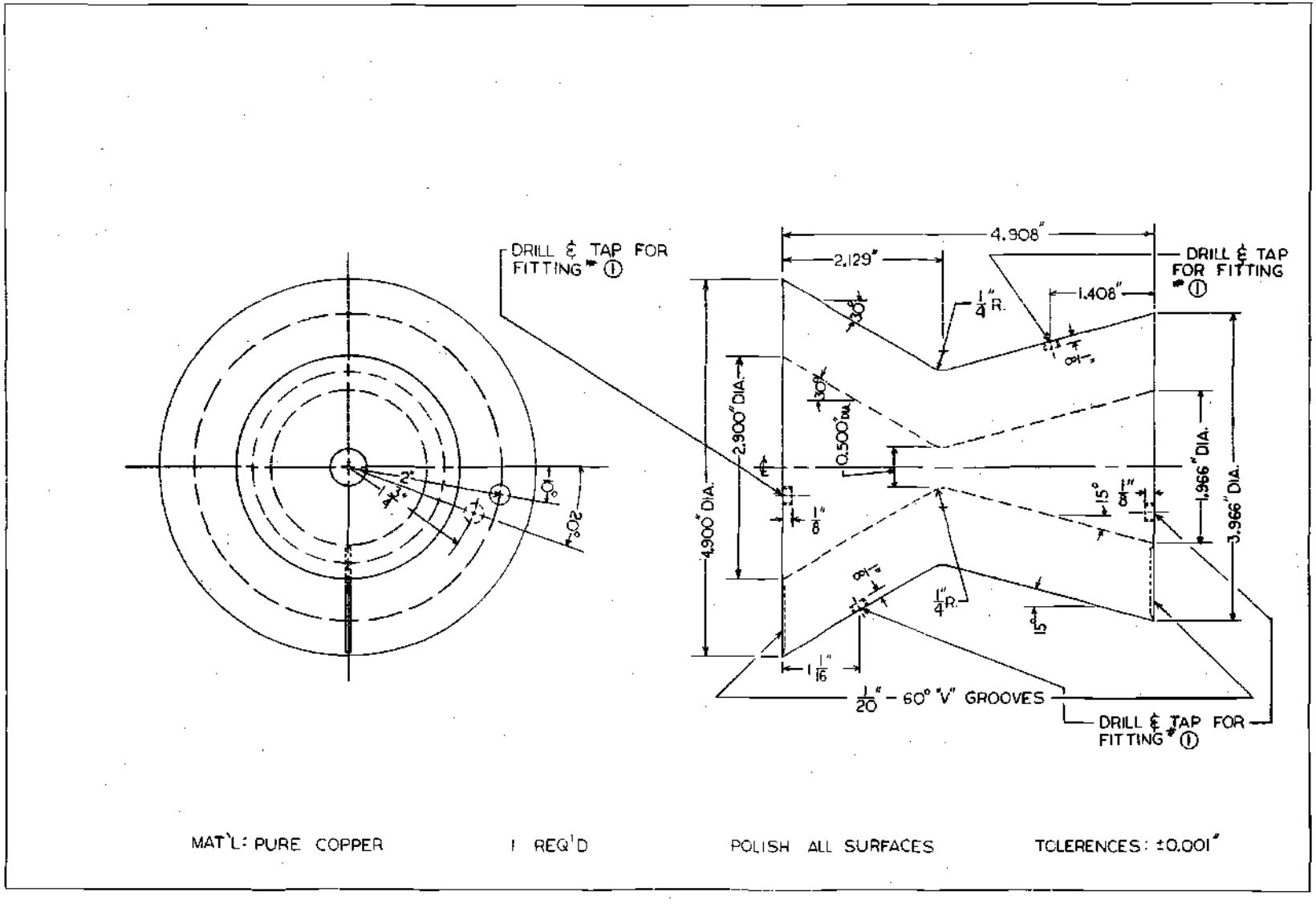

FIGURE 13. NOZZLE BODY

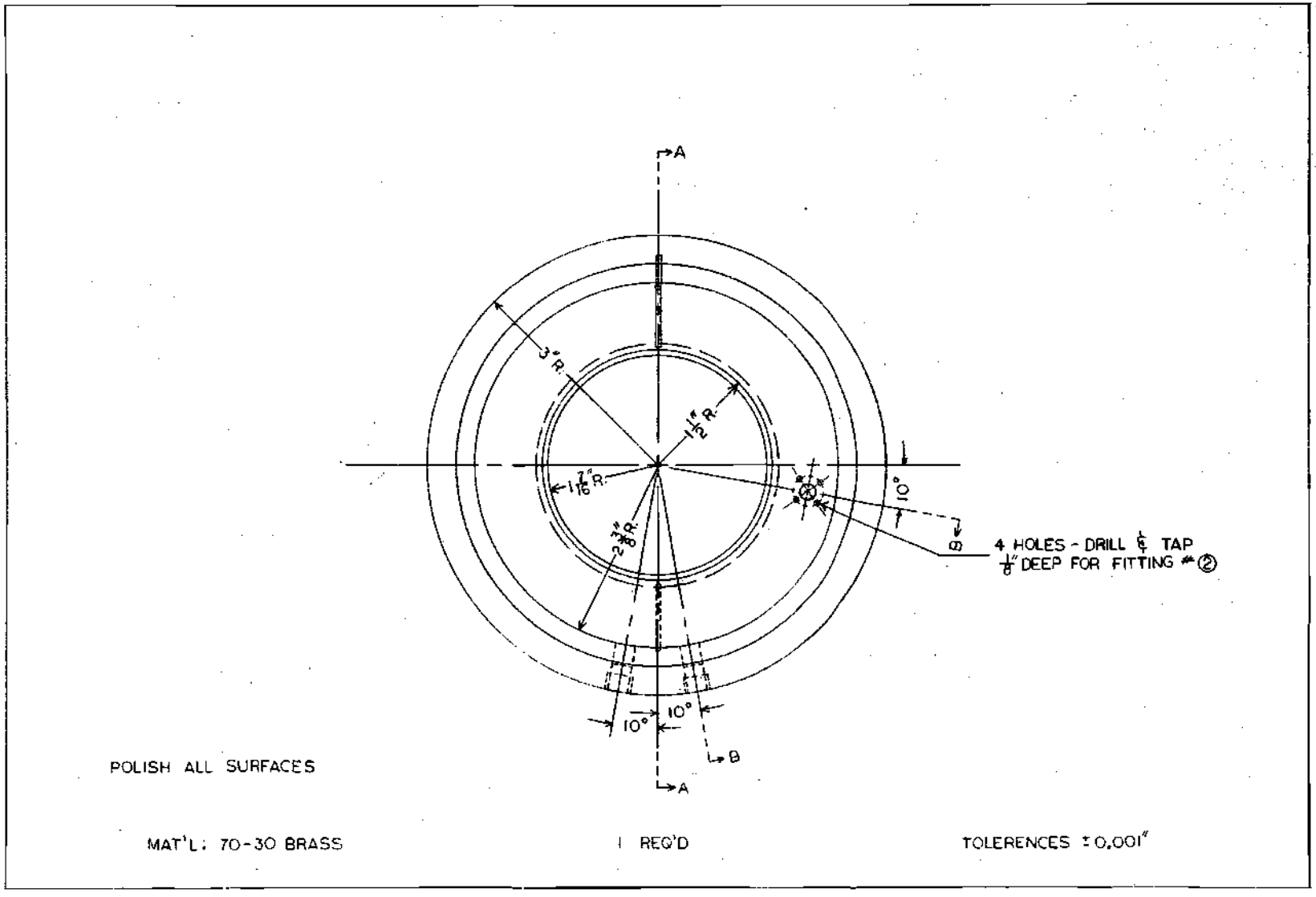

FIGURE 14. FIRST ENTRANCE END PLATE

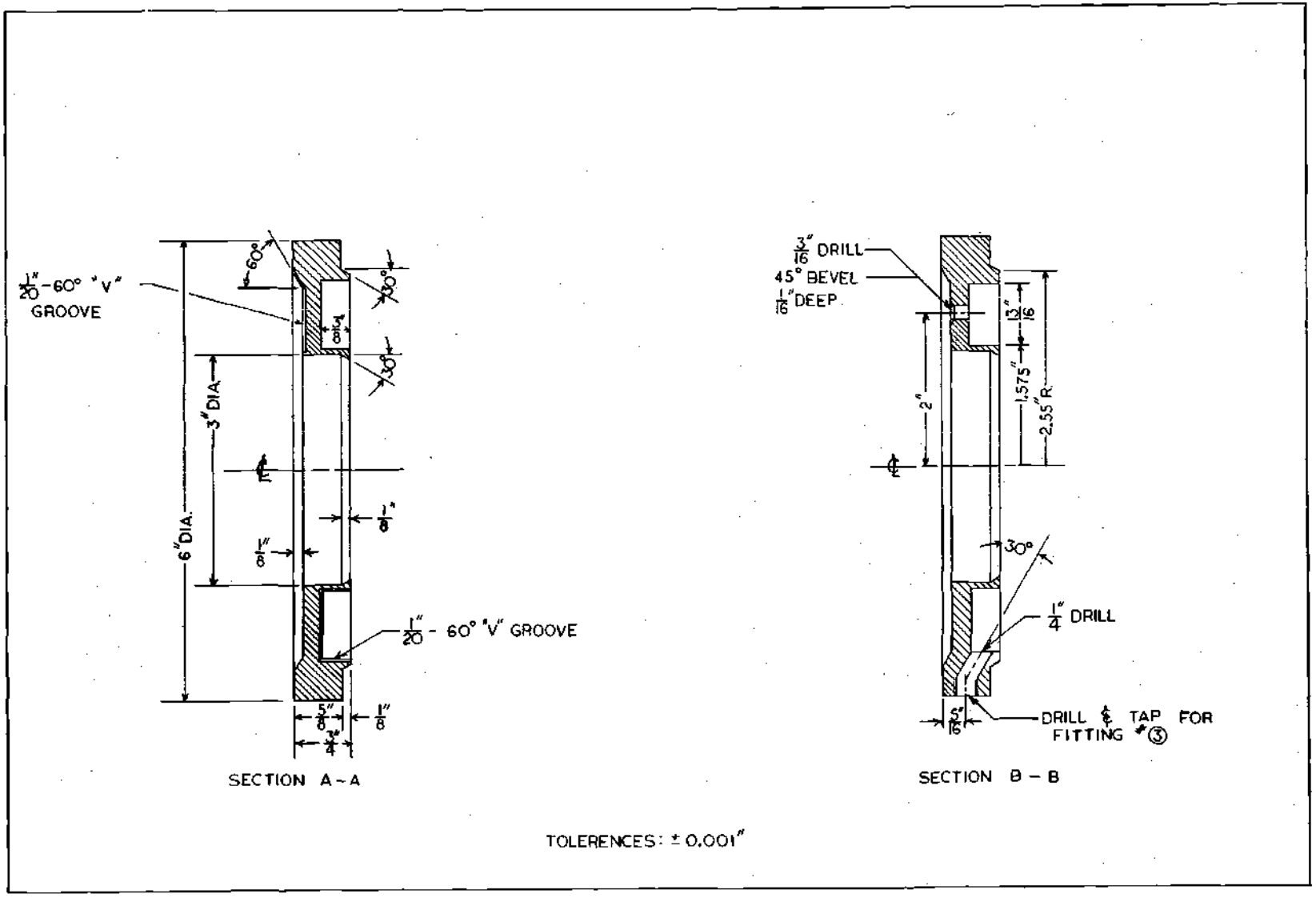

FIGURE 15. FIRST ENTRANCE END PLATE - SECTIONS

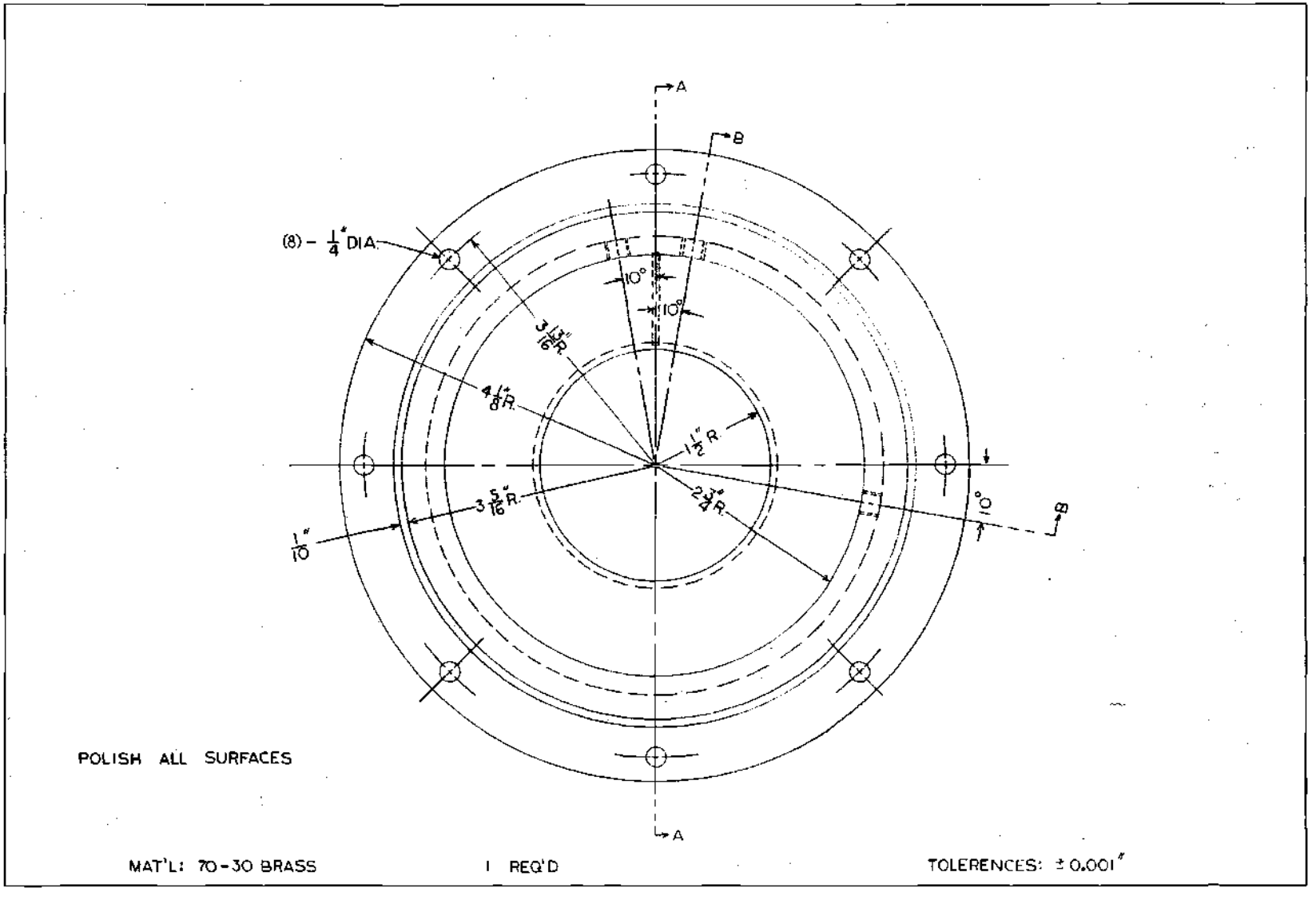

FIGURE 16. SECOND ENTRANCE END PLATE

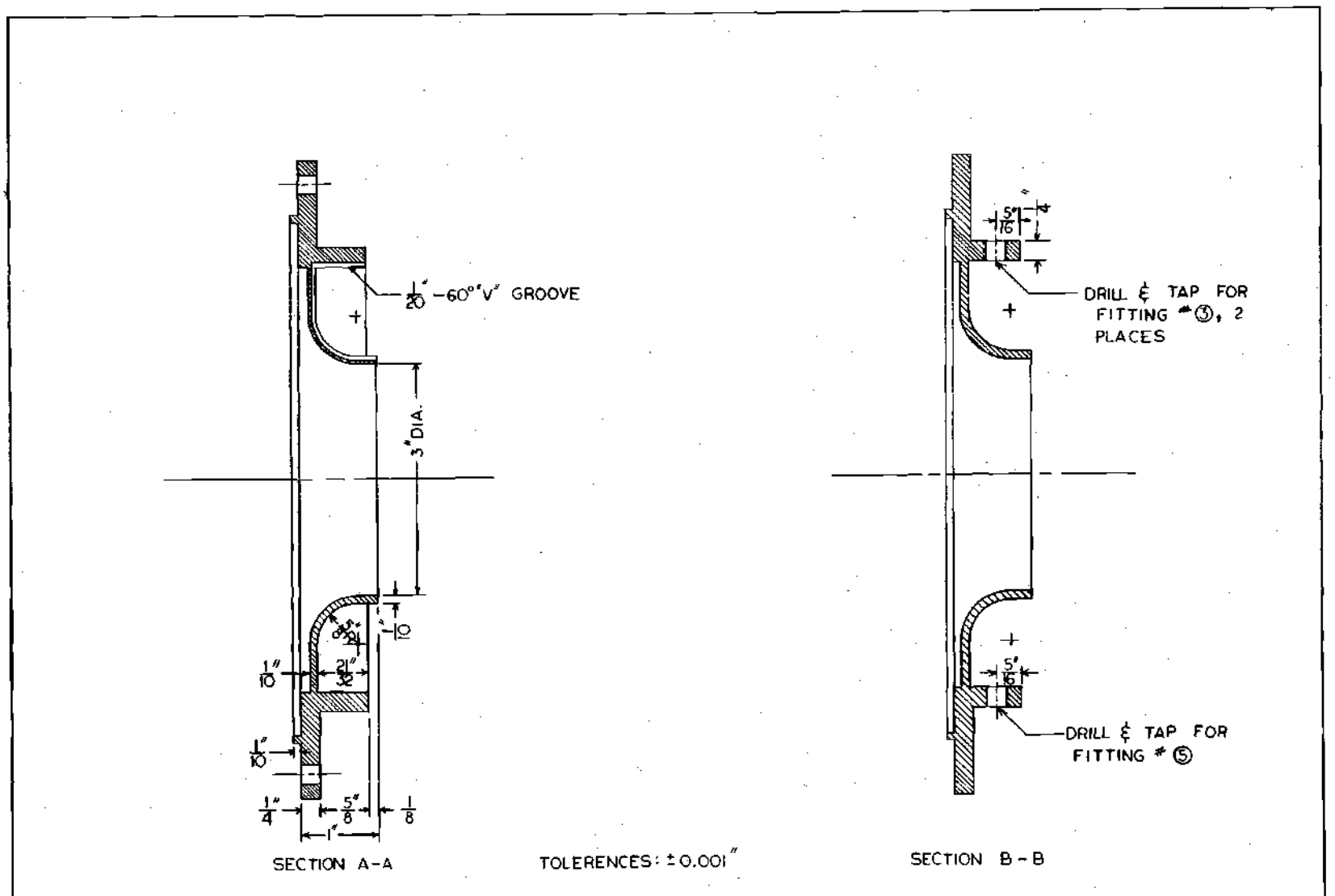

FIGURE 17. SECOND ENTRANCE END PLATE - SECTIONS

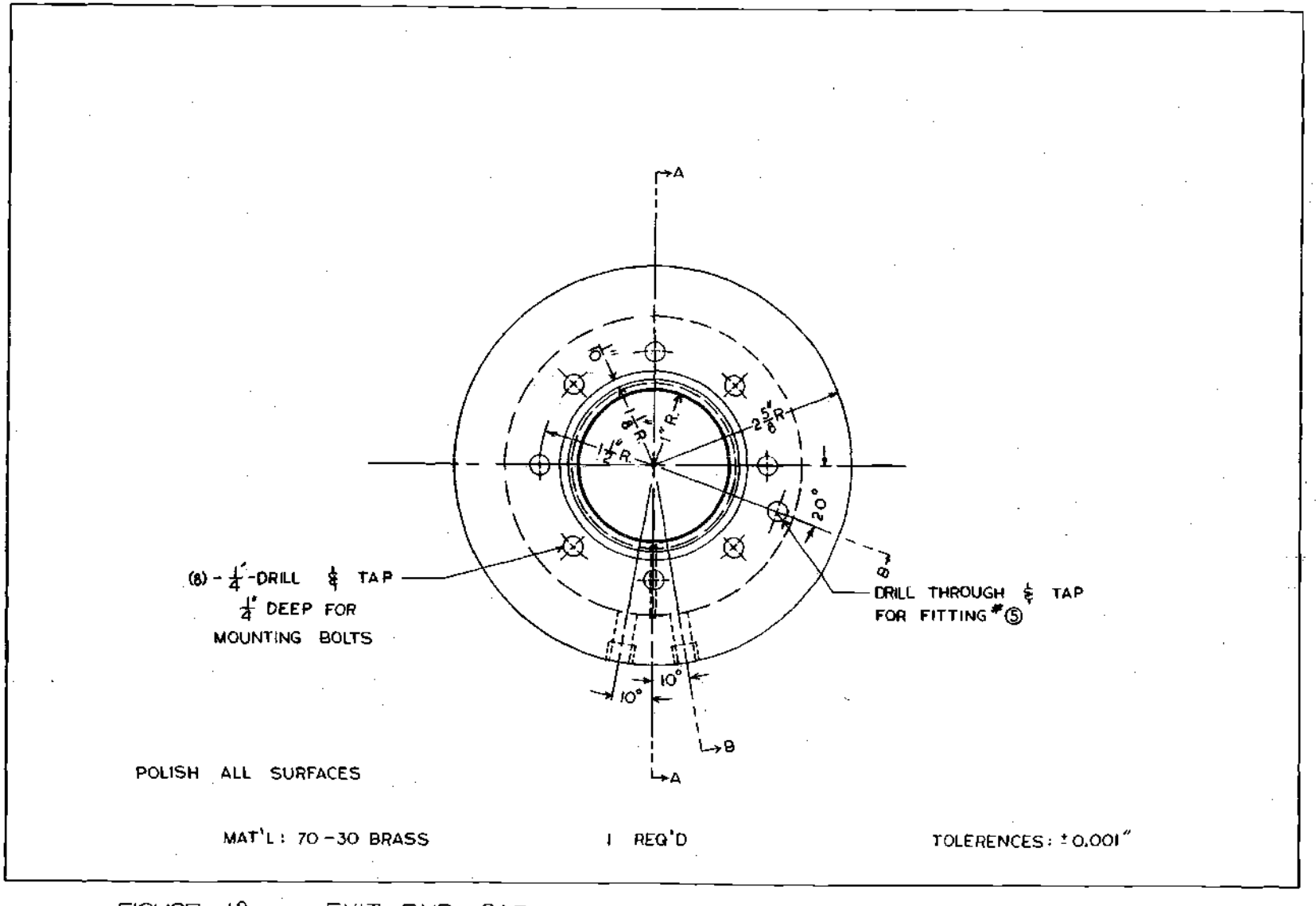

FIGURE 18. EXIT END CAP

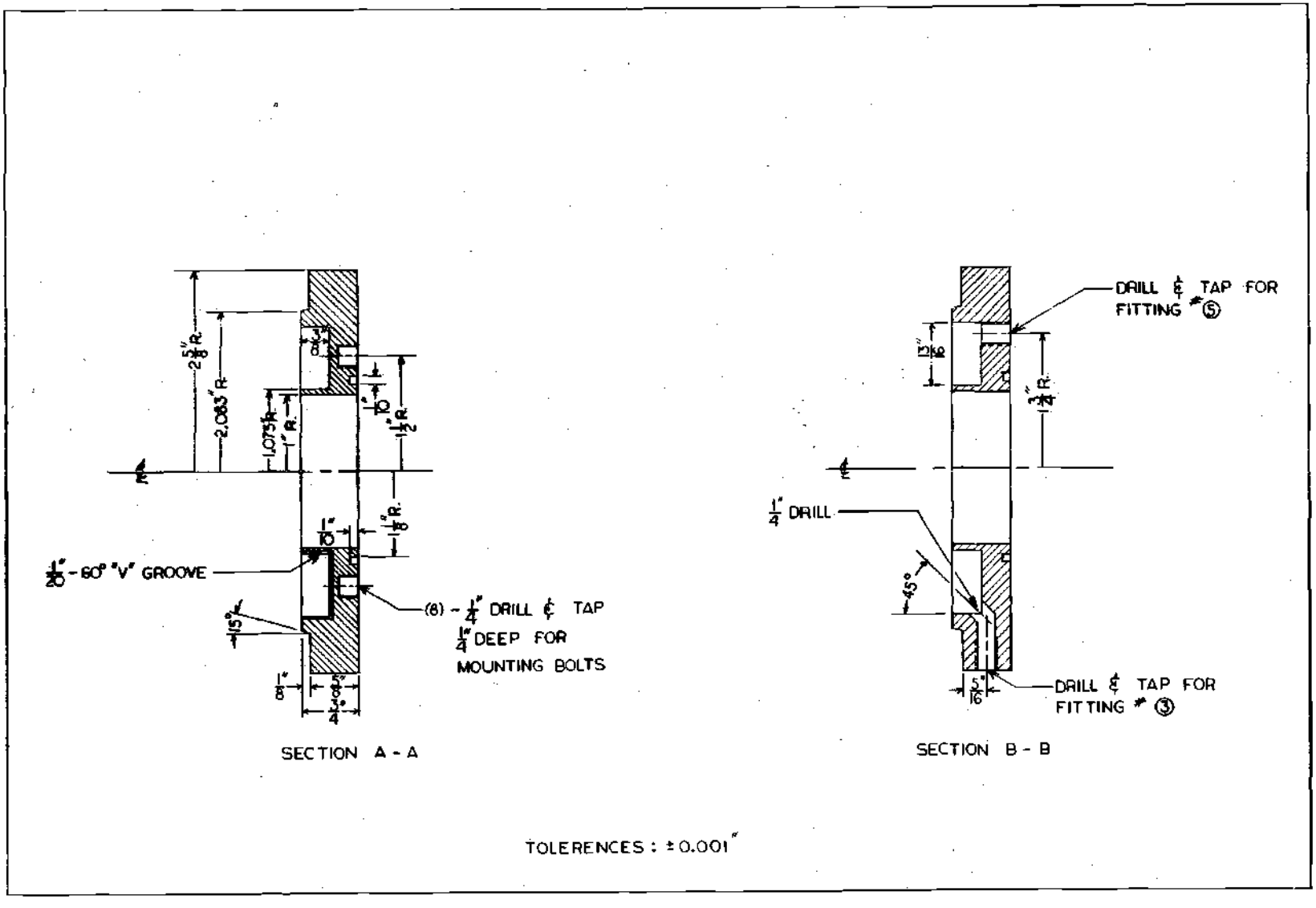

FIGURE 19. EXIT END CAP - SECTIONS

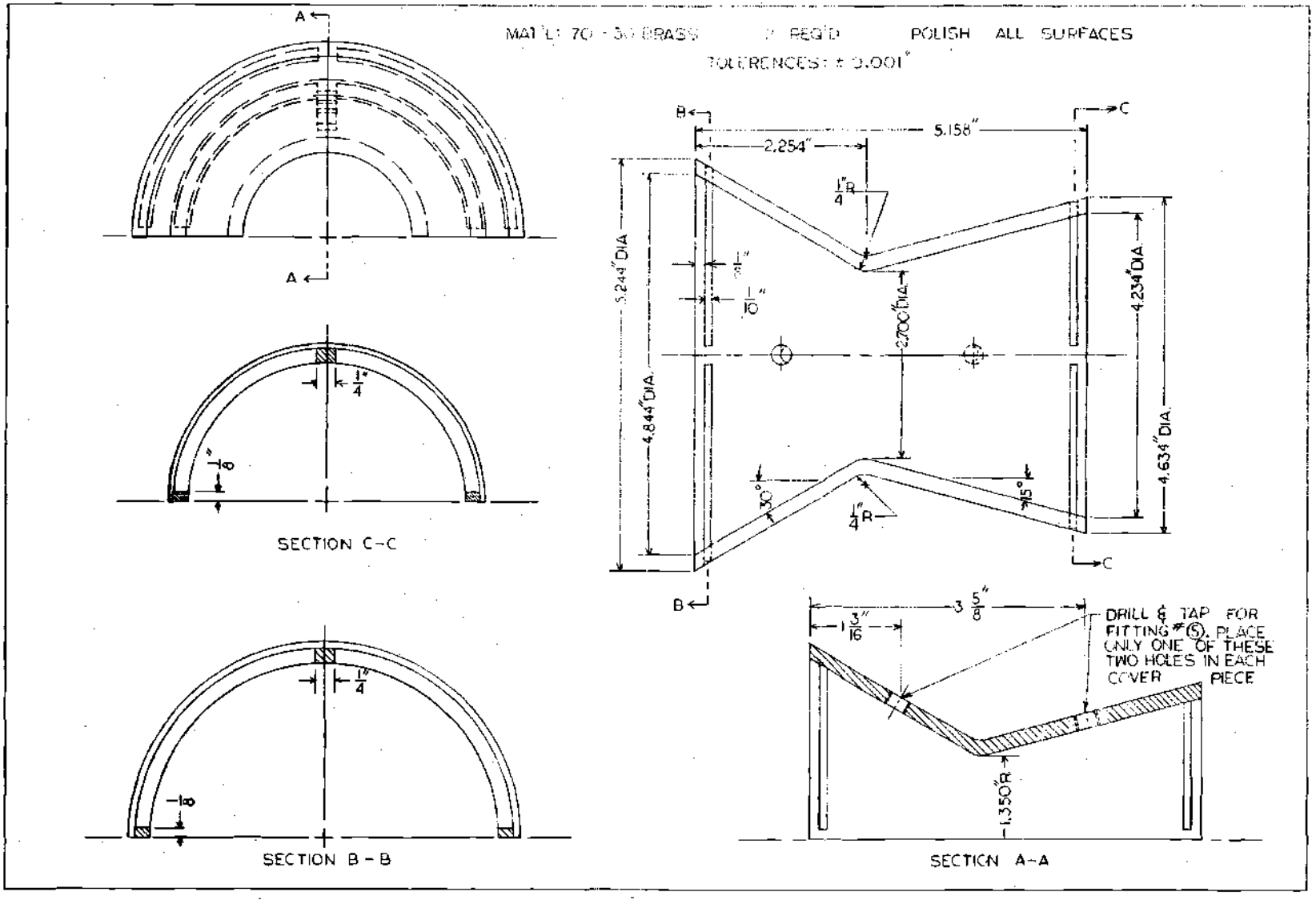

FIGURE 20. AXIAL COVER

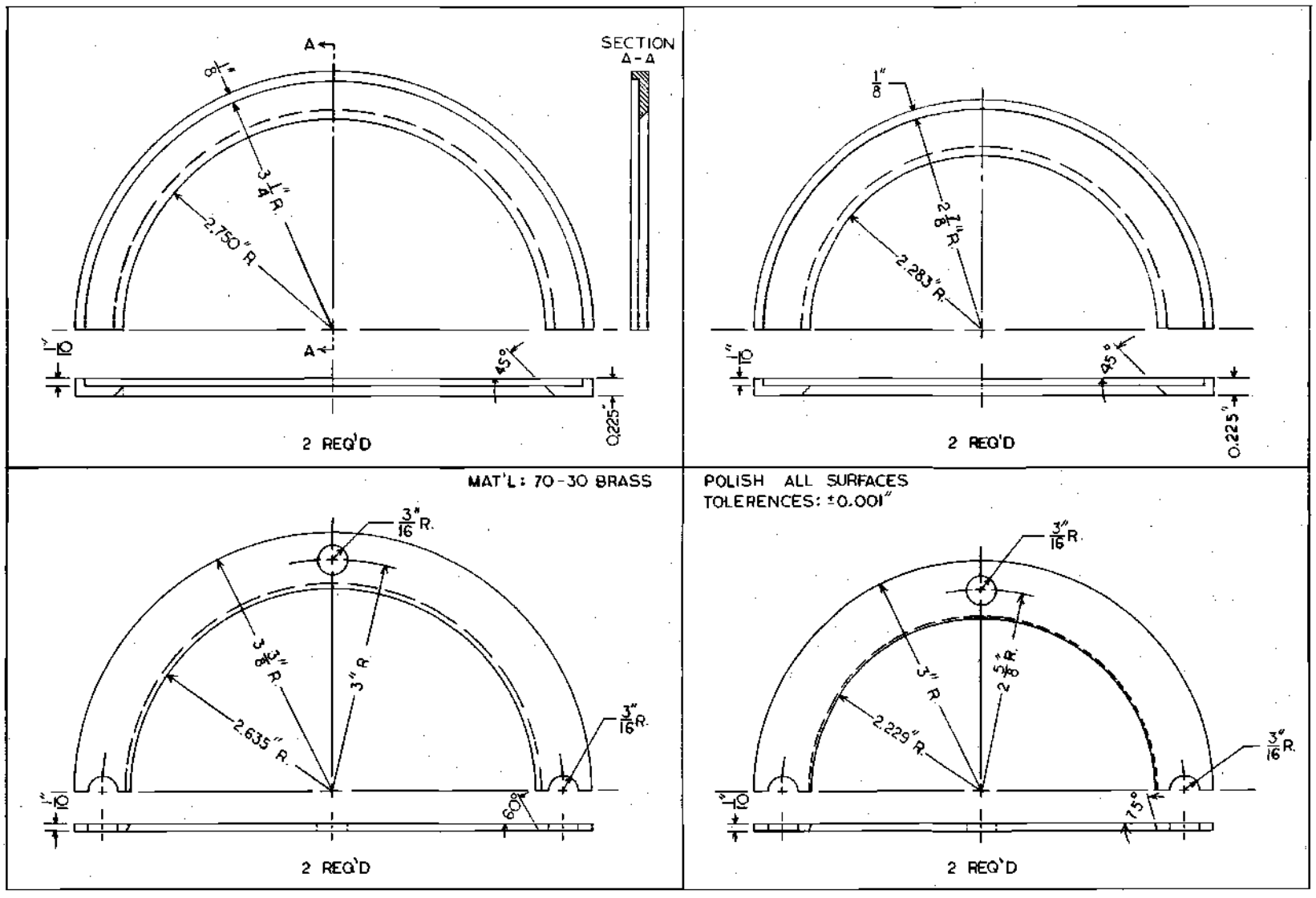

FIGURE 21. COLLECTOR RING PARTS

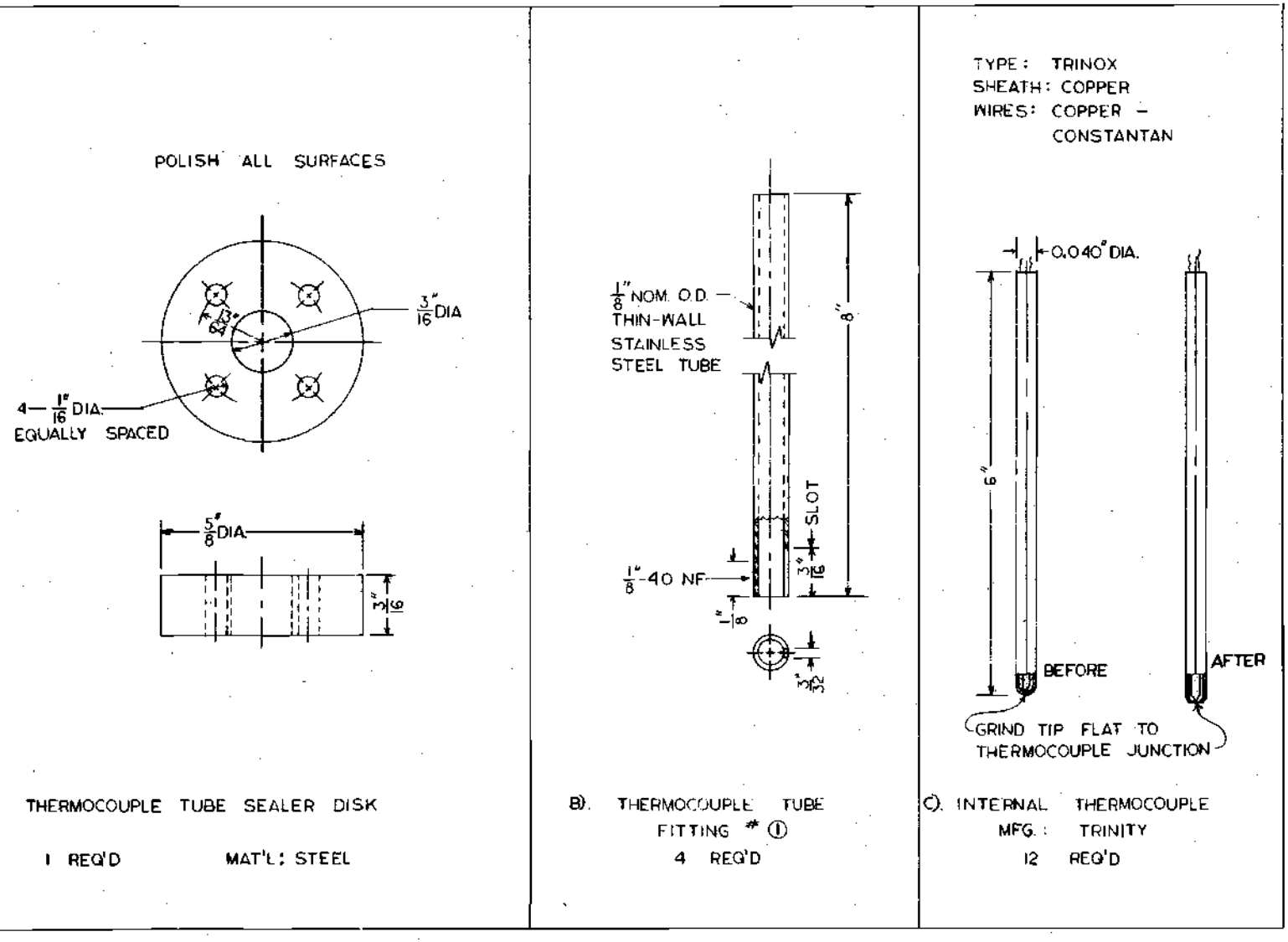

FIGURE 22. SPECIAL PARTS

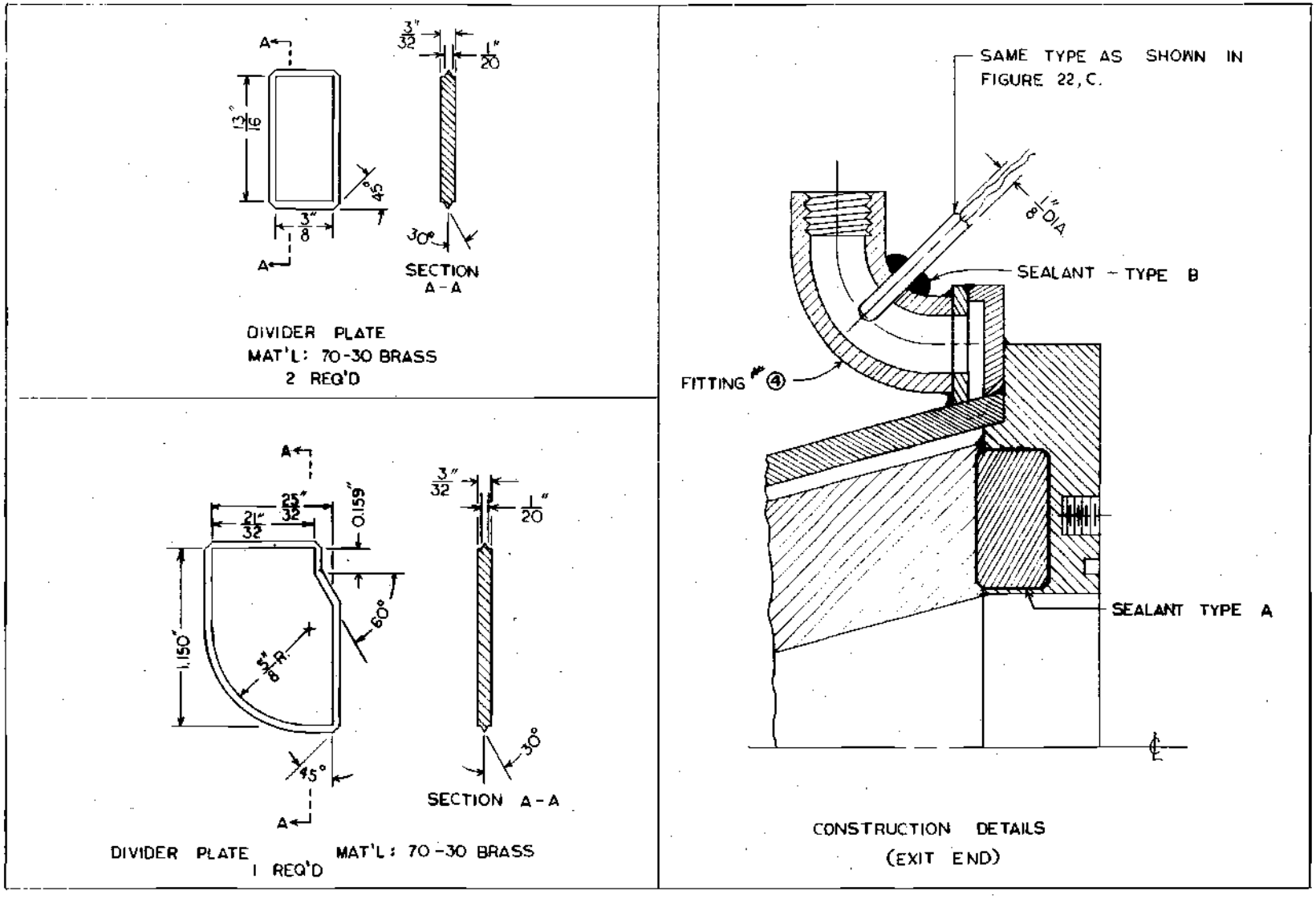

FIGURE 23. DIVIDER PLATE AND CONSTRUCTION DETAILS

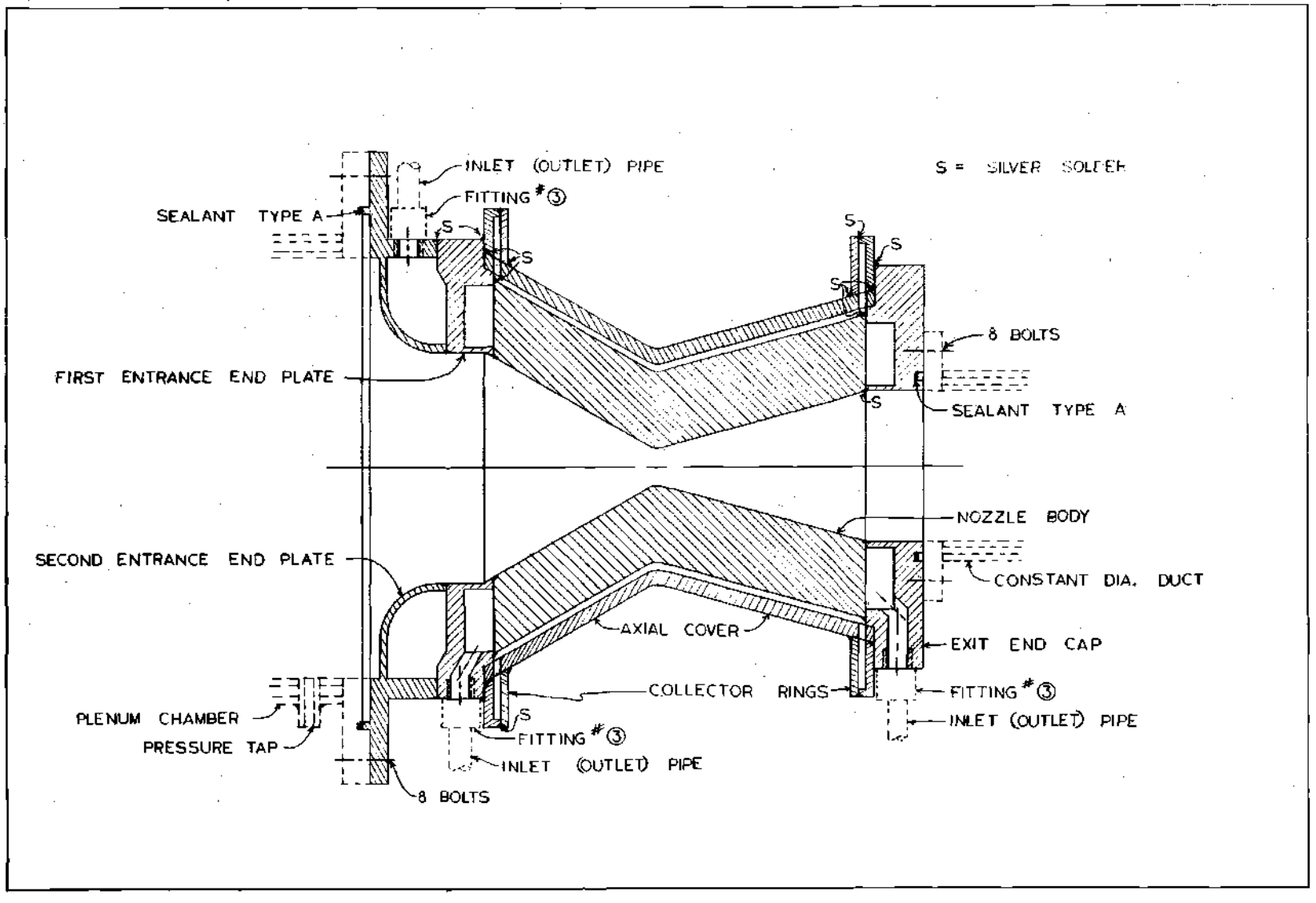

FIGURE 24. CONSTRUCTION DETAILS

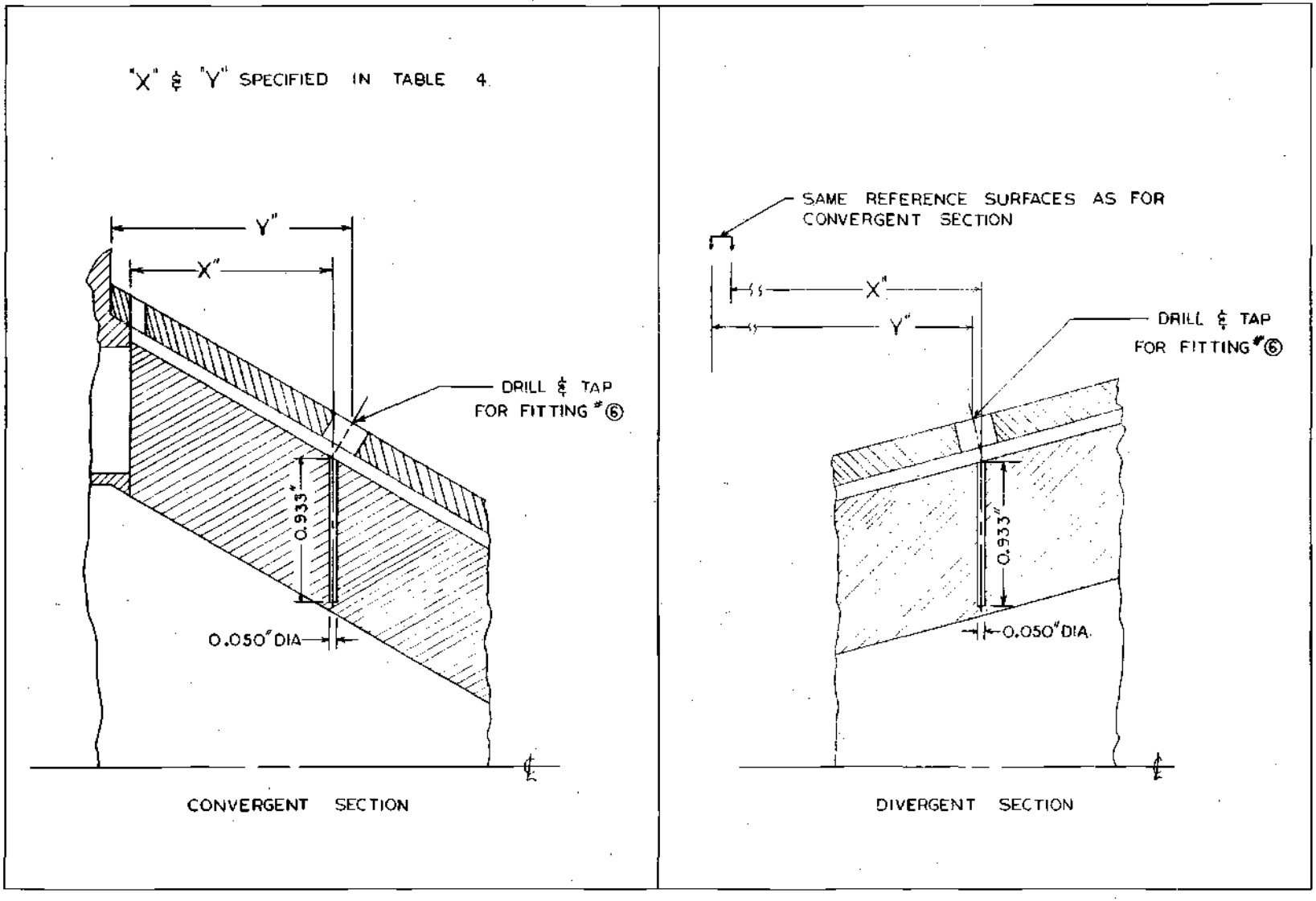

FIGURE 25. INTERNAL THERMOCOUPLE HOLES

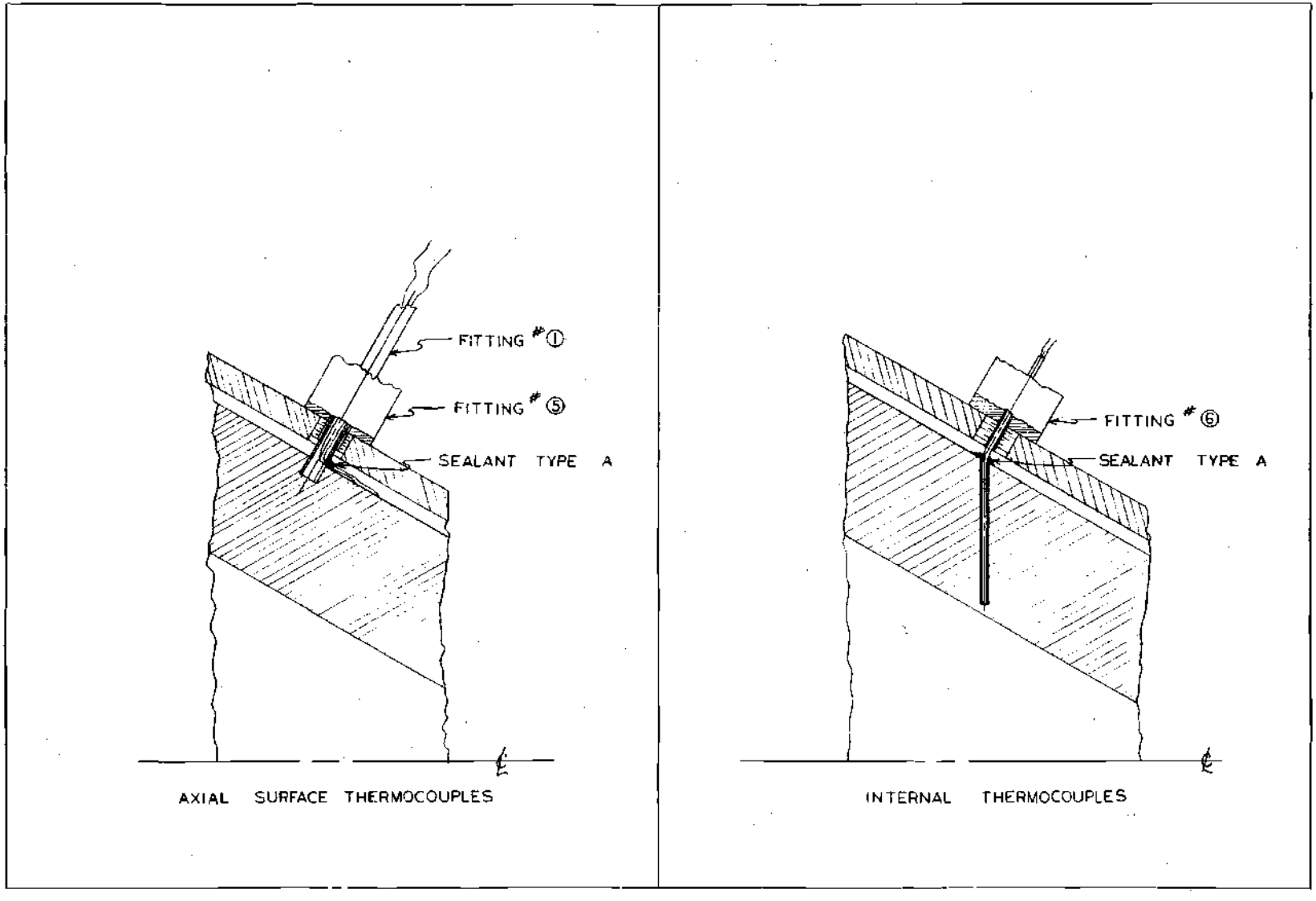

FIGURE 26. THERMOCOUPLE MOUNTING DETAILS

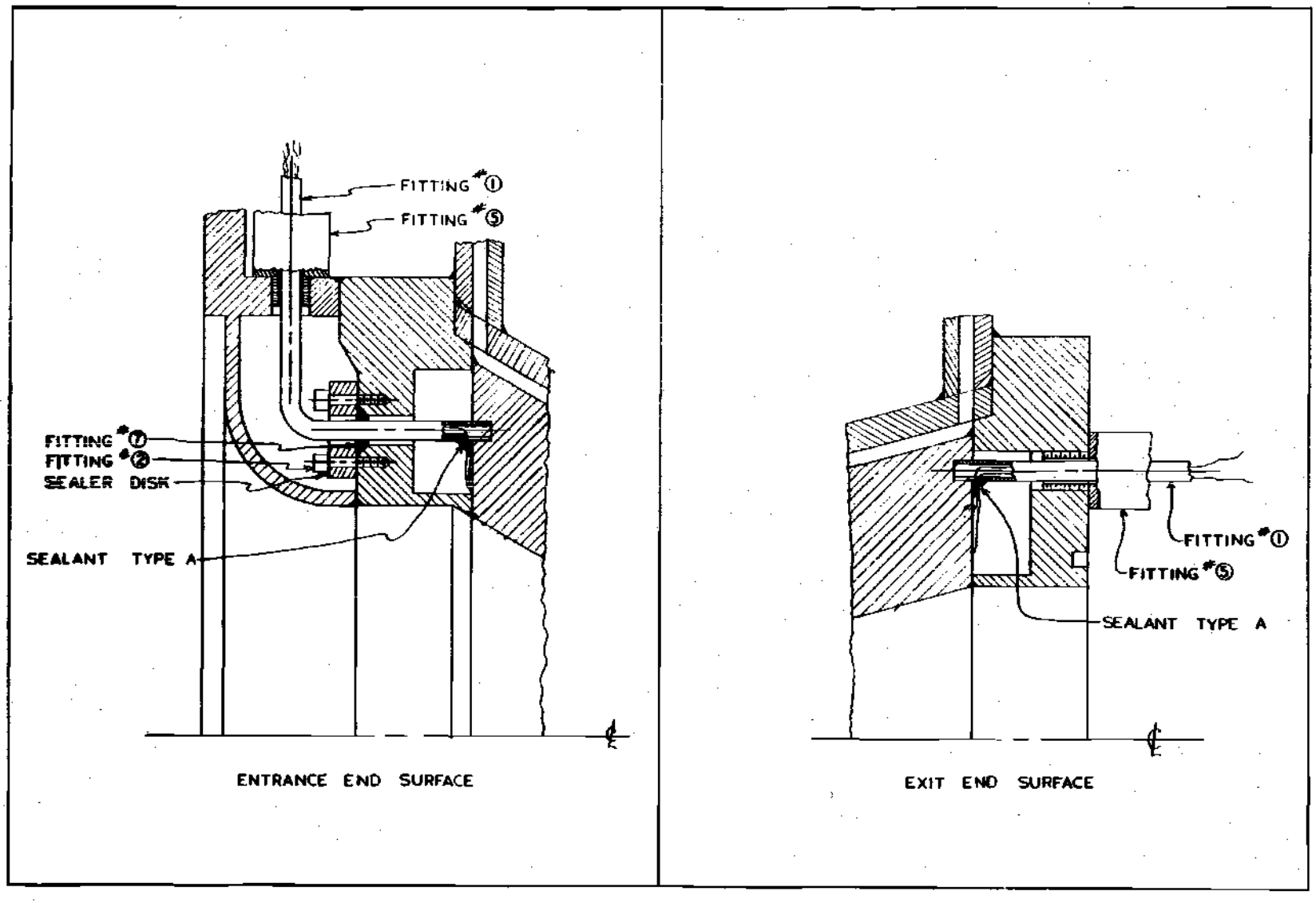

FIGURE 27. THERMOCOUPLE MOUNTING DETAILS

Table 1. Parts and Material Lists

A. Fittings

Fitting Number	Description
1.	Thermocouple tube; quantity - 4; see Figure 22.
2.	Sealer disk bolt; quantity - 4; No. 0 Fillister Head Am. Std. machine screw; shaft length - 5/16"; thread length - 3/16".
3.	End cap coolant connectors; standard 1/4" nom. o.d. copper tubing threaded fittings; quantity - 6.
4.	Collector ring connector; quantity - 8; 90° - 3/8" nom. i.d. copper pipe elbows; threaded on one end only.
5.	Thermocouple tube locking unit; quantity - 4; mfr. - Trinity; unit - Trinox P6 adjustable fitting with packing bland; size - 1/4" NPT; packing material - polyethylene.
6.	Internal thermocouple locking unit; quantity - 12; mfr. - Trinity; unit - Trinox P6 adjustable fitting with packing gland; size - 1/8" NPT; packing material - polyethylene.
7.	O-ring; ring inner diameter - 1/8"; thickness - 1/8" diameter; material - high temperature rubber (200°F).

B. Materials

Part	Description
Constantan Wire	33 B&S gage constantan lacquered thermocouple wire; total length - 120 ft.; cut into 2-ft. lengths.
Copper Wire	33 B&S gage copper lacquered thermocouple wire; total length - 16 ft.; cut into 2-ft. lengths.
Sealant Type A	10021-C Glyptal paint; mfr. - Central Scientific Co., Division of Cenco Instrument Co.
Sealant Type B	Insa-Lute adhesive cement, No. 1 paste, Sovereisen Cements Co.

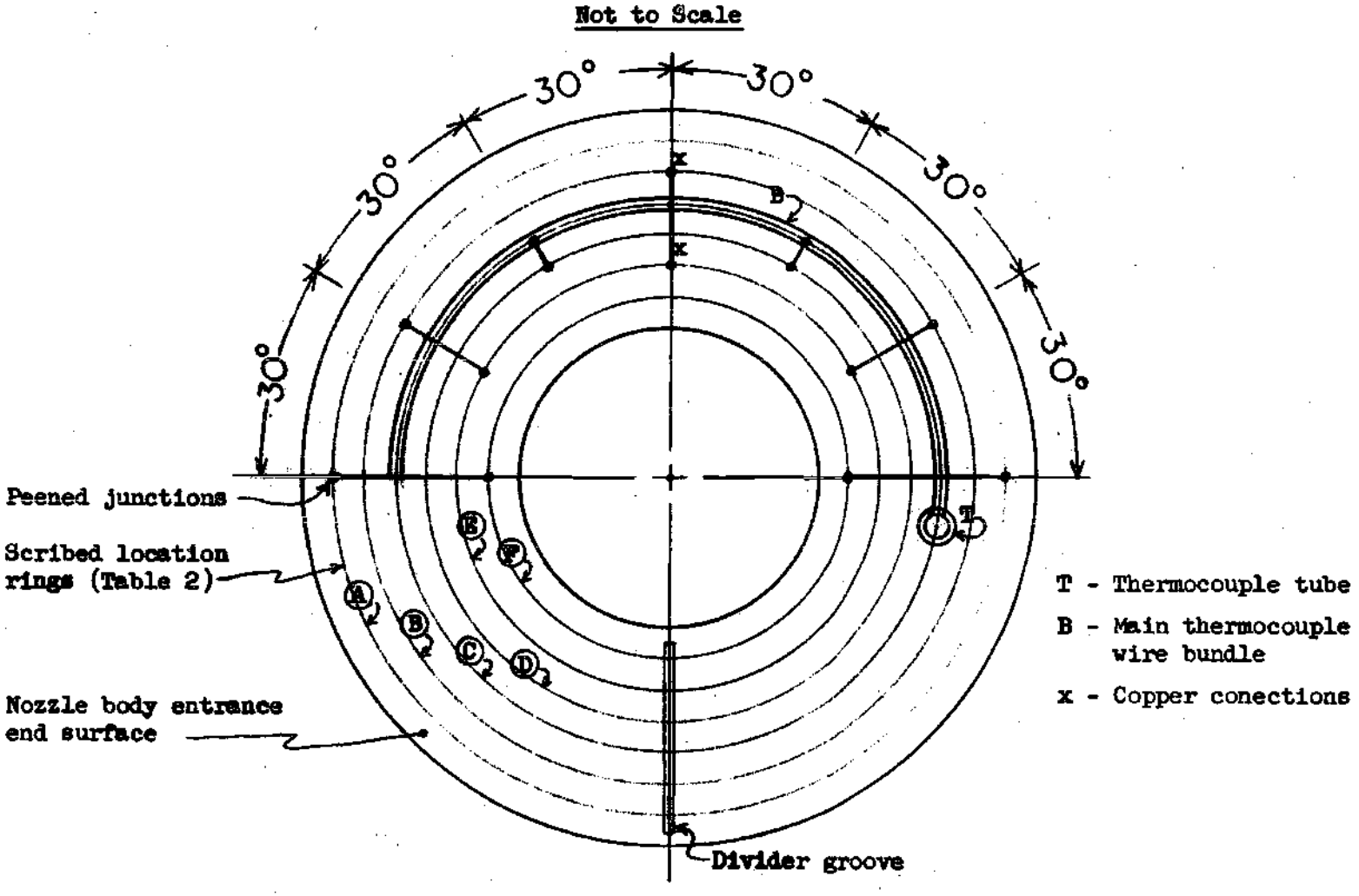

Figure 28. Entrance End Surface Thermocouple Locations

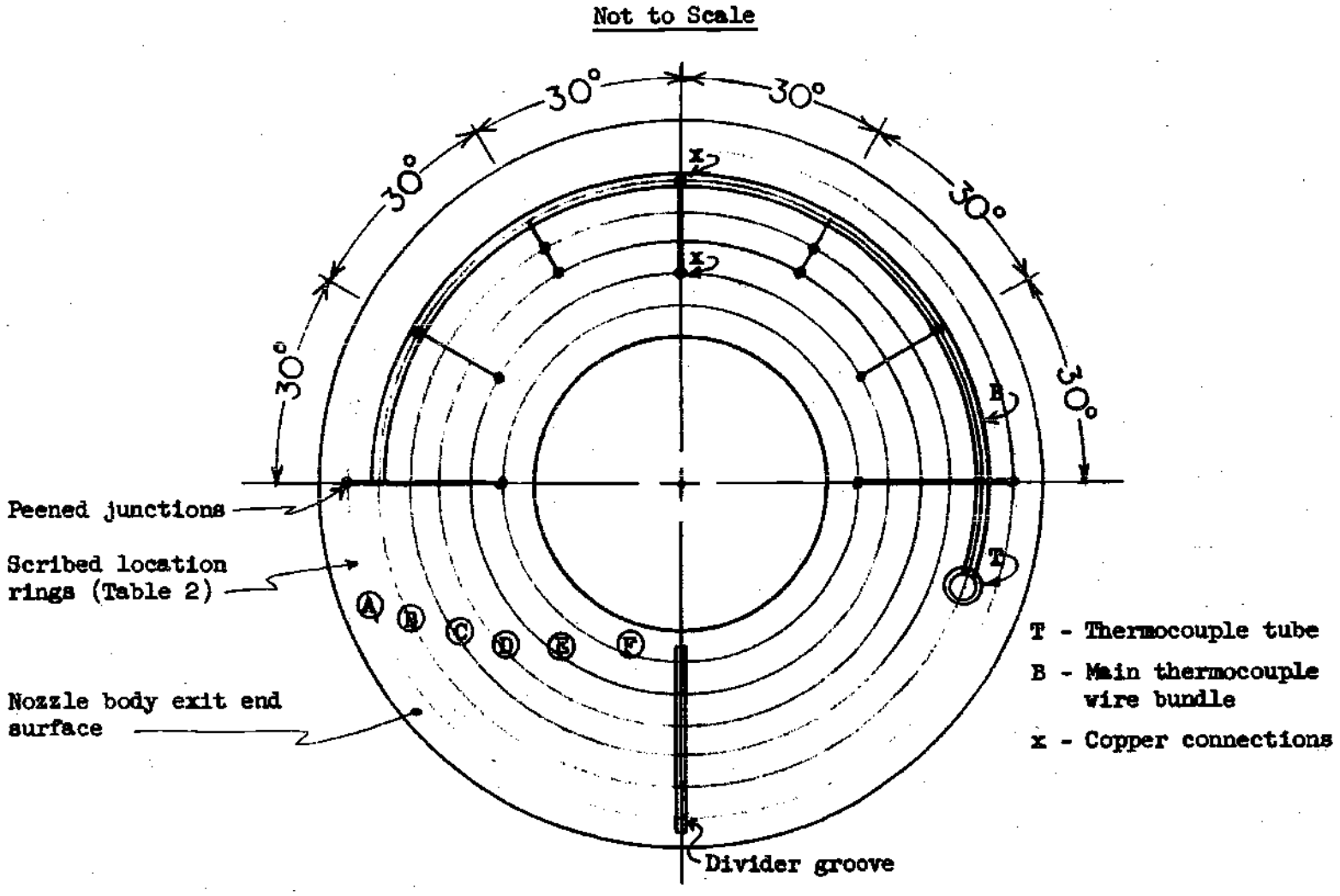

Figure 29. Exit End Surface Thermocouple Locations

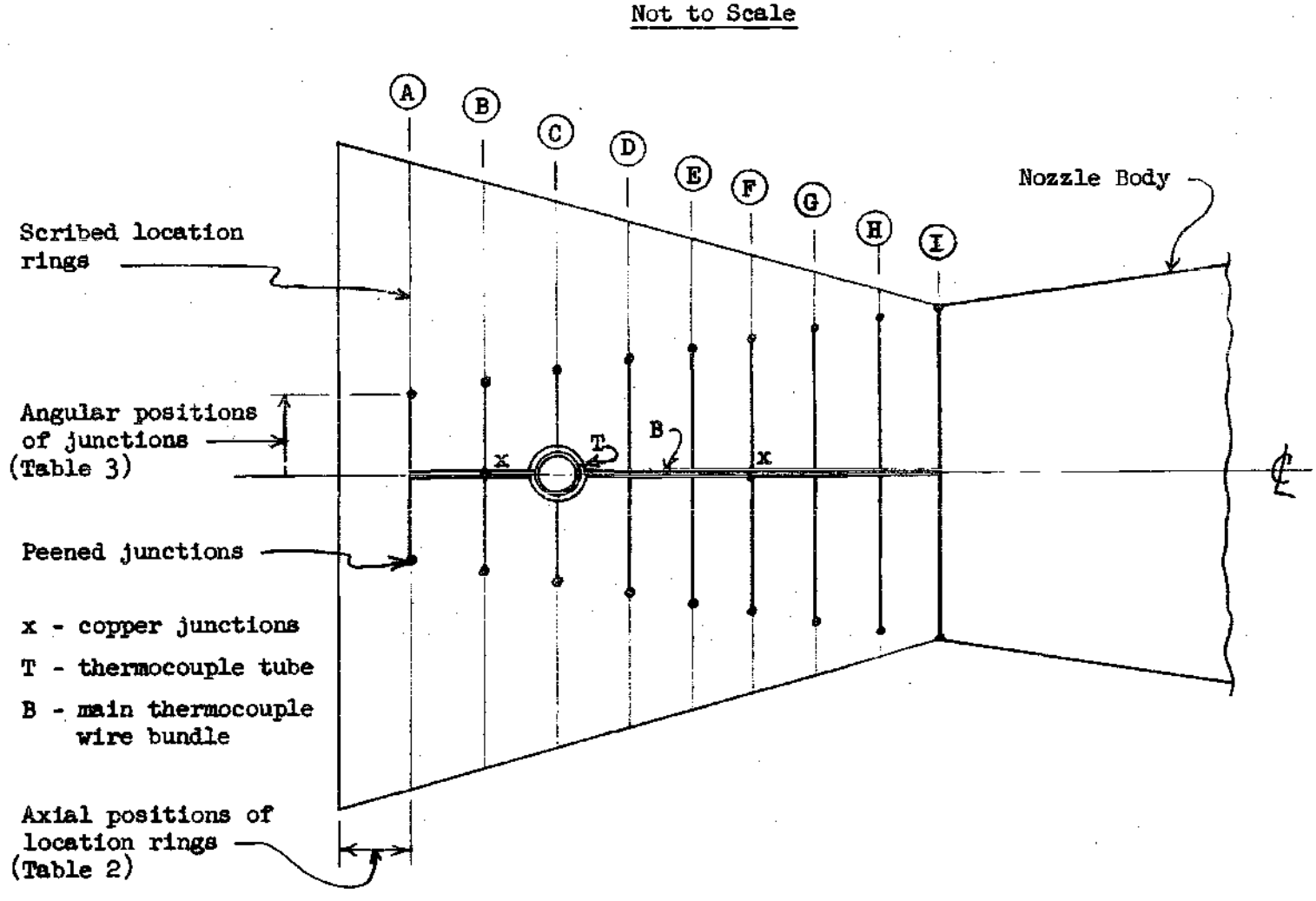

Figure 30. Convergent Section Surface Thermocouple Locations and Wire Patterns

Not to Scale

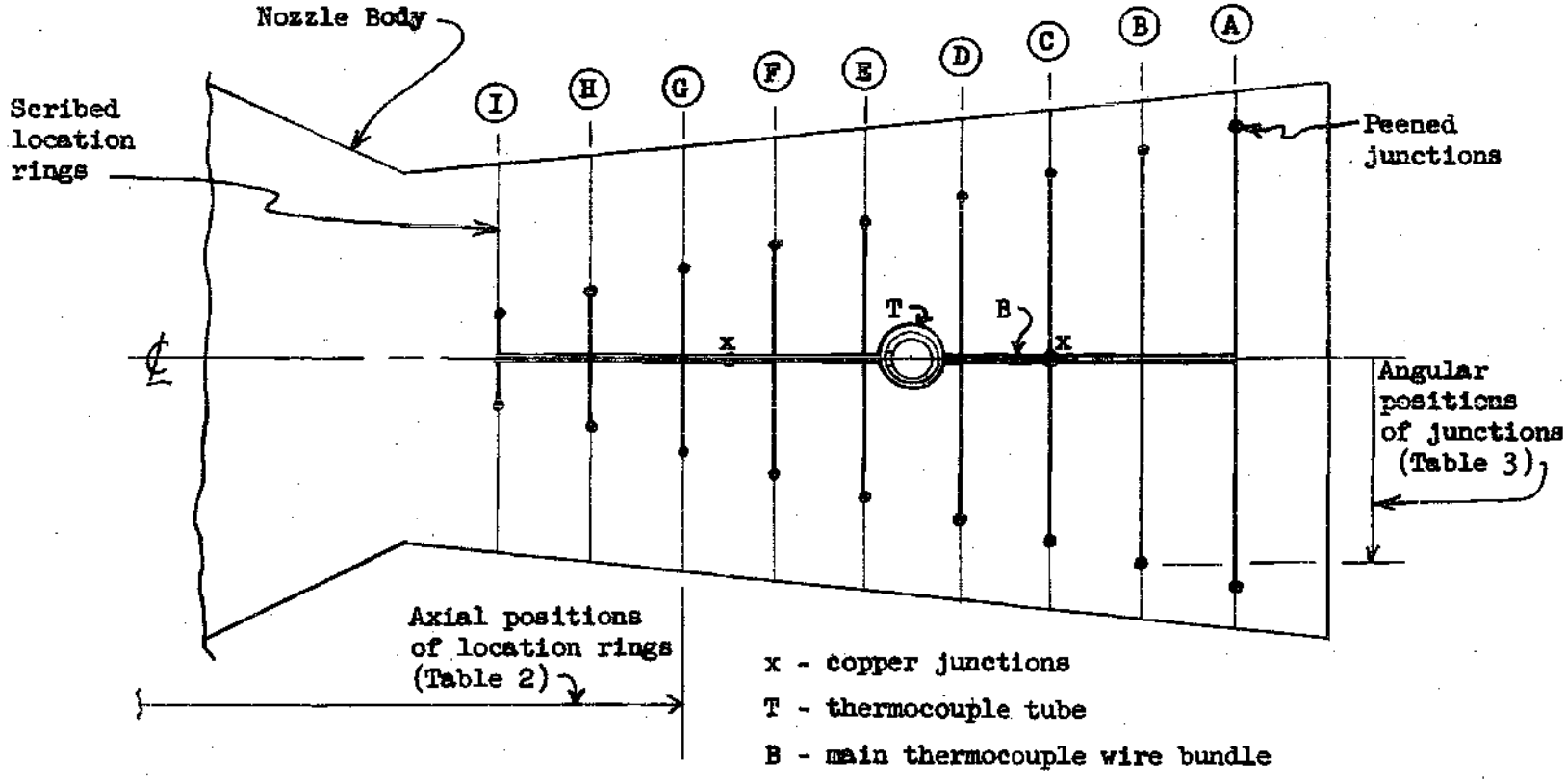

Figure 31. Divergent Section Surface Thermocouple Locations and Wire Patterns

Table 2. Positions of Scribed Location Rings

A. Entrance End Surface

Location Ring	Radius Inches
A	1.583
B	1.717
C	1.850
D	1.983
E	2.117
F	2.250

B. Exit End Surface

Location Ring	Radius Inches
A	1.117
B	1.250
C	1.383
D	1.517
E	1.650
F	1.783

C. Convergent End Axial Surface

Location Ring	Distance from Entrance End Surface - Inches
A	0.401
B	0.630
C	0.859
D	1.088
E	1.317
F	1.546
G	1.775
H	2.038
I	2.129

D. Divergent End Axial Surface

Location Ring	Distance from Entrance End Surface - Inches
A	2.270
B	2.536
C	2.786
D	3.036
E	3.285
F	3.535
G	3.784
H	4.034
I	4.284

Tolerances on all location dimensions are $\pm$ 0.001 inch.

Table 3. Angular Position of Axial Thermocouples

A. Convergent End

Location Ring	Degrees from Axial ℄ thru Tube ℄
A	± 15°
B	± 30°
C	± 45°
D	± 60°
E	± 75°
F	± 90°
G	±105°
H	±120°
I	±135°

Copper connections are on ℄

B. Divergent End

Location Ring	Degrees from Axial ℄ thru Tube ℄
A	± 135°
B	± 120°
C	± 105°
D	± 90°
E	± 75°
F	± 60°
G	± 45°
H	± 30°
I	± 15°

Table 4. Positions of Internal Thermocouple Holes and Axial Cover Holes

A. Convergent End

Thermocouple Number	"X"-Inches*	"Y"-Inches*	Angular ** Position Degrees
1	0.457	0.707	0°
2	0.687	0.937	30°
3	1.031	1.281	60°
4	1.374	1.624	90°
5	1.718	1.968	120°
6	1.947	2.197	150°
7	2.129	2.129	180°

B. Divergent End

8	2.411	2.474	210°
9	2.661	2.724	240°
10	3.160	3.223	270°
11	3.660	3.722	300°
12	4.159	4.221	330°

* See Figure 25 for definition of "X" and "Y".

** Reference Line is centerline of entrance end surface divider groove. Angles measured clockwise when facing entrance end surface.

Tolerances on "X" and "Y" are ± 0.001 inch.

Tolerances on angular positions are ± 1 degree.

APPENDIX D

CONSTRUCTION SEQUENCE

I. Surface Thermocouple Assembly

A. Cut thermocouple wires into two-foot lengths.

B. Carefully twist into bundles.

1. Entrance end surface bundle--12 constantan and 2 copper.

2. Exit end surface bundle--12 constantan and 2 copper.

3. Convergent end axial surface--18 constantan and 2 copper.

4. Divergent end axial surface--18 constantan and 2 copper.

C. Carefully thread each bundle into a thermocouple tube.

D. Bend bundles into slot at end of tube and seal both ends of the tubes with sealant, type B.

E. Check each wire in each bundle for electrical shorts either to other wires or to the tube itself.

II. Exit End Cap Assembly

A. Insert exit end surface thermocouple tube into nozzle body and screw tight.

B. Coat nozzle exit end surface thermocouple paths with thin layer of sealant, type A.

C. Bend thermocouple wires into shape to follow pattern shown in Figure 29 in Appendix C.

D. Peen thermocouple wires to surface at locations specified in Appendix C after wire lacquer has been removed at the specific point the wire is to be peened.

E. Secure and seal all wires to the surface with sealant, type A, being careful to avoid covering the junctions.

F. Trim excess wire ends off and seal thermocouple tube slot with sealant, type A.

G. Line divider plate grooves in the nozzle body and the exit end cap with sealant, type A, and place divider plate in place.

H. Place exit end cap in place over thermocouple tube and divider plate and silver solder to nozzle body on inner surface and outer surface.

I. Install both coolant passage connectors and the thermocouple tube locking unit and tighten them.

III. Entrance End Cap Assembly

A. Insert entrance end surface thermocouple tube into nozzle body and screw tight.

B. Coat nozzle entrance end surface thermocouple paths with thin layer of sealant, type A.

C. Bend wires into shape to follow pattern shown in Figure 28, Appendix C.

D. Peen thermocouple wires to surface at locations specified in Appendix C after lacquer has been removed at the specific point the wire is to be peened.

E. Secure and seal all wires to the surface with sealant, type A, being careful to avoid covering the junctions.

F. Trim excess wire ends off and seal thermocouple tube slot with sealant, type A.

G. Line divider plate grooves in the nozzle body and the first

entrance end plate with sealant, type A, and place divider plate in place.

H. Place first entrance end plate in place over thermocouple tube and divider plate and silver solder to nozzle body on inner surface and outer surface.

I. Install 0-ring and sealer disk over thermocouple tube and insert and tighten sealer disk bolts.

J. Bend thermocouple tube to fit through second entrance end plate hole as shown in Figure 27 in Appendix C.

K. Line divider grooves in first and second entrance end plates with sealant, type A, and place divider plate in place.

L. Place second entrance end plate in place over thermocouple tube and divider plate and silver solder to first entrance end plate on inner and outer surfaces.

M. Install all four coolant passage connectors into first and second entrance end plates and tighten.

N. Install the thermocouple tube locking unit over the thermocouple tube in the second entrance end plate and tighten.

IV. Axial Cover Assembly

A. Insert both convergent and divergent outer surface thermocouple tubes into the nozzle body and screw tight.

B. Coat outer surface of nozzle body only on surface thermocouple paths shown in Figures 30 and 31 in Appendix C with a thin layer of sealant, type A.

C. Bend wires into shape to follow pattern shown in Figures 30 and 31 in Appendix C.

D. Peen thermocouple wires to surface at the locations specified in Appendix C after lacquer has been removed at the specific point each wire is to be peened.

E. Secure and seal all wires to the surface with sealant, type A, being careful to avoid covering the junctions.

F. Trim excess wire ends off and seal both thermocouple tube slots with sealant, type A.

G. Place the first half of the axial cover in place and silver solder it to the entrance end plate and the exit end plate.

H. Repeat step G for the second half of the axial cover.

I. Silver solder the two halves together.

J. Locate the back plates of the collector rings on each end of the axial cover and silver solder them to the cover and the end plates.

K. Locate the other plates of the collector rings and silver solder them to the cover and to the collector ring back plates. Silver solder the ring halves together. In locating the ring pieces on the cover, make sure the inlet holes to the rings are located over the closed portions of the axial cover slots and not over the open places.

L. Insert the internal thermocouples into their holes in the nozzle body and seal the nozzle body holes around the thermocouples at the nozzle body outer surface with sealant, type A.

M. Place over the internal thermocouples and the thermocouple tubes their locking units and tighten them when the sealant has dried.

N. Silver solder the collector ring connectors in place.

0. Insert the coolant thermocouples and seal them in place with sealant, type B.

APPENDIX E

COMPUTER PROGRAMS

Nomenclature Translation

A = a

A(M) = A_{cj} (for j = 1,2,3)

B = b

Cj = C_j (for j = 1,2,3,...15)

DR = Δr

H(M) = h_m

Kj = $\bar{k}_j$ (for j = 1,2,3,...6)

L1 = L_1

L2 = L_2

LOG = ln

M = m

N = n

Q(M) = $q_{m,i}$

QFLUX(M) = $q''_{m,i}$

R(M,N) = $r_{m,n}$

RREF = $r_{1,1}$

SQRT = $\sqrt{\quad}$ or $[\quad]^{\frac{1}{2}}$

TA(M,N) = $t^a_{m,n}$

TB(M,N) = $t_{m,n}$

TG = T_{og}

TOTAL = total heat input to nozzle wall inner surface

$$= \sum_{m}^{\bar{m}} q_m$$

Z(M) = z_m

```
2 COMMENT BAC - 220  STANDARD VERSION  2/1/62                          $
2 COMMENT PROGRAM FOR CALCULATING TWO-DIMENSIONAL TEMPERATURE
2         DISTRIBUTION. ERIC KUNZ. 6/10/64.                            $
2 INTEGER I,J,M,N $
2 ARRAY   TA(30,16), TB(30,16), R(30,16), Z(30), H(30) $
2         READ($$CONSTS) $
2         READ($$DATA1) $
2         READ($$DATA2) $
2         READ($$DATA3) $
2 COMMENT CALCULATION OF RADIUS MATRIX $
2         FOR M = (1,1,19)$ FOR N = (1,1,16)$
2         R(M,N) = RREF - (M + N - 2.0).DR $
2         FOR M = (20,1,30)$ FOR N = (1,1,16)$
2         R(M,N) = RREF - (36.0 + N - M).DR $
2 COMMENT THIS SECTION MAINTAINS SURFACE TEMPERATURES CONSTANT $
2         FOR N = (1,1,16) $ TB(1,N) = TA(1,N) $
2         FOR M = (2,1,29) $ TB(M,1) = TA(M,1) $
2         FOR N = (1,1,16) $ TB(30,N) = TA(30,N) $
2         WRITE($$TITLE1) $
2         WRITE($$OUT1,FMT1) $
2         WRITE($$TITLE3) $
2 COMMENT TEMPERATURE CALCULATION CYCLE STARTS $
2         FOR I = (1,1,200) $
2         BEGIN
2 COMMENT ENTRANCE SECTION TEMPERATURE CALCULATIONS $
2 START.. FOR M = (2,1,18) $
2   BEGIN FOR N = (2,1,16) $
2   BEGIN IF N LEQ 15 $ GO TO FONA $ GO TO FONB $
2 FONA..  K1 = A + (0.5).B.(TA(M+1,N-1) + TA(M,N)) $
2         K2 = A + (0.5).B.(TA(M-1,N+1) + TA(M,N)) $
2         K3 = A + (0.5).B.(TA(M,N+1) + TA(M,N)) $
```

```
2          K4 = A + (0.5)*B*(TA(M,N-1) + TA(M,N)) $
2          C1 = ((2.0)*(R(M,N))*DR)/(Z(M+1) - Z(M)) $
2          C2 = ((2.0)*(R(M,N))*DR)/(Z(M) - Z(M-1)) $
2          C3 = (Z(M+1) - Z(M-1))/(LOG(R(M,N)) - LOG(R(M,N) - DR)) $
2          C4 = (Z(M+1) - Z(M-1))/(LOG(R(M,N) + DR) - LOG(R(M,N))) $
2          TB(M,N) = (K1*C1*TA(M+1,N-1) + K2*C2*TA(M-1,N+1)
2          + K3*C3*TA(M,N+1) + K4*C4*TA(M,N-1))/(K1*C1 +  K2*C2 + K3*C3
2          + K4*C4) $
2          GO TO FINI1 $
2 FONR..   K1 = A + (0.5)*B*(TA(M+1,N-1) + TA(M,N)) $
2          K4 = A + (0.5)*B*(TA(M,N-1) + TA(M,N)) $
2          C5 = (2.0)*R(M,N)*(SQRT((DR)**2.0 +
2               ((Z(M+1) - Z(M-1))**2.0)/(4.0))) $
2          C6 = ((1.5)*R(M,N)*DR + (0.125)*((DR)**2.0))/(Z(M+1) - Z(M))  $
2          C7 = ((Z(M+1) - Z(M))*((2.0)*R(M,N) + DR) + (Z(M) -
2               Z(M-1))*(R(M,N) + (0.75)*DR))/(((2.0)*R(M,N) +
2               + DR)*(LOG(R(M,N) + DR) - LOG(R(M,N)))) $
2          TB(M,N) = (H(M)*C5*TG + K1*C6*TA(M+1,N-1) +
2          K4*C7*TA(M,N-1))/(H(M)*C5 + K1*C6 + K4*C7) $
2          GO TO FINI1 $
2 FINI1..  END $
2          END $
2 COMMENT CALCULATION OF THROAT LINE TEMPERATURES $
2          M = 19 $
2          FOR N = (2,1,16) $
2   BEGIN  IF N LEQ 14 $ GO TO EQNC $ GO TO CHECK1 $
2 CHECK1.. IF N EQL 15 $ GO TO EQND $ GO TO EQNE $
2 EQNC..   C1 = ((2.0)*R(M,N)*DR)/(Z(M+1) - Z(M)) $
2          C2 = ((2.0)*R(M,N)*DR)/(Z(M) - Z(M-1)) $
2          C3 = (Z(M+1) - Z(M-1))/(LOG(R(M,N)) - LOG(R(M,N) - DR)) $
```

```
     2          K2 = A + (0.5)*B*(TA(M-1,N+1) + TA(M,N))  $
     2          K3 = A + (0.5)*B*(TA(M,N+1) + TA(M,N)) $
     2          K4 = A + (0.5)*B*(TA(M,N-1) + TA(M,N)) $
     2          K5 = A + (0.5)*B*(TA(M+1,N+1) + TA(M,N)) $
     2          TB(M,N) = (K5*C1*TA(M+1,N+1) + K2*C2*TA(M-1,N+1)
     2          + K3*C3*TA(M,N+1) + K4*C4*TA(M,N-1))/(K5*C1 + K2*C2 + K3*C3
     2          + K4*C4) $
     2          GO TO FIN12 $
     2 FOND..   K2 = A + (0.5)*B*(TA(M-1,N+1) + TA(M,N)) $
     2          K3 = A + (0.5)*B*(TA(M,N+1) + TA(M,N)) $
     2          K4 = A + (0.5)*B*(TA(M,N-1) + TA(M,N)) $
     2          K5 = A + (0.5)*B*(TA(M+1,N+1) + TA(M,N)) $
     2          C12 = ((Z(M) - Z(M-1))*((DR + L1)*(R(M,N) - (0.25)*DR
     2          - (0.25)*L1) - ((1.0)/(12.0))*((DR - L1)**2.0)) +
     2          (Z(M+1) - Z(M))*((DR + L2)*(R(M,N) - (0.25)*DR + (0.25)*L2)
     2          - ((1.0)/(12.0))*((DR - L2)**2.0)))/(((2.0)*R(M,N)*DR
     2          - (DR)**2.0)*(LOG(R(M,N)) - LOG(R(M,N) - DR))) $
     2          C13 = (Z(M+1) - Z(M-1))/(LOG(R(M,N) + DR) - LOG(R(M,N)))$
     2          C14 = (R(M,N)*DR + (0.25)*((DR)**2.0) + (1.5)*R(M,N)*L2
     2          - ((2.0)/(3.0))*((L2)**2.0))/(Z(M+1) - Z(M)) $
     2          C15 = (R(M,N)*DR + (0.25)*((DR)**2.0) + (1.5)*R(M,N)*L2
     2          - ((2.0)/(3.0))*((L2)**2.0))/(Z(M) - Z(M-1)) $
     2          TB(M,N) = (K3*C12*TA(M,N+1) + K4*C13*TA(M,N-1)
     2          + K5*C14*TA(M+1,N+1) + K2*C15*TA(M-1,N+1))/(K3*C12 + K4*C13
     2          + K5*C14 + K2*C15) $
     2          GO TO FIN12 $
     2 FONE..   K4 = A + (0.5)*B*(TA(M,N-1) + TA(M,N)) $
     2          C10 = ((2.0)*R(M,N) + DR - L1)*(SQRT(((DR - L1)**2.0)
     2          + (0.25)*((Z(M) - Z(M-1))**2.0))) + ((2.0)*R(M,N) + DR
     2          - L2)*(SQRT(((DR - L2)**2.0) + (0.25)*((Z(M+1) - Z(M))**2.0))) $
     2          C11 = ((Z(M) - Z(M-1))*(R(M,N)*(DR + L1) + (DR)**2.0
```

```
2          - ((1.0)/(3.0)).((DR - L1)*2.0)) + (Z(M+1)
2          - Z(M)).(R(M,N).(DR + L2) + (DR)*2.0 - ((1.0)/(3.0)).((DR
2          - L2)*2.0)))/(((2.0).R(M,N).DR + (DR)*2.0).(LOG(R(M,N) + DR)
2          - LOG(R(M,N)))) $
2          TB(M,N) = (H(M).C10.TG + K4.C11.TA(M,N-1))/(H(M).C10
2          + K4.C11) $
2          GO TO FINI2 $
2 FINI2..  END $
2 COMMENT  CALCULATION OF EXIT SECTION TEMPERATURES $
2          FOR M = (20,1,29) $
2   BEGIN  FOR N = (2,1,16) $
2   BEGIN  IF N LEQ 15 $ GO TO EQNF $ GO TO EQNG $
2 EQNF..   K3 = A + (0.5).B.(TA(M,N+1) + TA(M,N)) $
2          K4 = A + (0.5).B.(TA(M,N-1) + TA(M,N)) $
2          K5 = A + (0.5).B.(TA(M+1,N+1) + TA(M,N)) $
2          K6 = A + (0.5).B.(TA(M-1,N-1) + TA(M,N)) $
2          C1 = ((2.0).(R(M,N)).DR)/(Z(M+1) - Z(M)) $
2          C2 = ((2.0).(R(M,N)).DR)/(Z(M) - Z(M-1)) $
2          C3 = (Z(M+1) - Z(M-1))/(LOG(R(M,N)) - LOG(R(M,N) - DR)) $
2          C4 = (Z(M+1) - Z(M-1))/(LOG(R(M,N) + DR) - LOG(R(M,N))) $
2          TB(M,N) = (K5.C1.TA(M+1,N+1) + K6.C2.TA(M-1,N-1)
2          + K3.C3.TA(M,N+1) + K4.C4.TA(M,N-1))/(K5.C1 + K6.C2 + K3.C3
2          + K4.C4) $
2          GO TO FINI3 $
2 EQNG..   K4 = A + (0.5).B.(TA(M,N-1) + TA(M,N)) $
2          K6 = A + (0.5).B.(TA(M-1,N-1) + TA(M,N)) $
2          C5 = (2.0).R(M,N).(SQRT((DR)*2.0 + ((Z(M+1)
2          - Z(M-1))*2.0)/(4.0))) $
2          C8 = ((1.5).R(M,N).DR + (0.125).((DR)*2.0))/(Z(M) - Z(M-1)) $
2          C9 = ((Z(M) - Z(M-1)).((2.0).R(M,N) + DR) + (Z(M+1)
2          - Z(M)).(R(M,N) + (0.75).DR))/(((2.0).R(M,N)
```

```
2          + DR)*(LOG(R(M,N) + DR) - LOG(R(M,N))) $
2          TB(M,N) = (H(M)*C5*TG + K6*C8*TA(M-1,N-1)
2          + K4*C9*TA(M,N-1))/(H(M)*C5 + K6*C8 + K4*C9) $
2          GO TO FINI3 $
2 FINI3**  END $
2          END $
2 COMMENT  THIS SECTION REPLACES TEMPS TA WITH TEMPS TB     $
2          FOR M = (1,1,30)$ FOR N = (1,1,16)$ TA(M,N) = TB(M,N)$
2 COMMENT  CONDITIONAL PRINT-OUT        $
2          FOR J = 1,(10,10,200) $
2   BEGIN
2          IF I EQL J $ GO TO ANS $ GO TO SKIP $
2 ANS**    WRITE($$TITLE2B) $
2          WRITE($$OUT2,FMT2) $
2 SKIP**   END$
2          END$
2 INPUT CONST(TG,A,B,L1,L2,DR,RREF) $
2 INPUT    DATA1(FOR M = (1,1,30)$ FOR N = (1,1,16)$ TA(M,N)) $
2 INPUT    DATA2(FOR M = (2,1,29)$ H(M)) $
2 INPUT    DATA3(FOR M = (1,1,30) $ Z(M)) $
2 OUTPUT   OUT1(FOR M = (2,1,29) $ (M,H(M))) $
2 OUTPUT OUT2(FOR M = (1,1,30)$ (M, FOR N = (1,1,16)$ TA(M,N))) $
2 FORMAT   TITLE1(*ORIGINAL VALUES OF H(M)              *,W3)$
2 FORMAT   FMT1(B10,*H(*,I2,*) =*,ST.6,W0) $
2 FORMAT   TITLE3(*TEMP DISTRIBUTIONS IN THE FOLLOWING ORDER*,
2          * I = 1,10,20,30,ETC *,W4,W1) $
2 FORMAT   TITLE2B(*M=   N=1  N=2    N=3    N=4    N=5    N=6    N=7   *,
2                  * N=8    N=9    N=10   N=11   N=12   N=13   N=14   *,
2          *N=15   N=16*,W0   $
2 FORMAT   FMT2(I2,B1,16(S6.5,B1),W4) $
2          FINISH $
```

```
-2 COMMENT BAC - 220  STANDARD  VERSION   2/1/62                          $
 2 COMMENT CALCULATION OF HEAT FLUX AND TOTAL HEAT INPUT TO NOZZLE.
 2         ERIC KUNZ. X 456 $
 2 INTEGER M $
 2 ARRAY   TA(30), H(30), R(30), Z(30), A(30), QFLUX(30), Q(30) $
 2         READ($$CONSTS) $
 2         READ($$DATA1) $
 2         READ($$DATA2) $
 2         READ($$DATA3) $
 2 COMMENT CALCULATION OF RADII OF INNER SURFACE IN FEET. $
 2         FOR M = (1,1,19) $
 2         R(M) = RREF - ((1.0)/(12.0) + (M - 1.0).DR) $
 2         FOR M = (20,1,30) $
 2         R(M) = RREF - ((1.0)/(12.0) + (37.0 - M).DR) $
 2 COMMENT CALCULATION OF AREAS OF INNER SURFACE IN SQUARE FEET. $
 2 COMMENT ENTRANCE POINT AREA. $
 2         A(1) = (3.14159).((1.5).R(1) + (0.5).R(2)).(0.5).(SQRT((R(1)
 2         - R(2))*2.0 + (Z(2) - Z(1))*2.0)) $
 2 COMMENT ENTRANCE SECTION AREAS. $
 2         FOR M = (2,1,18) $
 2         A(M) = (3.14159).(R(M) + (0.5).(R(M-1) +
 2         R(M+1))).(0.5).(SQRT((R(M-1) - R(M+1))*2.0 + (Z(M+1) -
 2         Z(M-1))*2.0)) $
 2 COMMENT THROAT AREA POINT. $
 2         A(19) = (3.14159).(SQRT((R(18) - L1 - R(19))*2.0 +
 2         ((0.5).(Z(19) - Z(18)))*2.0)).(R(18) + R(19) - L1) +
 2         (3.14159).(SQRT((R(18) - L2 - R(19))*2.0 + ((0.5).(Z(20) -
 2         Z(19)))*2.0)).(R(18) + R(19) - L2) $
 2 COMMENT EXIT SECTION AREAS. $
 2         FOR M = (20,1,29) $
 2         A(M) = (3.14159).(0.5).(SQRT((R(M+1) - R(M-1))*2.0 +
```

```
2          (Z(M+1) - Z(M-1))*2.0)).(R(M) + (0.5).(R(M+1) + R(M-1))) $
2 COMMENT EXIT POINT AREA . $
2          A(30) = (3.141591.(0.5).(SQRT((R(30) - R(29))*2.0 +
2          (Z(30) - Z(29))*2.0)).((1.5).R(30) + (0.5).R(29)) $
2 COMMENT CALCULATION OF LOCAL HEAT FLUXES $
2          FOR M = (1,1,30) $
2          QFLUX(M) = H(M).(TG - TA(M)) $
2 COMMENT CALCULATION OF LOCAL HEAT INPUT. $
2          FOR M = (1,1,30) $
2          Q(M) = QFLUX(M).A(M) $
2 COMMENT CALCULATION OF TOTAL HEAT INPUT TO NOZZLE $
2          TOTAL = 0.0 $
2          FOR M = (1,1,30) $
2          TOTAL = TOTAL + Q(M) $
2          WRITE($$TITLE1) $
2          WRITE($$OUT2,FMT2) $
2          WRITE($$TITLE2) $
2          WRITE($$OUT1,FMT1) $
2          WRITE($$TITLE3) $
2 INPUT    CONSTS(TG,L1,L2,RREF,DR) $
2 INPUT    DATA1(FOR M = (1,1,30)$ TA(M)) $
2 INPUT    DATA2(FOR M = (1,1,30) $ H(M)) $
2 INPUT    DATA3(FOR M = (1,1,30) $ Z(M)) $
2 OUTPUT   OUT1(FOR M = (1,1,30) $ (M,QFLUX(M),Q(M))) $
2 OUTPUT   OUT2(TOTAL) $
2 FORMAT   TITLE1(*LOCAL HEAT FLUXES, LOCAL HEAT INPUT, AND TOTAL HEAT *,
2          *INPUT TO NOZZLE*,W0) $
2 FORMAT   TITLE2(B3,*M =  *,B5,*LOCAL HEAT FLUX = *,B5,*LOCAL HEAT *,
2          *INPUT = *,W4) $
2 FORMAT   FMT1(B4,I2,B14,F11.5,B13,F11.5,W4) $
2 FORMAT   FMT2(*TOTAL HEAT INPUT TO NOZZLE IS*,F11.5,B2,*BTU/HR.*,W4) $
```

```
2 FORMAT  TITLE3(*UNITS ARE AS FOLLOWS..*,W4,*LOCAL HEAT FLUX = *,
2         *BTU/HR.-SQ.FT.  *,W4,*LOCAL HEAT INPUT = BTU/HR.*,W4) $
2         FINISH $
```

LITERATURE CITED

1. P. F. Massier and M. B. Noel, "Heat Transfer from Ionized Gases," *Space Program Summary 37-19*, Vol. IV, Jet Propulsion Laboratory, California Institute of Technology, (December 1962), p. 119.

2. P. F. Massier, M. B. Noel and L. H. Back, "Heat Transfer from Ionized Gases," *Space Program Summary 37-22*, Vol. IV, Jet Propulsion Laboratory, California Institute of Technology, (June 1963), p. 119.

3. P. F. Massier, M. B. Noel, L. H. Back and A. B. Witte, "Heat Transfer from Ionized Gases," *Space Program Summary 37-23*, Vol. IV, Jet Propulsion Laboratory, California Institute of Technology, (August 1963), p. 109.

4. P. F. Massier, "Heat Transfer to Convergent-Divergent Nozzles from Ionized Argon," *Space Program Summary 37-24*, Vol. IV, Jet Propulsion Laboratory, California Institute of Technology, (October 1963), p. 105.

5. A. B. Witte and E. Y. Harper, "Heat Transfer in Rocket Motors," *Research Summary 36-10*, Vol. I, Jet Propulsion Laboratory, California Institute of Technology, (June 1961), p. 87.

6. A. B. Witte, E. Y. Harper, P. F. Massier and H. L. Gier, "Heat Transfer in Rocket Motors," *Research Summary 36-11*, Jet Propulsion Laboratory, California Institute of Technology, (August 1961), p. 80.

7. A. B. Witte and E. Y. Harper, "Heat Transfer in Rocket Motors," *Research Summary 36-12*, Vol. I, Jet Propulsion Laboratory, California Institute of Technology, (October 1961), p. 132.

8. A. B. Witte and E. Y. Harper, "Heat Transfer in Rocket Motors," *Research Summary 36-13*, Vol. I, Jet Propulsion Laboratory, California Institute of Technology, (December 1961), p. 127.

9. W. E. Welch, Jr. and A. B. Witte, "A Comparison of Analytical and Experimental Local Heat Fluxes in Liquid-Propellant Rocket Thrust Chambers," *Technical Report 32-43*, Jet Propulsion Laboratory, California Institute of Technology, (February 1961).

10. A. B. Witte and E. Y. Harper, "Experimental Investigation and Empirical Correlation of Local Heat-Transfer Rates in Rocket-Engine Thrust Chambers," *Technical Report 32-244*, Jet Propulsion Laboratory, California Institute of Technology, (March 1962).

11. W. B. Powell, G. W. Howell and J. P. Irving, "A Method for the Determination of Local Transient Heat Flux in Uncooled Rocket Motors," *Technical Report 32-257*, Jet Propulsion Laboratory, California Institute of Technology, (July 1962).

12. L. H. Back, P. F. Massier and H. L. Gier, "Convective Heat Transfer in a Convergent-Divergent Nozzle," *Technical Report 32-415*, Jet Propulsion Laboratory, California Institute of Technology, (November 1963).

13. A. B. Witte, "Heat Transfer in Rocket Motors," *Research Summary 36-9*, Vol. I, Jet Propulsion Laboratory, California Institute of Technology, (April 1961), p. 85.

14. R. E. Lee, "Heat Transfer to the Throat Region of a Solid Propellant Rocket Nozzle," *NOL Technical Report 62-72*, U. S. Naval Ordnance Laboratory, Maryland, (February 1963).

15. C. H. Liebert, J. E. Hatch and R. W. Grant, "Application of Various Techniques for Determining Local Heat Transfer Coefficients in a Rocket Engine from Transient Experimental Data," *NASA Technical Note D-277*, National Aeronautics and Space Administration, Lewis Research Center, Ohio, (April 1960).

16. J. D. Clem, Jr., W. H. Groetzinger, III, J. E. Johnson and C. H. Parr, "Experimental Determination of Heat Transfer Film Coefficients in Uncooled Rocket Nozzles," *Quarterly Progress Report on Weapons Research (U) P-57-5*, Redstone Arsenal Research Division, Rohm and Haas Co., (December 1956), p. 1.

17. J. Nanigian, "Temperature Measurements and Heat Transfer Calculations in Rocket Nozzle Throats and Exit Cones," *Nav Weps Report 8022, Technical Report 122*, U. S. Naval Propellant Plant, Maryland, (December 1962).

18. L. Ongkiehong and J. Van Duijn, "Construction of a Thermocouple for Measuring Surface Temperatures," *Journal of Scientific Instruments*, Vol. 37, (June 1960), p. 221.

19. S. Greenfield, "Determination of Rocket-Motor Heat-Transfer Coefficients by the Transient Method," *Journal of the Aeronautical Sciences*, Vol. 18, No. 8, (August 1951), p. 512.

20. R. L. Perry and W. P. Berggren, "Transient Heat Conduction in Hollow Cylinders after Sudden Change of Inner Surface Temperature," *Publications in Engineering*, Vol. 5, No. 3, University of California, (1944), p. 59.

21. H. S. Carslaw and J. C. Jaeger, *Conduction of Heat in Solids*, Second Edition, London: Oxford University Press, (1959).

22. R. V. Churchill, *Fourier Series and Boundary Value Problems*, First Edition, New York: McGraw-Hill Book Co., Inc., (1941).

23. C. R. Wylie, Jr., *Advanced Engineering Mathematics*, Second Edition, New York: McGraw-Hill Book Co., Inc., (1960).

24. B. Gebhart, *Heat Transfer*, New York: McGraw-Hill Book Co., Inc., (1961).

25. P. J. Schneider, *Conduction Heat Transfer*, Massachusetts: Addison-Wesley Publishing Co., Inc., (1955).

26. G. M. Dusinberre, *Heat-Transfer Calculations by Finite Differences*, Pennsylvania: International Textbook Co., (1961).

27. W. H. McAdams, W. E. Kennel, C. S. Minden, R. Carl, P. M. Picornell and J. E. Dew, "Heat Transfer at High Rates to Water with Surface Boiling," *Journal of Industrial and Engineering Chemistry*, Vol. 41, No. 9, (1949), p. 1945.

28. M. Jakob, *Heat Transfer*, Vol. I, New York: John Wiley and Sons, Inc., (1962).

29. M. Jakob, *Heat Transfer*, Vol. II, New York: John Wiley and Sons, Inc., (1963).

30. G. P. Sutton, *Rocket Propulsion Elements: an Introduction to the Engineering of Rockets*, Third Edition, New York: John Wiley and Sons, Inc., (1963).

31. J. Todd, *Survey of Numerical Analysis*, New York, McGraw-Hill Book Co., Inc., (1962).